

**SYNTHESIS AND FABRICATION OF  
NANOSTRUCTURED FUNCTIONAL POLYMERIC  
MATERIALS via PLASMA PROCESSES AND POLYMER  
MODIFICATION**

**ZONG BAOYU**

**NATIONAL UNIVERSITY OF SINGAPORE**

**2009**

**SYNTHESIS AND FABRICATION OF  
NANOSTRUCTURED FUNCTIONAL POLYMERIC  
MATERIALS via PLASMA PROCESSES AND POLYMER  
MODIFICATION**



**ZONG BAOYU**  
**(B. Sci., MBA)**

**A THESIS SUBMITTED  
FOR THE DEGREE OF DOCTOR OF PHILOSOPHY  
DEPARTMENT OF CHEMICAL AND BIOMOLECULAR  
ENGINEERING  
NATIONAL UNIVERSITY OF SINGAPORE  
2009**

## ACKNOWLEDGEMENT

First of all, I wish to express my cordial gratitude to my supervisors, Prof. **Kang En-Tang** and Prof. **Neoh Koon-Gee**, for the heartfelt guidance, valuable suggestions, profound discussions, and warm encouragements throughout this research work. The invaluable knowledge, which I have learnt from them on how to do research work and prepare scientific papers, will benefit me in my future research career.

I would like to thank all my group members and laboratory officers of the Department of Chemical and Biomolecular Engineering for their kind help and assistance. In particular, thanks to Dr Xu Fujian, Dr Lin Qidan, Dr Fu Guodong, Dr Yuan Ziliang, Mr Shang Zhenhua, Dr Shi Zhilong, and Dr Hu Feixiong for their helpful advices and discussions. It is my great pleasure to work with all of them.

I am deeply grateful for the supports from the top management and my research group members at the Data Storage Institute of A-Star.

Last but not least, I would like to give my special thanks to my parents, wife, daughter, and family members for their continuous encouragements.

## TABLE OF CONTENTS

<b>Acknowledgement .....</b>	<b>I</b>
<b>Table of Contents .....</b>	<b>II</b>
<b>Summary .....</b>	<b>V</b>
<b>Nomenclatures .....</b>	<b>VIII</b>
<b>List of Figures .....</b>	<b>XI</b>
<b>List of Tables .....</b>	<b>XVI</b>
<b>Chapter 1 Introduction .....</b>	<b>1</b>
1.1 Background of Research .....	2
1.2 Research Objectives and Scope .....	5
<b>Chapter 2 Literature Survey .....</b>	<b>9</b>
2.1 Fluoropolymers and Plasma Polymerization .....	10
2.2 Polymer Modification and Fine Polymer Nanostructures .....	28
<b>Chapter 3 Synthesis of Highly Hydrophobic Fluoropolymer Films of Nanospheres via Plasma Polymerization of Fluoromonomers.....</b>	<b>30</b>
3.1 Introduction .....	31
3.2 Experimental Section .....	33
3.3 Results and Discussion .....	35
3.4 Conclusions .....	48
<b>Chapter 4 Porous Fluoropolymer Nanospheres and Thin Film Prepared via Plasma Polymerization .....</b>	<b>49</b>
4.1 Introduction .....	50
4.2 Experimental Section .....	52
4.3 Results and Discussion .....	54

4.4	Conclusions .....	67
<b>Chapter 5</b>	<b>Magnetic Mesoporous Fluoropolymer Nanospheres from Plasma Polymerization and Surface-Initializing Adsorption of Magnetic Nanoparticles .....</b>	<b>68</b>
5.1	Introduction .....	69
5.2	Experimental Section .....	71
5.3	Results and Discussion .....	73
5.4	Conclusions .....	87
<b>Chapter 6</b>	<b>Magnetic Mesoporous Fluoropolymer Nanospheres from Plasma Polymerization/Etching and Adsorption of Surface-Functionalized Magnetic Nanoparticles .....</b>	<b>88</b>
6.1	Introduction .....	89
6.2	Experimental Section .....	91
6.3	Results and Discussion .....	93
6.4	Conclusions .....	106
<b>Chapter 7</b>	<b>Sterically Aligned Fluoropolymer Nanospheres from Self-Assembly During Plasma Polymerization .....</b>	<b>107</b>
7.1	Introduction .....	108
7.2	Experimental Section .....	110
7.3	Results and Discussion .....	112
7.4	Conclusions .....	126
<b>Chapter 8</b>	<b>0 - 3 Dimensional Conductive and Magnetic Nanostructures Prepared from Colloidal Polypyrrole Dispersions .....</b>	<b>127</b>
8.1	Introduction .....	128
8.2	Experimental Section .....	130
8.3	Results and Discussion .....	135
8.4	Conclusions .....	151

**Chapter 9 Conclusions and Recommendation for Future Work ..... 152**

**References..... 157**

**List of Publications ..... 182**

## SUMMARY

Plasma processes and polymer modification are two versatile tools for the fabrication of polymer nanostructures and nanopatterns. Nanostructures of functional polymers, such as fluoropolymers, electroactive polypyrrole (PPY), and others, can be prepared potentially via plasma processes or polymer modification. The aim of this work was to develop simple and novel methods for the fabrication of fine polymer nanostructures and nanopatterns from fluoromonomers and pyrrole via plasma polymerization, plasma etching, or polymer modification. It was also the objective of this work to explore useful functionalities and potential applications for these nanostructured polymers after characterization.

Initially, via plasma polymerization and deposition at room temperature, highly hydrophobic fluoropolymers were synthesized by exploring various polymerization parameters, such as the wide range of system pressures (13 – 107 Pa) and glow discharge powers (100 – 400 W), and the natures of fluoromonomers of different boiling points (b. p.), molecule weight (MW), and degree of saturation. Mesoporous fluoropolymer nanospheres were prepared via the agglomeration of fine poly(heptadecafluorodecyl acrylate) (pp-HDFA) nanoparticles from plasma polymerization and deposition. Relationships between particle size and glow discharge duration during the high energy plasma polymerization of the HDFA monomer were elucidated. With these mesoporous nanospheres, a series of ultra-thin (< 100 nm) and low dielectric constant nanoporous films were obtained by means of one-round or multiple pulse plasma polymerizations. In addition, by carefully controlling the monomer concentrations and polymerization parameters, two-dimensionally and three-dimensionally self-assembled pp-HDFA

nanospheres on hydrogen-terminated Si(100) (H-Si) wafers were fabricated in dry ambience. The morphology of horizontally aligned particles could be changed from particle 'chains' to particle 'bars' by reducing the particle distribution density on the wafer surface. The vertically assembled nanoparticles in the form of pyramids were obtained under a very low initial monomer concentration and the effect of the electric field in the reaction chamber. Furthermore, by carefully controlling the input plasma power, system pressure, and glow discharge duration, mesoporous poly(pentafluorostyrene) (pp-PTFS) nanospheres and films were synthesized from the PTFS monomer. The porous nanospheres can be used to fabricate magnetic porous nanospheres upon thermal-decomposition of the adsorbed pentacarbonyl iron.

By using the two different plasma functions (viz. plasma polymerization and plasma etching) in a plasma system, mesoporous fluoropolymer nanospheres of 200 - 300 nm in size were prepared directly via one-pot plasma polymerization and deposition, followed by controlled argon plasma dry etching. The porous fluoropolymer nanospheres can be used as substrate to adsorb PtFe nanoparticles, and thus imparting magnetic functionality on the mesoporous nanospheres.

Finally, via polymer modification in wet process, functional micro- and nano-structures from conductive aqueous PPY colloidal dispersions were created. The stable PPY colloidal dispersions were prepared via oxidative polymerization of pyrrole by  $\text{FeCl}_3$  in the presence of surfactants in an aqueous medium. Zero to three dimensional (0 - 3D) PPY nanostructures, such as 0D nanoparticles, 1D nanofibres, 2D nanofilms, and 3D nanoflowers were fabricated by casting, coating, or spraying. When using these PPY



nanospheres as substrates, magnetic CoFe shell/conductive PPY core nanospheres, hollow magnetic CoFe nanospheres, and conductive microspheres with magnetic handles were also prepared.

## NOMENCLATURE

0 – 3D	Zero to three dimension
AFM	Atomic force microscope
BEs	Binding energies
b. p.	Boiling point
CAP mechanism	The principle of competitive ablation and polymerization
D. C.	Direct current
$D_m$	Particle size (mean particle diameter)
EDX	Energy dispersive X-ray
FESEM	Field emission scanning electron microscope
FTIR	Fourier transform infrared spectroscopy
HDFA	Heptadecafluorodecyl acrylate
HFB	Hexafluorobenzene
H-Si wafer	Hydrogen-terminated silicon wafer
IC	Integrated-circuit
IPA	Isopropanol or 2-Propanol
$\kappa$	Dielectric constant
M	Molarity or molar concentration (units: mol/L)
M-H loop	Magnetization-hysteresis loop
MW	Molecular weight
NaDS	Sodium dodecyl benzene sulfonate
OLED	Organic light-emitting-device

PCB	Printed circuit board
PET	Polyethylene terephthalate
PFH	Perfluoroheptane
PFS	2,3,4,5,6- Pentafluorostyrene
pp-HDFA	Plasma polymerized heptadecafluorodecyl acrylate
pp-HFB	Plasma polymerized hexafluorobenzene
pp-PFH	Plasma polymerized perfluoroheptane
pp-PFS	Plasma polymerized pentafluorostyrene
PPY	Polypyrrole
pp-Zonyl <sup>TM</sup>	Plasma polymerized Zonyl <sup>TM</sup>
PVA	Poly(vinyl alcohol)
$R_a$	Average surface roughness
RF	Radio frequency
sccm	Standard cubic centimeter per minute
SD	Standard deviation
SIA	Semiconductors Industry Association
TEM	Transmission electron microscopy
Tg	Glass transition temperature
ToF-SIMS	Time-of-flight secondary ion mass spectrometry

VSM	Vibrating sample magnetometer
W/FM	Composite parameter in plasma polymerization, where: W - RF power (in J/s), F - monomer flow-rate (in mol/s), M - molecular weight of monomer (in kg/mol)
XPS	X-ray photoelectron spectroscopy

## LIST OF FIGURES

### Chapter 3

- Figure 3.1 FESEM images of (a) pp-PFS and (b) pp-Zonyl<sup>TM</sup> polymer films deposited at a system pressure of 80 Pa, RF power of (1) 100 and (2) 400 W.
- Figure 3.2 AFM images of (a) pp-PFH and (b) pp-HFB films deposited at RF power of 400 W and different pressures of (1) 27, (2) 80, and (3) 107 Pa.
- Figure 3.3 AFM image of pp-Zonyl<sup>TM</sup> film obtained at monomer temperature of (a) 25 or (b) 60°C on Si substrate with room temperature, or (c) 25°C on Si substrate with high temperature of 78°C, under a RF power of 400 W and system pressure of 13 Pa.
- Figure 3.4 FTIR reflectance spectra of (a) pp-PFS and (b) pp-Zonyl<sup>TM</sup> films deposited at 80 Pa. The RF powers for pp-PFS are 100, 300, and 400 W while for pp-Zonyl<sup>TM</sup> 50, 100, 200, and 400W.

### Chapter 4

- Figure 4.1 Scheme for the fabrication of porous polymer nanospheres and film via plasma polymerization and deposition.
- Figure 4.2  $3 \times 3 \mu\text{m}$  2D AFM images of pp-HDFA nanospheres deposited at a system pressure of 7 Pa with various glow discharge duration: (a) 3, (b) 10, (c) 20, and (d) 30 s.
- Figure 4.3  $3 \times 3 \mu\text{m}$  2D AFM images of pp-HDFA nanoparticles polymerized at a system pressure of 13 Pa with various glow discharge duration. (a)-(f) stands for 3, 10, 20, 30, 60, and 120 s, respectively.
- Figure 4.4 pp-HDFA nanospheres polymerized under RF power of 500 W at a system pressure of 7 Pa by plasma-glow-discharge of 55 s. (a)  $3 \times 3 \mu\text{m}$  AFM 3D image and (b)  $0.5 \times 0.5 \mu\text{m}$  2D AFM topographical image. (c) FESEM image (scale bar: 10 nm) of one big nanosphere in (b).
- Figure 4.5 ToF-SIMS spectra of the pp-HDFA nanospheres deposited at a system pressure of 7 Pa with various glow discharge durations.

Figure 4.6 (a<sub>1</sub>) and (b<sub>1</sub>) are 3 × 3 μm 3D AFM images of porous pp-HDFA films polymerized under RF power of 500 W at a system pressure of 13 Pa by plasma-glow-discharge of 38 s for one and four rounds, respectively. (a<sub>2</sub>) FESEM lateral view image of (a<sub>1</sub>) porous film on Si wafer. The inset is a high magnification FESEM image at a magnification of 250,000× (scale bar = 30 nm). (b<sub>2</sub>) FESEM image of a porous pp-HDFA film via multiple depositions. The scale bar is 100 nm.

## Chapter 5

Figure 5.1 Fabrication scheme of magnetic porous polymer nanospheres via plasma polymerization, surfactant-initiated surface adsorption, and thermal decomposition.

Figure 5.2 AFM image of pp-PTFS (a) solid particles prepared under a system pressure of 27 Pa and RF power of 200 W with a plasma discharge duration of 60 s. (b) Mesoporous films prepared under a system pressure of 13 Pa and glow discharge power of 500 W with a glow discharge time of 20 s. The inset in (b) is a 200 × 200 nm FESEM image. (c) Mesoporous films compiled nanospheres synthesized under a system pressure of 13 Pa and glow discharge power of 400 W with a plasma discharge duration of 60 s.

Figure 5.3 (a) FESEM image of pp-PTFS porous nanospheres prepared under a system pressure of 27 Pa and RF power of 400 W with glow discharge time of 20 s. The inset is a TEM image focusing on a nanosphere. The scale bar is 50 nm. (b) AFM image of pp-PTFS mesoporous nanospherical film deposited via 4 rounds of multi-plasma polymerization under the same polymerization parameters as (a).

Figure 5.4 High-resolution XPS C 1s core-level spectra of pp-PTFS nanostructured polymers deposited under different polymerized parameters. (a) solid particles, (b) porous nanospheres, (c) porous film.

Figure 5.5 (a) FESEM images of one porous pp-PTFS nanosphere with immobilized iron oxide nanoparticles. (b) TEM image of one part of ~300 nm pp-PTFS nanosphere loaded with iron oxide nanoparticles. The scale bars of (a) and (b) are 100 and 20 nm, respectively. (c) and (d) are the respective VSM and EDX analysis results of the magnetic nanospheres on a 10 × 8 mm Si substrate. In (c), the open symbol (-◇-) and solid symbol (-■-) stand for the magnetic moment of the mesoporous pp-PTFS nanospheres prior to and after immobilization of the iron oxide nanoparticles,

respectively. (e) TEM image of one part of a magnetic pp-PTFS nanosphere after HCl washing.

## Chapter 6

Figure 6.1 Scheme illustrating (a) the preparation of mesoporous fluoropolymer nanospheres via plasma polymerization and plasma etching, (b) the preparation of surface-functionalized PtFe nanoparticles, and (c) the adsorption of magnetic PtFe nanoparticles on the porous polymer nanospheres.

Figure 6.2 FESEM images of (a) solid pp-HDHF particles polymerized under an input RF power of 200 W, system pressure of 40 Pa and glow discharge time of 45 s, and the solid particles after (b) 5 s and (c) 22 s of Ar plasma etching under the same RF power and system pressure. The scale bars in the images of parts (a) and (b) are 1  $\mu\text{m}$ , and of part (c) is 100 nm, while the scale bars for the 3 insets are 100 nm.

Figure 6.3 ToF-SIMS spectra of the pp-HDFA spheres (a) before and (b) after 8 s of plasma etching.

Figure 6.4 XPS wide scan spectra and C 1s core-level spectra of the pp-HDFA spheres before etching (a, b) and after 5 s (c, d) and 8 s (e, f) of plasma etching.

Figure 6.5 Images of a porous pp-HDFA nanosphere (from 5 s of plasma etching of the solid nanosphere) with adsorbed magnetic PtFe nanoparticles: (a) FESEM image, (b) TEM image. The scale bars in (a) and (b) are 100 and 20 nm, respectively.

Figure 6.6 VSM analysis results of a 250-nm thick layer of the magnetized pp-HDFA nanospheres on a  $5 \times 3 \text{ mm}^2$  Si substrate. The open symbol (- $\diamond$ -) and solid symbol (- $\blacksquare$ -) stand for the magnetization of the mesoporous pp-HDFA nanospheres prior to and after adsorption of the PtFe nanoparticles, respectively.

## Chapter 7

Figure 7.1 Schematic illustration of plasma deposition under different glow discharge conditions.

Figure 7.2  $3 \times 3 \mu\text{m}$  AFM image of (a) the pp-HDFA porous film deposited under a pressure of 13 Pa, RF power of 400 W, and glow discharge time of 60 s. (b) and (c) 2D (linearly) aligned pp-HDFA nanospheres chains deposited under a pressure of 53 and 107 Pa, respectively, RF power of 400 W, and plasma glow discharge time of 60 s. The plasma chamber was charged with the HDFA monomer for 60, 30, and 30 s for (a), (b), and (c), respectively, prior to plasma polymerization.

Figure 7.3  $3 \times 3 \mu\text{m}$  AFM image of the 2D aligned pp-HDFA particle bars deposited under a pressure of 53 Pa and RF power of 400 W, with glow discharge time of 15 s for (a) and (b) (one round deposition), and (c) (two rounds deposition). The plasma chamber was feed with the monomer for 20, 15, and 15 s, respectively, before polymerization. The inset of (b) is a  $1 \times 1 \mu\text{m}$  AFM image of the wafer rotated by about  $90^\circ$  before scanning while keeping the scanning direction of the tip unchanging.

Figure 7.4  $3 \times 3 \mu\text{m}$  AFM images of the pp-HDFA particles deposited under a pressure of 53 Pa and the RF power of 400 W with glow discharge time of (a) 5, (b) 15, and (c) 40 s, respectively. The plasma chamber was initially charged with the monomer for 5 s. The inset of (c) is  $1 \times 1 \mu\text{m}$  AFM image, which shows pyramids of  $\sim 50$  nm nanoparticles.

Figure 7.5 C 1s core-level spectra of the pp-HDFA nanoparticle pyramids (a), and the nanoparticle pyramids after storing in  $\text{CO}_2$  (b) and  $\text{O}_2$ , respectively, for two days.

## Chapter 8

Figure 8.1 Fabrication schemes of (a) PPY dispersion, 0D solid PPY nanospheres, and 1 - 3D nanostructures, (b) PPY core-CoFe shell nanospheres, (c) hollow magnetic CoFe shell nanospheres, and (d) magnetic PPY spheres by means of chemical oxidation polymerization, magnetic film sputtering, and solution treatment processes.

Figure 8.2 FESEM images of (a) PPY nanospheres synthesized via drop-wise addition of PPY dispersion into acetone under stirring at a speed of 1000 rpm, (b) PPY nanowires prepared via casting PPY dispersion into alumina filter, baking, and dissolving the alumina filter, (c) PPY nanowires synthesized via casting of liquid PPY dispersion into acetone through an alumina filter with a pore size of 150 nm, (d) PPY porous film fabricated via sprinkling PPY and acetone solution onto Si wafer surface and drying under reduced pressure, (e) PPY flat film prepared via spin-coating PPY dispersion on Si wafer and drying in air, and (f) PPY



nanoflowers synthesized via sprinkling PPY and H<sub>2</sub>O mixture on Si wafer, followed by cooling in liquid N<sub>2</sub> and drying under reduced pressure. The scale bars in the images of (a) and (b) are 100 nm; (c), (e) and the inset of (f) are 1 μm; (d) and (f) are 10 μm.

Figure 8.3 FESEM images of (a) a thick layer of PPY nanospheres laid on Si wafer surface, (b) one layer of PPY nanospheres on Si wafer surface prepared via spin-coating for 20 s at a speed of 2000 rpm, (c) magnetic CoFe shell/conductive PPY core nanospheres, (d) and (e) hollow magnetic CoFe nanospheres. The inset is a TEM image, and (f) magnetic handle microspheres. The scale bars in the FESEM images of (a), (b) and inset of (f) are 1 μm, (c)-(e) are 100 nm while (f) is 10 μm. The scale bars for the TEM image in the inset of (e) is 5 nm.

Figure 8.4 XPS wide scan spectra of the solid conductive PPY nanostructures: (a) planar film from drying PPY dispersion in air, (b) porous film from drying the mixture of PPY dispersion and acetone under reduced pressure, and (c) solid nanospheres from drop-wise addition of PPY dispersion into acetone under vigorous stirring.

Figure 8.5 EDX results of (a) PPY nanospheres, (b) hollow magnetic CoFe nanospheres, (c) handle of magnetic PPY microsphere, and (d) 3D PPY nanoflower.

Figure 8.6 PPY nanosensor measurement circuit (a) and measurement results (b). In (b), the line (—) stands for sensor results without any addition (before 150 s) and addition of liquid toluene (at 150 s), while (—○—) and (—◇—) stand for addition of liquid N<sub>2</sub> or acetone, and addition of distilled water then acetone, respectively.

## LIST OF TABLES

### Chapter 3

Table 3.1 Chemical structures and properties of the 4 monomers.

Table 3.2 Surface morphological properties of 4 fluoropolymer films obtained at different RF power and system pressure on the Si substrates.

Table 3.3 Water contact angles for the 4 fluoropolymer surfaces.

### Chapter 4

Table 4.1 Assignments of positive ions in the ToF-SIM spectra of the pp-HDFA nanospheres.

Table 4.2 Physical properties of the transparent porous pp-HDFA films deposited via polymerization and deposition at input RF power of 500 W.

### Chapter 5

Table 5.1 Property comparisons of the pp-PTFS polymers deposited at different plasma (RF) energy.

Table 5.2 Assignments of positive ions and ToF-SIMS spectra of pp-PTFS.

### Chapter 6

Table 6.1 Assignments of the positive ion fragments in the ToF-SIMS spectra of pp-HDFA nanospheres.

Table 6.2 XPS results of pp-HDFA nanospheres before and after Ar plasma etching.

Table 6.3 EDX analysis results of magnetized pp-HDFA nanospheres.

### Chapter 7

Table 7.1 Physicochemical properties of the pp-HDFA nanostructures.

### Chapter 8

Table 8.1 Physicochemical properties of conductive PPY dispersion and nanostructures.

**CHAPTER 1**

**INTRODUCTION**

### 1.1 Background of Research

Preparation of nano-/micro-structured polymers and innovative applications of these polymers are two recent objectives in polymer science. Nanostructured organic materials are of increasing importance in microelectronics, bioactive-device, nanotechnology, semiconductor industry, and other advanced technologies. For example, in order to match the increasing memory capacity and faster processing speed of computers, continuous development of highly integrated microchips requires the semiconductor industry to evolve towards electronic devices with ever decreasing feature dimensions on each chip [Callister et al., 2003; Sermon et al., 2004]. Hence, ultra-low dielectric constant ( $\kappa$ ) interlayer films are essential in the new generation of high density integrated circuits (IC) for reducing the time delay, cross-talk, and power dissipation of the resistive capacitance in electronic devices. In this aspect, the widely used silicon dioxide insulator ( $\kappa = 3.9 - 4.2$ ) can no longer meet the requirement ( $\kappa < 2.5$ ) of the new generation of ultra-large scale ICs [Yu et al., 2004; Sermon et al., 2004]. Nanostructured fluoropolymers are potential materials for applications in this area due to their lowest  $\kappa$  values among all the bulk materials, their good chemical and thermal stabilities, and reasonable costs of production [Stevens, 1999; Yasuda, 1990; Inagaki, 1996]. However, fluoropolymer applications in the sub-micron and nanoscale electronics are hindered by difficulties in fabrication [Yasuda, 1990; Biederman, 1992]. Fortunately, plasma polymerization is a simple technique for the deposition of polymer films on a variety of substrates from a wide range b. p. of monomers and molecules [Mijs, 1992; Biederman, 1992]. Furthermore, plasma polymerization is a convenient way to deposit polymers of controlled thicknesses and properties. The other merits of polymer fabrication via plasma

processes is the possibility of carrying out the reaction under a wide range of temperature (including room temperature) in dry ambience and in the absence of a solvent. In addition, plasma process possesses two inverse functions, viz. plasma polymerization and plasma etching. Thus, the processing problem of fluoropolymers can be overcome by plasma processes [Inagaki, 1996; Stevens, 1999]. Furthermore, differing from conventional methods, through the plasma process in dry ambience, different morphologies of fluoropolymers involving nano-/micro-structures or nanopatterns can be synthesized [Shi, 1996]. However, even though plasma process is a simple process, the parameters in plasma polymerization and deposition, such as plasma power, monomer concentration, system pressure, chemical and physical properties of the monomers, have two opposite functions to affect the resulting polymers and the reproducibility. On one hand, the parameters can significantly affect the morphology, property, and the reproducibility of the resulting polymers [Shi, 1996; Fu et al., 2003]. On the other hand, the parameters can also be used as variables for achieving various nanostructured materials. Currently despite numerous reports on the use of plasma polymerizations for the synthesis of types of bulk and micro-/submicro-structured fluoropolymers, studies on how to control the parameters of plasma polymerization and use the two opposite functions (plasma polymerization and plasma etching) of plasma process to fabricate nanostructured fluoropolymers are still of great interest, as few studies and reports are available in the literature.

Besides the importance of nanofluoropolymers, nanostructured organic electronic conductors (such as polypyrrole or PPY) are also important polymers in the field of microelectronics, biotechnology, and nanoprocess [Ghosh et al. 2004; Zou et al., 2001].

In comparison to other conductive polymers, PPY possesses some unique properties, such as low-toxicity, excellent environment stability, high electrical conductivity, and interesting redox properties [Kang et al., 1987; Benseddik, 1998; Saxena and Malhotra, 2003]. Hence conductive PPY nanopolymers have potential applications as electroactive materials for batteries, capacitors, actuators, membranes, smart windows, and communication tools in microelectronics [Cawdery et al., 1998; Li et al., 2001; Lu et al., 2004]. However, nanostructured pyrrole nanopolymers synthesized by chemical or electrochemical oxidative polymerization are largely intractable [Makhlouki, 1992; Saunders, 1999]. Up to now, the synthesized aqueous and non-aqueous colloidal PPY dispersions face the problems of stability and phase-transfer [Makhlouki, 1992]. Therefore, PPY applications in nanodevice fabrication are currently limited [Benseddik, 1998; Saunders, 1999].

### 1.2 Research Objectives and Scopes

Based on the developing situations and challenges in the fabrication of fine nanostructured fluoropolymers and pyrrole polymers, the specific goals of this PhD study are as follows:

- 1) To prepare low dielectric constant and highly hydrophobic nanostructured fluoropolymers from different monomers by controlling the parameters in plasma polymerization.
- 2) To develop new techniques of polymer self-assembly in dry ambience for the preparation of well-defined fluoropolymer nanostructures or nanopatterns.
- 3) To combine the two different functions of plasma process (plasma polymerization and etching) as a novel approach for the fabrication of nanoporous fluoropolymers.
- 4) To prepare stable aqueous colloidal dispersions of conductive PPY, which are suitable for the fabrication of 0 – 3D functional PPY nanostructures via phase transfer.
- 5) To explore new functions and applications for the as-synthesized polymer nanostructures.

This thesis will focus on plasma process and polymer modification for the fabrication of various functional nanostructures. The work consists of nine chapters. This chapter provides a general introduction to the subject. Chapter 2 presents an overview of the related literature.

Chapter 3 describes the synthesis of highly hydrophobic nanostructured fluoropolymers on silicon substrates via plasma polymerization and deposition. Four monomers with

different b. p. and chemical structures are used as precursors for the preparation of polymers under varying glow discharge conditions. From the experimental results, the influences of the polymerization parameters on the morphologies, properties, and deposition rates of the resulting polymers will be revealed. The monomers used include perfluoroheptane (PFH, linear saturated structure), hexafluorobenzene (HFB, contains an unsaturated aromatic ring), pentafluorostyrene (PFS, contains an aromatic ring and one unsaturated C=C bond), and Zonyl<sup>TM</sup> fluoromonomer (Zonyl<sup>TM</sup>, linear structure with one C=C bond).

Chapter 4 states a series of ultra-thin (< 100 nm) and highly porous fluoropolymer films prepared from the aggregation of mesoporous nanospheres via plasma polymerization and deposition in a controlled manner. The synthesized mesoporous fluoropolymer nanospheres have an average size of down to 18 nm, which depends on the plasma-glow-discharge duration and system pressure. The pore size of the nanospheres was 2 - 6 nm. The thickness of the thin fluoropolymer films (20 – 100 nm) can be controlled by means of one-time or multiple pulse plasma polymerizations.

Chapter 5 illustrates simple approach to the synthesis of ordered mesoporous nanospheres in dry ambience via plasma polymerization and deposition. This method allows mesoporous fluoropolymer nanospheres and films to be prepared from one monomer (PFS) under controlled high energy of plasma polymerizations. The synthesized porous fluoropolymer nanospheres are about 300 nm in size. The pores of the nanospheres were about 20 nm. After thermal-decomposition of adsorbed pentacarbonyl iron, these



mesoporous nanospheres were transferred to magnetic porous nanospheres, which can potentially be used in biotechnologies and catalysis as multifunctional delivery tools.

Chapter 6 reports the mesoporous fluoropolymer nanospheres of 200 - 300 nm in size, prepared directly via one-pot plasma polymerization and deposition of solid fluoropolymer nanospheres, followed by controlled argon plasma dry etching. Films of the assembled mesoporous fluoropolymer spheres exhibited an ultra-low dielectric constant of about 1.7. Adsorption of surface-modified PtFe nanoparticles of about 3 nm in size onto the mesoporous structure resulted in mesoporous fluoropolymer spheres with super-paramagnetic properties.

Chapter 7 presents the methodologies for self-assembly of horizontally and vertically aligned fluoropolymer nanospheres via plasma polymerization and deposition. Two-dimensionally (horizontally) and three-dimensionally (vertically) assembled fluoropolymer nanospheres on H-Si(100) wafer can be deposited in a controlled manner. The direction of the horizontally aligned nanoparticles is along the crystal epitaxis line of the Si(100) substrate. Particles of sizes ranging from 15 to 40 nm are generated at reduced initial monomer concentration in the glow discharge chamber and by varying the system pressure. The vertically assembled nanoparticles in the form of pyramids are obtained at a very low initial monomer concentration and high glow discharge power of  $\geq 400$  W under the effect of the plasma electric field. This self-assembly method can be potentially applied to the fabrications of other nanopatterns.

Chapter 8 demonstrates methods for preparing 0 – 3D functional micro- and nano-structures from modified conductive polypyrrole (PPY) colloidal aqueous dispersions.

The stable PPY colloidal dispersions are prepared via oxidative polymerization of pyrrole by  $\text{FeCl}_3$  in the presence of surfactants in an aqueous medium. 0D nanoparticles, 1D nanofibres, 2D nanofilms, and 3D nanoflowers are prepared by casting, coating, or spraying. The PPY nanostructures have various applications. From PPY colloids, magnetic CoFe shell/conductive PPY core nanospheres, hollow magnetic CoFe nanospheres, and conductive microspheres with magnetic handles are prepared via combined processes of metal sputtering and solution treatment.

Finally, in Chapter 9, the conclusion and recommendation for further work are given.

**CHAPTER 2**

**LITERATURE SURVEY**

## 2.1 Fluoropolymers and Plasma Polymerization

### 2.1.1 Applications of Plasma Polymerized Fluoropolymers

Fluoropolymer nanostructures and nanopatterns have broad applications in advanced technologies, such as in optics, microelectronics, and material-separation processes with membranes [Yang et al., 2003; Fu et al., 2004]. There are two major driving forces in the implementation of nanostructured fluoropolymers. Firstly, fluoropolymers possess the lowest dielectric constant value ( $\kappa \leq 2.2$ ) among all organic and polymer materials. Secondly, fluoropolymers can be prepared in the form of nanostructures with distinguished characteristic that cannot be found in the bulk phase [Zhang et al., 2002]. These specific properties can satisfy the requirements in the nanoscale regime of the advanced technologies. Thus, nanostructured fluoropolymer-based materials are of increasingly demand [Yasuda, 1984]. Furthermore, in IC manufacturing, the next generation of polymer interlayer dielectrics for sub-micron and nano-level electronics must also satisfy a variety of requirements, such as chemical inertness, good thermal stability, low moisture adsorption, and good adhesion to semiconductor and metal substrates. Nanostructured fluoropolymers with ultra-low  $\kappa$  as interlays can be used to alleviate these stringent requirements. Thus, there is a constant need to develop more nanostructured fluoropolymer materials [Mijs, 1992; Zhang et al., 2003].

Furthermore, nanoporous polymer films have been found important new applications. They are developed to be used as delivery beds for bio-materials or substrates for catalysis, and in purification of water or synthesis of fine solid organics [Nalwa, 1999; Martin et al., 2000; Maier, 2001]. Nanoporous fluoropolymers prepared from plasma polymerization exhibit a wide range of low  $\kappa$  applications, as compared to other

polymers. Porous nanospherical fluoropolymer films exhibit an even higher hydrophobicity and lower  $\kappa$  in comparison to bulk fluoropolymers. It is because the rougher surface and incorporation of air, which has a  $\kappa$  value of about 1, reduces the  $\kappa$  of the any resulting nanoporous structures [Lagendijk et al., 1998; Chen et al., 2004]. Furthermore, fluoropolymer films can be readily deposited on an assortment of substrates by the dry process of plasma polymerization, which is known to have an advantage over the wet process in the fabrication of nano-level electronics [Shi, 1996]. In addition, the nanostructured fluoropolymer films exhibit other excellent physicochemical properties, such as low dissipation factor, good chemical stability, high hydrophobicity, and high thermal stability [Han and Timmons, 2000; Takahashi, 2003]. These advantages and merits of nanostructured fluoropolymer films determine their potential applications in fabricating nanosized electronics or biomedical devices. As such, a number of studies have been devoted to plasma polymerization of fluorine-containing monomers to produce nanostructured low  $\kappa$  films [Hadjadj et al., 2001].

### **2.1.2 Plasma Polymerization and Deposition**

Plasma polymerization and deposition is a simple and convenient tool for the fabrication of nanostructured fluoropolymer materials. The plasma polymerization parameters can greatly affect the morphologies and properties of resulting fluoropolymers. The polymerization mechanism, advantages, and factors affecting the deposited film can be summarized in the following.

**1) Mechanism of Plasma Polymerization and Deposition.** Plasma collisions generate ions and radicals that lead to plasma polymerization and etching [Loo, et al., 2001;

Inagaki, 1996]. When the relative kinetic energy in the system is high, all or part of the energy is absorbed into the potential energy of the electrons and inelastic collision occurs. Such collisions can occur between atoms, ions and electrons, but not in ion-ion and electron-electron systems. These interactions have an approximate equal probability of producing either excitation or ionization of atoms. The interactions, however, have greater chance of producing excitation than ionization in molecules. In cases where the absorbed energy from collision is larger than the ionization energy of the molecule itself, collision can lead to ionization [Biederman, 1992]. If the energy is more than excitation energy but less than ionization energy, electrons stay in an excited state for a short time of  $10^{-8}$  –  $10^{-9}$ s, after which the electrons decay to the ground state and excess energy is emitted as photons. Ionization or dissociative ionization of the activated species is possible through further inelastic collisions with another particle. These collisions occur when the lifetime of the activated species is longer or equal to  $10^{-4}$  s (metastable states). Similarly for the energy transfer by photon absorption, absorbed photon energy greater or lesser ionization energy can result in photoionization or photoexcitation, respectively [Yasuda, 1990].

Plasma polymerization processes were first noticed from the deposition of organic compounds on the container walls via a discharge generated in acetylene. In the early nineteenth century, it was already known that electric discharge in a glass tube forms oily or solid-like products on the surface of the electrodes [Inagaki, 1996]. These products were treated as by-products, and not much attention was given to them until the start of 1960s when it was recognized that electric discharge could initiate polymerization of monomers to form polymer products. Through plasma

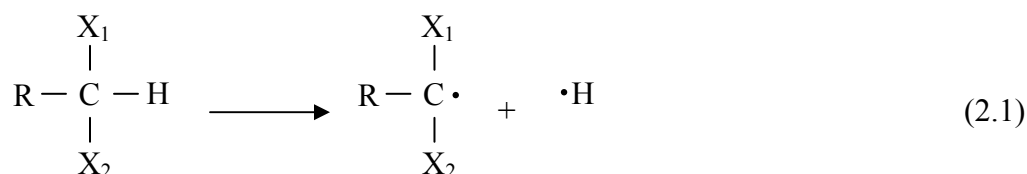
polymerization, the preparation of ultra-fine polymer particles, which cannot be achieved by other methods, is possible.

Plasma polymerization is a process in which polymer films are deposited directly on surfaces of substrates without any fabrication. In this process, the transformation of monomers into polymers occurs under low pressure, with the assistance of plasma energy produced by a glow discharge through organic gas or vapor. The liquid monomer evaporates and the vapor is pumped into a vacuum chamber. A glow discharge initiates the polymerization. When the energies of the plasma species are higher than the ionization energies or bond energies of the monomers, formation of electrons, radicals, ions and excited molecules occurs. While ionization is essential for sustaining the glow discharge, the free radicals are the dominant species that control the deposition of an organic compound in the plasma [Yasuda, 2003]. The extent of fragmentation of the monomer molecules depends very much on the operating conditions of the plasma polymerization process, including the electron density, input power, the starting monomer, the monomer flow-rate, etc. The process involves reactions between plasma species, between plasma and surface species, and between surface species. Some of the typical mechanisms proposed are ionic mechanism, radical mechanism and atomic polymerization [Zhang, 2002].

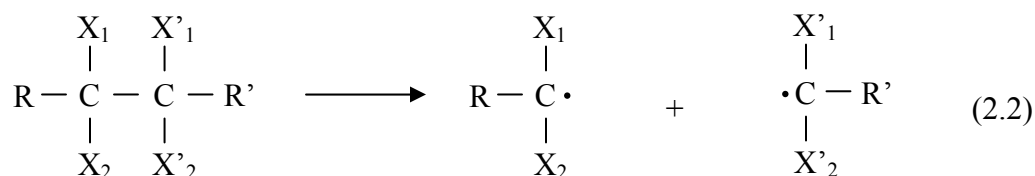
In the cases of a free-radical mechanism, two types of reaction may be postulated, namely plasma-induced polymerization and plasma-state polymerization. Plasma-induced polymerization is the conventional free radical-induced polymerization of

molecules containing unsaturated carbon bonds, triggered by the influence of the plasma. The molecules are activated without fragmentation and rearrangement [Inagaki, 1996; Dai, 1997]. For plasma-state polymerization, polymerization process occurs only in plasma of an electric discharge ignited in an organic gas. The elemental reactions are the fragmentation of monomer molecules, the formation of radicals and the recombination of these active fragments by free radical termination reaction. Free radicals trapped in the films can continue to react and change the polymer network over time. The film can also be altered by reacting with oxygen and water vapor in the atmosphere. The process does not require polymerizable bonds, such as double bonds, triple bonds or cyclic structure. Therefore, it allows the formation of polymer films from unconventional starting materials, such as saturated alkenes or benzene that do not polymerize under normal chemical polymerization conditions. The propagation reaction in polymerization is a stepwise recombination of the radicals formed by hydrogen elimination and C-C bond scission, instead of just simple chain reactions through double bonds.

- Hydrogen elimination



- C-C bond scission





### **2) Advantages of the Plasma Polymerization Process**

As mentioned above, conventional polymerization is essentially a chain reaction that involves chemical bonding of monomers with unsaturated bonds to form a macromolecule consisting of repeating units. The chemical structures of the starting monomers are retained, with small variation like the removal of small fragments, such as a water molecule, from two monomers. Consequently, the chemical composition of the final polymer can be predicted.

In contrast to the conventional chemical method, plasma polymerization is known not to be restricted to a monomer having a double bond or an unsaturated bond. Unlike the conventional polymers, plasma polymers do not contain regularly repeating units, and are characterized by a three-dimensional structure rather than a one-dimensional chain structure. The chains are branched and randomly terminated with high degree of cross-linking [Takahashi, 2001]. The initial molecular structure of the monomer is destroyed through the introduction of high-energy plasma into the process chamber. Due to this partial preservation of chemical structures, cross-linking and rearrangement of the monomer molecules in the plasma, it is not possible to predict the resulting chemical structure from that of the initial monomer [Yasuda, 1984]. In many cases, the chemical and physical properties of polymers formed by plasma polymerization can be rather different from those of the conventional polymers derived from the same starting materials.

During plasma polymerization, the fluoropolymer film is deposited by exposing the monomers to a glow discharge at a set of input power, system pressure, and temperature. This technique can be used to produce nanostructured organic compounds that do not form bulk polymers, which is from conventional chemical methods, as plasma polymerization requires electron impact-induced dissociation and ionization for chemical reactions. The nanostructured polymers produced can have additional features, such as highly corrosion resistance, which are not attainable using conventional chemistry [Inagaki, 1996]. Thus, plasma polymerization is a simple method for preparing nanostructured organic nanomaterials with various properties.

Some other advantages of the plasma process compared to the conventional polymer synthesis are stated below [Martinů et al., 1986; Nguyuen, 1999; Ibn-Eihaj and Schadt, 2001; Takahashi, 2001]:

- Polymerization can be achieved in dry ambience without the use of a solvent, making it easier to meet environmental restrictions.
- Polymer films have excellent coating adhesion on almost all substrates, including metal and plastic surfaces.
- Plasma treatment or deposition of thin polymeric coatings using plasma polymerization can modify the surface properties of polymers, with minimal effect on the bulk properties.
- Ultra-thin ‘pin-hole’ free and porous uniform films can both be produced.
- Polymer films have good chemical, thermal, and mechanical stabilities.

- The films are generally insoluble in organic solvents and have good corrosion resistance.
- It is possible to tailor the films with respect to specific chemical functionality and thickness by controlling the polymerization parameters.
- The process can be carried out at room temperature, making it possible to coat polymers on plastic substrates which have a low deflection temperature.
- Plasma polymerization only requires a relatively short process time, ranging from a few seconds to a few minutes.
- The starting material need not contain specific types of functional groups and can be any one of or several monomers or other organic materials, which are not flammable.

Therefore, plasma polymerization is an effective method for the deposition of fluoropolymers or for the modification of surface properties of substrates.

### **3) Factors Influencing the Result of Plasma Polymerization and Deposition**

In a plasma polymerization and deposition process, the structure of polymerized polymer is affected by the monomer type, energy per unit monomer molecules, deposition method, and substrate position. The effects of these factors are reflected on the monomer concentration or glow discharge energy in the reaction chamber during plasma process. In addition, the surface situations (e. g., temperature) and properties (e.g., texture structure) of the substrates will also affect the morphology of polymerized thin polymers. In general, monomer type, system pressure, flow-rate of the feed gas,

and feeding time of the monomer will determine the monomer concentration in reaction zone, while input power and plasma glow discharge time will govern the energy per unit monomer molecules. Thus, the monomer concentration and the plasma energy will directly determine the deposition rate and the structures of polymerized films. A high deposition rate normally leads to thick porous or bulk films while a low deposition rate can potentially result in thin films of nanospheres or nanostructured materials. The effects of plasma deposition parameters are summarized below.

### (1) Monomer type

Hydrocarbons can be classified into three major groups [Ibn-Eihaj and Schadt, 2001]:

- Aromatic or triple-bond containing compounds.
- Double bond containing and cyclic compounds.
- Saturated structure.

The chemical structure and boiling point of the monomer are the main factors governing the resultant polymer film morphology and deposition rate. When the feed flow-rate is kept constant, the ratio of the monomer to carrier gas molecules is determined by the boiling point of the monomer; when other process parameters are held constant, the maximum deposition rate increases by one order of magnitude with increasing degree of unsaturation in the starting molecule [Dai et al., 1997]. For example, ethane, methane, cyclohexane can be plasma polymerized at a slower rate than acetylene, ethylene and benzene. Thus, the minimum discharge power needed for the plasma polymerization of different monomers can differ significantly. The required discharge power is greater when the molecular weight of the starting material increases [Dai et al., 1997].

**(2) Feed gas and its flow-rate**

Apart from the monomer type, the carrier gas also has an effect on the monomer concentration and deposition rate [Chen et al., 1999; Øye et al., 2003]. Some of the carrier gases that can be used are Ar, CF<sub>4</sub>, H<sub>2</sub>, and N<sub>2</sub>. These gases do not form plasma polymers, and hence there is no material deposition from these carrier gases. The monomer with similar properties to the carrier gas always reaches higher concentration due to increased monomers evaporation in the chamber when the feed rate is fixed. Amongst these four gases, the non-reactive Ar plasma produces the highest deposition rate, followed by N<sub>2</sub>, CF<sub>4</sub>, and lastly H<sub>2</sub>.

With continuous increasing flow-rate while keeping other parameters constant, the deposition rate increases initially, and then decreases [Dai et al., 1997]. It is because at a low flow-rate the polymerization rate is limited by the supply of fresh monomer. At high flow-rate, residence time of the feed gases is lowered and active species may be prevented from reaching the substrate by being entrained in the monomer flow. The maximum deposition rate occurs where competing processes are balanced, and it shifts to higher flow-rates with increased unsaturation of the starting molecule.

The chemical structure of the polymer is also dependent on the feed gas flow-rate. An increase in flow-rate will push the domain of plasma polymerization from monomer deficient region to monomer rich region. In the monomer rich region, the monomer molecules are subjected to less fragmentation and less rearrangements. In the monomer deficient region, the deposition rate will show linear dependence on the monomer feed

rate at a given discharge power and system pressure [Øye et al., 2003]. There is heavy fragmentation and the plasma polymer undergoes more rearrangement. At the same time, there is a large loss of secondary groups, such as hydrogen, hydroxyl and carbonyl groups [Biederman, 1992].

### (3) Monomer feeding time

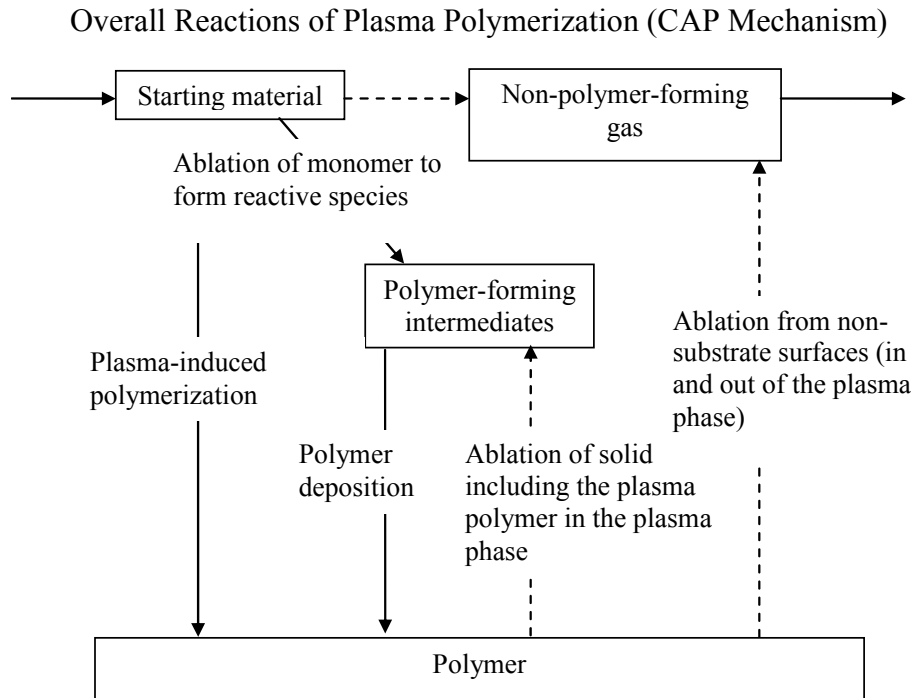
At a fixed feed flow-rate, when the monomer reaches saturation in the chamber, the monomer with high boiling point needs longer charging time in comparison to that of low boiling point. Before the monomer reaches saturation, the feeding time will directly determine the monomer concentration in the chamber and the deposition rate [Inagaki, 1996].

### (4) System pressure

High pressure promotes plasma polymerization as the residence time increases, the electron energy increases and the mean path decreases [Ibn-Eihaj and Schadt, 2001]. However, it can also bring about the inhomogeneity in deposition rate. For that reason, most operations are carried out at pressures below 130 Pa to obtain a more homogeneous film. With the flow-rate and discharge power held constant, the deposition rate increases initially and goes to maximum at increased pressure.

### (5) Input power

Power input in plasma polymerization is required for the production of the plasma as well as the fragmentation of the monomer molecule into activated small molecules. The polymers formed are constantly bombarded by the plasma until the polymerization



process completes, leading to degradation of the deposited film. Ablation or fragmentation, and polymerization could occur in a competitive manner in either plasma etching or plasma polymerization, and the balance depends on the overall system conditions. The chart below illustrates the principle of competitive ablation and polymerization (CAP) proposed by Yasuda [Yasuda, 2003].

In an energy deficient region, the polymer-forming process is predominant and the polymer deposition rate increases with increasing discharge power. If the plasma only consumes energy for activation of the monomer, the discharge power will be proportional to the density of energetic electrons as well as the concentration of activated molecules. Therefore, deposition rate at a constant flow-rate increases with power until the monomer molecules are completely consumed. Conversely, in the

energy rich region, polymer deposition rate decreases with further increase in discharge power beyond a threshold value due to the predominance of the polymer ablation process. This variation in the polymer deposition rate with discharge power indicates that the plasma contributes to both the polymer-forming and polymer-degrading processes. Plasma polymerization is therefore a balance between the polymer-forming and the ablation process, and the balance can shift in favor of one of the processes by changing the discharge power [Inagaki, 1996].

### (6) Volume and configuration of the chamber

The most frequently used plasma polymerization deposition systems are the bell-jar reactors with internal parallel plate metal electrodes and the tubular-type reactors with external ring electrodes or an external coil [Inagaki, 1996]. The inter-electrode separation will affect the breakdown of a gas in the chamber. When the inter electrode distance is too large at a given applied potential, the local electric field will be too low to supply sufficient energy to the electrons. On the other hand, electrode separation that is too small can result in the loss of electrons before any ionizing collisions with the gas atoms can occur. This phenomenon can be compensated by increasing the voltage. The apparatus geometry can influence the extent of ion bombardment on the substrate as well as electron energy distribution and active species production. The geometry of chamber will only have secondary effect on the experiment since the configuration is static and little can be done to vary this parameter.



## (7) Composite parameter (W/FM)

Parameters, such as discharge power, flow-rate and system pressure, are not independent of one another in determining the optimum conditions for a particular polymerization process. The fragmentation process depends on the electrical power supplied to maintain the plasma and the amount of monomer introduced into the plasma. Yasuda proposed a controlling parameter of W/FM for the deposition rate, where W, F, and M are the RF power (in J/s), the monomer flow-rate (in mol/s), and the molecular weight of the monomer (in kg/mol), respectively [Biederman, 1992; Inagaki, 1996]. The composite parameter represents the apparent input energy per unit of monomer molecule given in J/kg, and is considered to be proportional to the concentration of activated species in plasma. As such, a low W/FM value means that electrons of low energy level initiate the process.

It is important to note that the deposition rate is dependent on the composite parameter W/FM. An increase in flow-rate at a given discharge power has the same effect as decreasing the discharge power at a given flow-rate. The polymerization rate depends strongly on the structure of the feed gas when W/FM is below a certain threshold value, and is nearly independent of the structure at high W/FM values. The deposition rate increases by increasing the W/FM parameter in the monomer rich region, i.e. the region where the activated species have a far lower concentration than the monomer in the plasma. At the competitive region, the deposition rate is constant with an increase in W/FM. Lastly, in the monomer deficient region, the deposition rate decreases with increasing value of W/FM due to the lack of monomer molecules.

### (8) The effect of substrate temperature, position, and surface structure

It is well known that high power, high pressure, and low substrate temperature promote the generation of fine particles that are uniform in size [Nguyen et al., 1999]. High pressure and high plasma energy densities lead to the creation of high concentrations of condensable radicals and ions, as well as low diffusion path lengths of reactive species in the plasma. These conditions favor the gas phase reactions between radicals and other species. Therefore, rapid agglomeration and fine particle deposition onto the substrate surface are triggered. Substrate temperature can substantially affect the deposition of nanospheres [Boufendi et al., 2001]. A high substrate temperature will increase the surface mobility and the diffusion length of the deposited species. Furthermore, an increase in substrate temperature reduces the probability for nucleation, and inhibits or delays the formation of fine particle depositions.

Homogeneous thickness over a large substrate area is not easy to achieve. When placed at different locations in the reaction chamber, polymer films can exhibit significantly different deposition rates and chemical properties. The power deposition may not be uniform over the entire substrate surface during the polymerization process. Consequently, there is heterogeneity in the concentration of active species and monomers in the reaction chamber, leading to varying deposition rates. This inconsistency in deposition can be eliminated through the use of a moving substrate plate [Biederman and Osada, 1992].

### 2.1.3 Nanostructured Fluoropolymers Synthesized from Plasma Polymerization and Deposition

Fluoropolymers have been prepared by plasma polymerization and depositions, many of these polymers are synthesized for use as low  $\kappa$  and high hydrophobicity materials, due to the increasing demand for miniaturization in the microelectronics industry. The use of ultra-low  $\kappa$  interlayer can reduce the resistance-capacitance (RC) time delay, cross talk, and power dissipation in the new generation of higher-density integrated circuits [Maier, 2001]. According to the Semiconductors Industry Association (SIA) roadmap, the dielectric constant of interlays should be less than 2.0 when the feature dimension in integrated circuits decreases to less than 0.13  $\mu\text{m}$  [Ramos, 1997]. Fluoropolymers are potential candidates for interlay dielectric applications because of their low  $\kappa$  and good chemical and thermal properties. Perfluorinated aliphatic polymers exhibit the lowest dielectric constant ( $\kappa$ : 2.0 - 2.1) among all bulk polymeric materials. However, most of fluoropolymers, such as poly(perfluoroheptane) and poly(pentafluorostyrene), are insoluble in common organic solvents, and their decomposition temperatures are not far above the melting temperatures [Maier, 2001]. Thus, these polymers cannot be processed through common methods, such as melt processing and solvent casting. The difficulties in processing hinder their wide-spread applications in sub-micrometer and nanometer-scale electronics.

Ultra-low  $\kappa$  micro- and nano-structures can also be obtained by the introduction of air gaps into interconnected structures [Han et al., 2000; Fu et al., 2003] and nanopores into dielectric polymers [Ramos et al., 1997; Nguyen et al., 1999]. Air, which has a dielectric constant of about 1 (similar to that of vacuum ( $\kappa = 1$ )), can greatly reduce the

dielectric constant of the resulting porous structure. An approach of generating nanoporous film, which involves the fabrication of nanostructured fluoropolymers, is possible to prepare fluoropolymer films with  $\kappa$  value of less than 2.0 by introducing nanopores into fluoropolymers. Nanoporous poly(silsesquioxane)s [Han and Zheng, 2008] have been prepared by selective thermal decomposition of the sacrificial templates from the matrix films. This method provides an approach to produce porous film with controllable pore size and porosity by using sacrificial templates with different molecular weights. However, this method requires the matrix polymer to have a higher  $T_g$  than the decomposition temperature of the labile block. Hence, nanoporous fluoropolymer films cannot be prepared by this method because of the difficulty in processing, as well as the high  $T_g$  requirement in the polymeric matrix.

Plasma polymerization is a convenient way to prepare porous fluoropolymers. A variety of fluoropolymer films, such as poly(tetrafluoromethane), poly(hexafluoropropeneoxide) [Savage et al., 1991], and perfluoroallybenzne [Han et al., 2000], have been prepared by plasma polymerization and deposition. As mentioned above that in most cases, the fluoropolymer films prepared from plasma polymerization are insoluble, cross-linked, and lack defined chemical structures. Ultra-low  $\kappa$  nanoporous fluoropolymer films ( $\kappa < 1.9$ ) can be prepared by plasma polymerization of  $C_4F_8$  and extraction of the non-crosslinked polymers with tetrahydrofuran [Takahashi et al., 2003], or from nanoporous composites consisting of plasma-polymerized allylpentafluorobenzene [Fu et al., 2003]. However, the fluoropolymers are not widely used in microelectronic fields due to their uncontrollable pore size, porosity, and morphology [Takahashi et al., 2003; Zong et. al., 2007].

Accordingly, the preparation of nanostructured fluoropolymers with controllable particle size, pore size, and morphology by controlling the parameters in plasma processes is still of great interest. In addition, different fluoropolymer nanostructures with hydrophobic property, low dielectric constant, and other specific properties are in demand for high-tech applications.

**2.2 Polymer Modification and Fine Polymer Nanostructures**

Polymer modification can be achieved by means of amplifying the component or composition of the original polymer via mixing, doping, or adsorbing of other materials [Heeger, 2001]. It is usually used to overcome the limitation in properties or applications for existing polymers. In this way, various nanostructured polymers with improved performance, such as conductive and semi-conductive polypyrrole, can be achieved [Kumar et al., 1998; Cui, 2005].

Conductive polymers are a new class of materials which exhibit highly reversible redox behavior and possess the unusual combined properties of metal and plastics [Heeger, 2001]. Hence they have potential applications in a number of growing technologies, such as biomolecular electronics, telecommunication, display devices, memory devices, microwave absorption, drug-delivery, and electrochemical storage systems, and others [Yang et al., 2003; Ghosh et al., 2004]. In new technologies, molecular-scale electronics is rapidly evolving from physics, chemistry, biology, electronics, and information technology. It is because the advanced silicon chip can store about 16 million bytes of information within an area of less than 1 cm<sup>2</sup> [Saxena et al., 2003]. Organic materials, such as conducting polymers, have the potential to act same semi-conductive functions that are being performed by silicon. Thus, conductive polymers have attracted much attention and interests in the semiconductor area, and many efforts have been made to synthesize various functional semi-conductive polymers [Wessling, 1998; Skotheim et al., 1997; Rupprecht et al., 1999]. However, in the fabrication of functional devices with the polymers, the problem of processability (similar as fluoropolymers) is being encountered by most conductive polymers [Heeger, 2001].

For example, PPY is insoluble in most solvents and is infusible up to the decomposition temperature. Thus, PPY is extremely difficult to process, which in turn, limits its technological applications [Watanabe et al., 1998]. Polymer modification is an effective method to improve the processability and property of PPY [Heeger, 2001]. After chemical modification, electronic PPY materials can potentially exhibit full range of properties from insulator to superconductor [Saxena et al., 2003]. The properties of these modified PPY strongly depend on their microstructures. The PPY modification can be readily achieved by means of chemical doping or modifying the molecule structure [Heeger, 2001]. Currently, despite the numerous improvements in the modifications of PPY and other conductive polymers reported, the approach to nanostructures and nanodevices by using material-shaping method from these modified polymers is still a challenge [Wessling, 2005]. It is known that liquid or melt polymer can be easily cast or processed into various shapes and sizes (including nano-scale structures). But experimental attempts to prepare true solutions of intrinsically conductive polymers have failed [Wessling, 2005]. It is because of the difficulty to prepare stable conductive polymer solutions or melts. Thus, developing a stable conductive aqueous dispersion, which can be readily converted into any shape and size of nanostructures, via chemical modification for the nanodevice fabrication is highly demanded in current advanced technologies [Reisberg et al., 2008].

**CHAPTER 3**

**SYNTHESIS OF HIGHLY HYDROPHOBIC  
FLUOROPOLYMER FILMS OF NANOSPHERES VIA PLASMA  
POLYMERIZATION OF FLUOROMONOMERS**



**3.1 Introduction**

Fluoropolymers exhibit many unique physicochemical properties, such as high thermal stability, low flammability, excellent inertness, refractive index, oil and water repellence, and enhanced aging and weather resistances [Liu et al., 2004; Fu et al., 2003]. As a family of high-performance materials, fluoropolymers are widely used in various aggressive environments, such as chemical processing, oil well, motor vehicle engines, nuclear reactor, aerospace, aeronautics, optics, microelectronics, paints and coatings, and other engineering applications [Martinů et al., 1986; Han et al., 2000; Chen et al., 2004]. Despite the wide range of applications of fluoropolymers, the difficulties in processing these fluoropolymers hindered their applications in sub-micrometer and nanometer-scale electronics [Martinů et al., 1986; Takizawa, 2000; Takahashi et al., 2003]. In order to overcome this processing limitation, numerous studies have been carried out to prepare and deposit fluoropolymer films through thermal or gas-phase polymerization techniques [Zhang et al., 2002; Yang et al., 2003]. However, the progress is still limited. Hence an alternative approach to synthesize fluoropolymers with good properties remains of great interest.

Plasma polymerization is a simple technique for the deposition of polymer films on a variety of substrates from different monomers. Thus, the processing problem of fluoropolymers can be partially overcome by plasma processing [Takahashi and Tachibana, 2001; Takahashi et al., 2003; Wang et al., 2004]. Furthermore, by finding suitable polymerization parameters, plasma polymerization can potentially deposit fluoropolymer films of nanospheres with good properties. In this work, an approach to highly hydrophobic fluoropolymer nanospheres via plasma polymerization under

different conditions was demonstrated. Four monomers (e.g., perfluoroheptane, Zonyl<sup>TM</sup> fluoromonomer, hexafluorobenzene, and pentafluorostyrene) were used for the plasma polymerization process. The monomers have different boiling points and degrees of unsaturation. The fluoropolymer films deposited on hydrogen-terminated silicon substrates exhibited different deposition rates. The effects of various experimental parameters, such as input RF power, monomer type, system pressure, and monomer temperature, on the properties of the deposited fluoropolymer films were investigated. In addition, the relationships between the monomer type and plasma energy were revealed by the morphologies and compositions of the deposited films from the four monomers.

### 3.2 Experimental Section

#### 3.2.1 Materials

Silicon wafers ((100)-oriented single crystal, purchased from Silicon Valley Microelectronics, Inc. USA), having a thickness of about 0.65 mm and diameter of 150 mm, were used as deposition substrates. The wafers were polished on one side and doped as p-type. Before the experiment, the Si wafers were sliced into rectangular strips of about  $5 \times 10$  mm or other dimensions. To remove organic residues on the surface, the silicon substrates were washed in an ultrasonic bath with a “piranha” solution, a mixture of 98 wt% concentrated sulfuric acid (70 vol%) and hydrogen peroxide (30 vol%), since the organic residues can be decomposed by the solution and removed away under vigorous vibration. The cleaned silicon strips were then rinsed with copious amount of doubly distilled water before being immersed in 10 ml of hydrofluoric acid (HF: 10 vol%) for 5 minutes to become hydrogen-terminated surface [Fu et al, 2003]. The strips were later dried under an argon purge.

Monomers, such as perfluoroheptane (PFH, linear saturated structure), Zonyl<sup>TM</sup> fluoromonomer (Zonyl<sup>TM</sup>, linear with one unsaturated C=C bond), hexafluorobenzene (HFB, containing an unsaturated aromatic ring), and pentafluorostyrene (PFS, containing an aromatic ring and one C=C bond), were used for the plasma polymerization process.

#### 3.2.2 Plasma Polymerization

Plasma polymerization of the fluoromonomers was carried out at room temperature using a Plasma 80 Plus system (Oxford Instruments Plasma Technology Inc, Yatton, UK). The RF generator was operated at a frequency of 13.5 MHz. The fluoromonomers were introduced into the depositing chamber by a stream of argon carrier gas at a flow-rate of

30 standard cubic centimeters per min (sccm). Prior to and after the deposition of the plasma polymerized PFH, Zonyl<sup>TM</sup>, HFB, and PFS polymers (namely pp-PFH, pp-Zonyl<sup>TM</sup>, pp-HFB, and pp-PFS, respectively), the plasma chamber was purged with argon at a system pressure of 80 Pa for 2 and 5 min, respectively. The purging of Ar gas was to fully remove the residual reactants and other gaseous residues. The temperature of the chamber including the Si substrates was controlled at around room temperature ( $26 \pm 4^\circ\text{C}$ ) during plasma polymerization if there was not special illustration. For each plasma polymerization, the plasma chamber was charged with the monomers for 30 s and glow discharged of 30 s with presetting input power.

### 3.2.3 Characterization of the Fluoropolymer Films

The surface morphology of fluoropolymers was studied using a Dimension 3100 atomic force microscope (AFM, Digital Instruments Inc. Buffalo, NK, USA) and a JEOL 6320 field emission scanning electron microscope (FESEM, JEOL, Asia). For roughness ( $R_a$ ) measurements using AFM, a driving frequency of  $330 \pm 50$  kHz and a scan rate of 0.5 Hz were applied. The mean particle size ( $D_m$ ) and size standard deviation (SD) in the porous films of nanospheres were derived from 100 arbitrarily chosen particles in the FESEM images using Smile View<sup>®</sup> statistical software. SD was directly calculated from the square root of the  $D_m$  variance (the average squared  $D_m$  deviation from the mean). For each polymer, 3 batch samples (prepared with same parameters) were used to generate the average value. The thickness of the fluoropolymer films was determined using an Alpha-Step 500 Surface Profiler (KLA-Tencor Company, San Jose, CA). The chemical composition of fluoropolymers was analyzed by Fourier transform infrared (FTIR) spectroscopy.

### 3.3 Results and Discussion

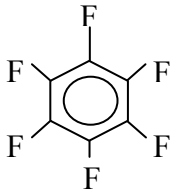
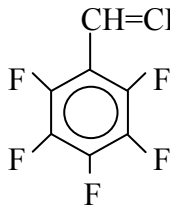
#### 3.3.1 Factors Affecting the Surface Morphologies of the Plasma Polymerized Fluoropolymer Films

By means of plasma polymerization and deposition, different fluoropolymer forms, including planar bulk films, granular powders, and films of nanospheres, were produced from the 4 fluoromonomers. In order to compare the as-synthesized polymers, the properties of the 4 monomers are elaborated in Table 3.1. In plasma polymerization, the system pressure, RF power, and other parameters were varied to investigate their effects on the morphologies and properties of the polymerized polymers. Representative results are summarized in Table 3.2. The result shows that the particle size, particle size distribution, and morphology of the synthesized fluoropolymer films are largely dependent on monomer property and glow discharge parameters. The generated fluoropolymer films, such as pp-HFB, pp-PFH, pp-PFS, and pp-Zonyl<sup>TM</sup>, from the 4 fluoromonomers, have different chemical structure and properties. Detailed results on the effect of experimental parameters on the as-synthesized polymers are given below.

##### 1) Effect of Input Power

The experimental data in Table 3.2 show that low RF power of 100 W leads to the formation of big particles or powdery films, whereas high RF power of 400 W results in film of fine spheres deposition. It is because at a constant flow-rate and system pressure, with the W/FM (W: power, F: monomer flow-rate, and M: molecular weight of monomer) composite parameter being taken into account, an increase in power will result in higher energy per monomer unit and higher density of energetic electrons, which subsequently lead to a high frequency of collisions [Yasuda, 2003]. As such, a greater

**Table 3.1** Chemical structures and properties of the 4 monomers

Monomers	Chemical Formula	Molecular Weight	b. p. (°C)
HFB		186	81
PFH	$\text{CF}_3(\text{CF}_2)_5\text{CF}_3$	388	82 - 84
PFS		194	139 - 140
Zonyl TM	$\text{H}_2\text{C}=\text{C}(\text{CH}_3)\text{CO}_2\text{CH}_2\text{CH}_2(\text{CF}_2)_n\text{F}$	534	210 - 350

level of fragmentation of the monomer molecules occurs, which in turn results in the formation of more reactive species and more nucleation sites [Barton et al., 2003; Yasuda, 2003]. Since the total amount of monomer molecules remains constant under a given flow-rate, more nucleation sites will lead to smaller particles [Zong et al., 2007]. Alternatively, the decrease in particle size with an increase in RF power can be explained by the different ways from which the particulates are derived. Particles from the plasma process originate from either the gas phase nucleation (homogeneous growth) or the fractured films deposited on the substrate surface (heterogeneous growth). At a low RF power, the particles are derived from both the gas phase and heterogeneous surface. On the other hand, gas phase reactions for the high concentration of radicals and ions are favored at high RF power [Yasuda, 2003]. As most of the particles are formed by homogeneous nucleation under a high RF power, the particles obtained have smaller

**Table 3.2** Surface morphological properties of 4 fluoropolymer films obtained at different RF power and system pressure on the Si substrates

Deposition Parameters		pp-PFH		pp-HFB		pp-PFS		pp-Zonyl™	
Pressure (Pa)	Power (W)	$D_m$ (nm)	$R_a$ (nm)	$D_m$ (nm)	$R_a$ (nm)	$D_m$ (nm)	$R_a$ (nm)	$D_m$ (nm)	$R_a$ (nm)
13	100	*	~ 0	-	-	-	-	*	~ 0
	400	62	3	190	6	256	20	42	2
27	100	*	~ 0	-	-	-	-	121	5
	400	55	1	160	3	242	18	38	1
80	100	57	2	186	8	248	35	37	52
	400	36	~ 0	155	7	218	12	25	3
107	100	60	~ 0	-	-	-	-	86	3
	400	21	1	80	2	201	14	23	~ 0

\* Bulk powdery film deposition, no particle was formed.  $D_m$  is the average diameter of both cluster and individual nanospheres on the substrates from 3 batch samples.

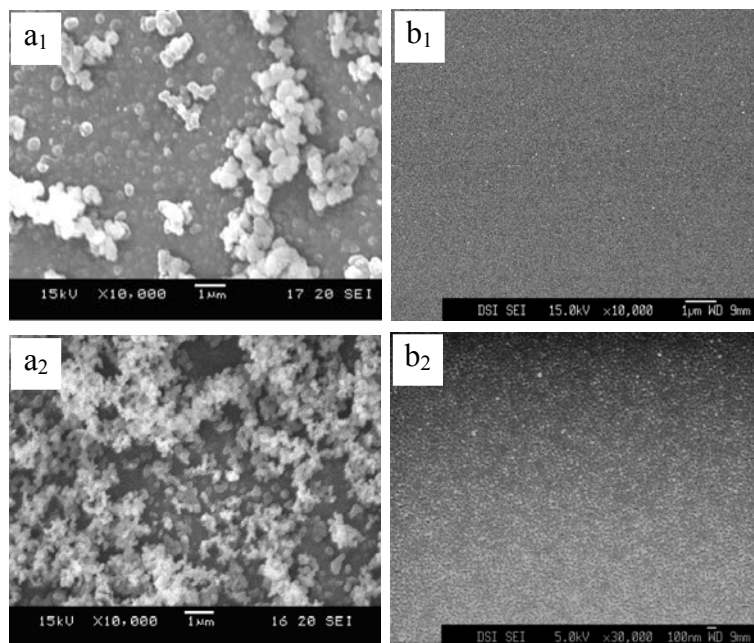


**Figure 3.1** FESEM images of (a) pp-PFS and (b) pp-Zonyl™ polymer films deposited at a system pressure of 80 Pa, RF power of (1) 100 and (2) 400 W.

mean diameters and greater uniformity compared to that of particles formed under a low RF power. FESEM images of the pp-PFS and pp-Zonyl<sup>TM</sup> films deposited under RF power of 100 and 400 W are shown in Figures 3.1(a) and (b), respectively. Table 3.2 shows that when the system pressure is kept constant at 80 Pa and the RF power is increased from 100 to 400 W for pp-PFS films, the mean particles diameter in the pp-PFS films decreased from 248 to 218 nm (shown in Figures 3.1 (a<sub>1</sub>) and (a<sub>2</sub>), respectively). As for pp-Zonyl<sup>TM</sup> films, the mean particles diameter in the films decreased from 37 to 25 nm (shown in Figures 3.1(b<sub>1</sub>) and (b<sub>2</sub>), respectively), while SD decreased from 11 to 3 nm. Thus, the results from both fluoropolymers suggest that the particle size depends on the plasma polymerization energy of unit monomer molecules. Increasing the RF power can reduce the mean diameter and size distribution of the particles. High RF power applied during plasma polymerization is favorable in fabricating fluoropolmer films of nanospheres. For plasma polymerization of the same monomer, the particle size is determined by the plasma energy. For the plasma polymerization of different monomers, the particle size depends on the monomer type and its boiling point when other parameters (e.g., the input RF power, system pressure, feeding gas flow-rate, glow discharge time, etc) are kept constant. PFS has lower boiling point compared to Zonyl<sup>TM</sup>. There is a high concentration of monomer in the chamber for PFS due to its higher evaporation rate at the same temperature and ambient pressure, resulting in low energy per unit monomer molecule. Hence in this energy deficient region for the polymerization, the polymer-forming process was predominant and the polymer deposition rate increased with the increase of RF power, which yielded a rougher deposited film. The FESEM images match the experimental data of the two polymerized monomers in Table 3.2.



**2) Effect of System Pressure**

The data in Table 3.2 also show the dependence of particle size and size distribution on the system pressure. For the plasma polymerization and deposition of pp-PFH and pp-HFB under a constant RF power of 400 W, as the system pressure increases from 27 to 107 Pa, the data show that there is a reduction of particle size in the deposited pp-PFH films from 55 to 20 nm, with the SD also decrease from 19 to 2 while roughness  $R_a$  is roughly same. In the deposited pp-HFB films, there is a decrease in particle size from 160 to 80 nm, with the SD and  $R_a$  decrease from 30 to 4, 3 to 2 nm, respectively.

The AFM images depicted in Figure 3.2 show similar variation as the data in Table 3.2 for the deposited pp-PFH and pp-HFB films under varying system pressure. At a low pressure of 27 Pa, larger particles of irregular shapes and sizes are produced due to the increased collision and aggregation of nucleation sites. However, at a higher pressure of 107 Pa, the particles formed are spherical and well defined. It is because an increase in the system pressure will reduce the relative concentration of the fluoromonomer in the Ar carrier gas. Subsequently, there is a lower collision frequency between the activated species generated in the glow discharge chamber, which results in the formation of smaller particles with a smaller size distribution. In terms of monomer flow, the vaporization rate of the monomer at lower system pressure is greater than that at higher system pressure. Thus, comparing the pressure of 27 Pa to those of 80 and 107 Pa, there is a higher concentration of monomer in the carrier gas and reaction chamber, which leads to a lower plasma energy per unit monomer. In plasma polymerization,

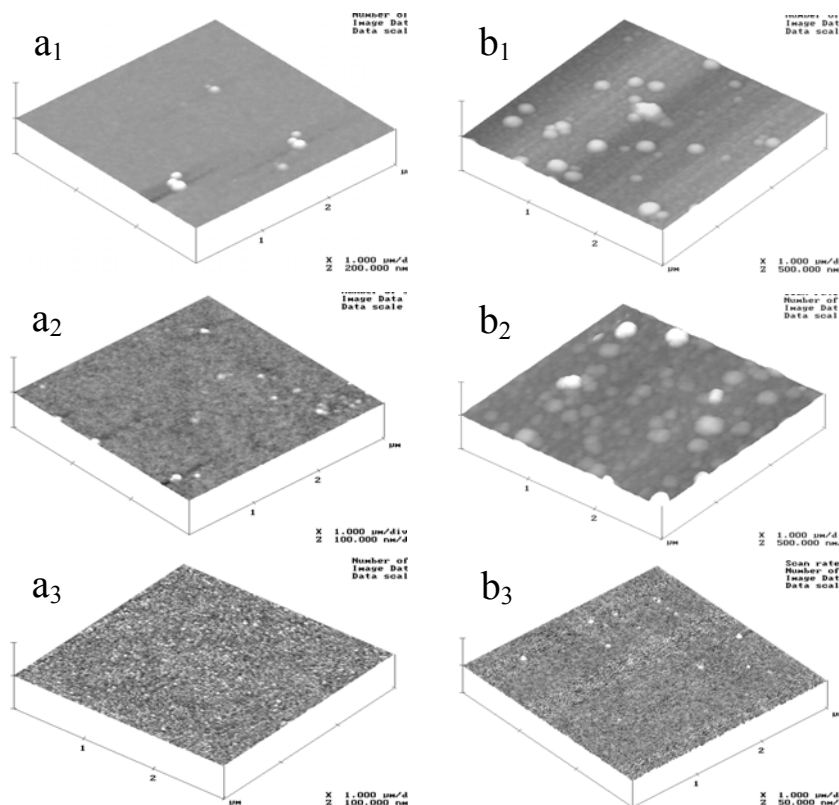


**Figure 3.2** AFM images of (a) pp-PFH and (b) pp-HFB films deposited at RF power of 400 W and different pressures of (1) 27, (2) 80, and (3) 107 Pa.

lower energy results in lower concentration of activated sites, which in turn causes the formation of larger particle size.

### 3) Effect of Monomer Temperature

Figures 3.3(a) and (b) show the AFM images of pp-Zonyl™ films obtained at monomer temperatures of 25 and 60°C, respectively, while maintaining the system pressure at 13 Pa and the RF power at 50 W. The temperature of the inlet monomer was varied using a water bath to warm the monomer bottle for at least 15 min with different temperatures. At  $25 \pm 2^\circ\text{C}$ , the mean diameter of the particles was about 55 nm while the SD was 10 nm.

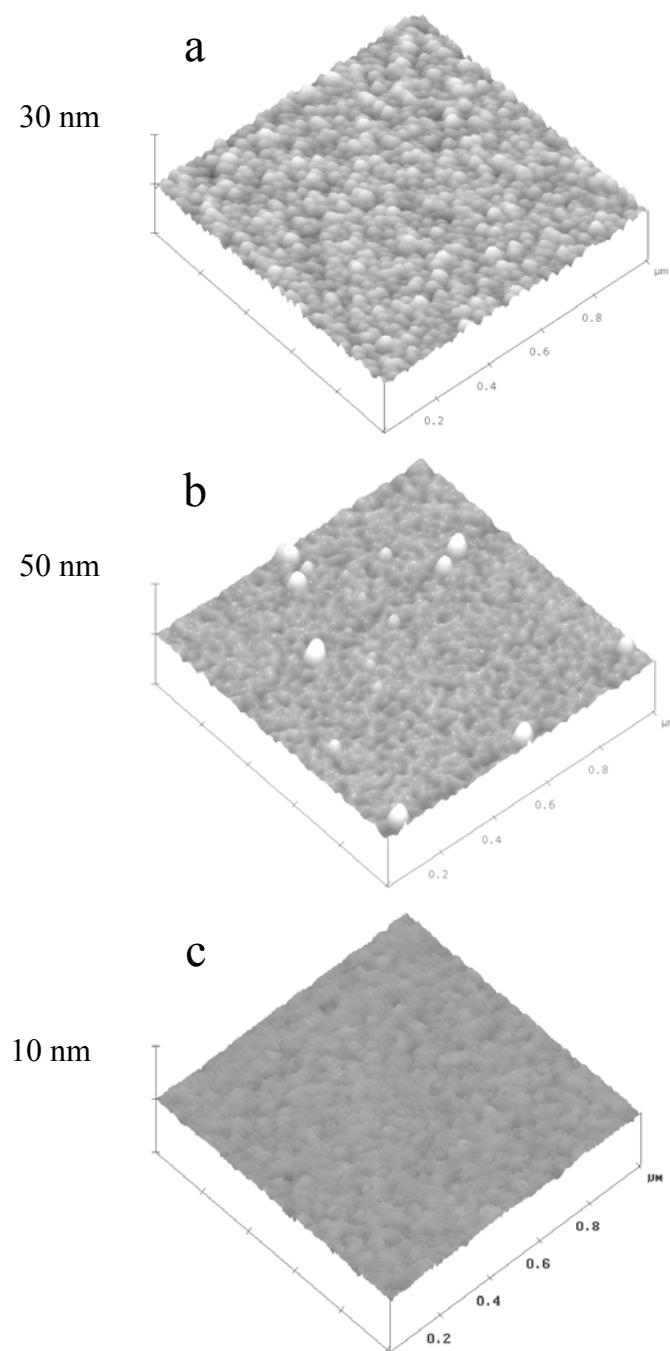


**Figure 3.3** AFM image of pp-Zonyl<sup>TM</sup> film obtained at monomer temperature of (a) 25 or (b) 60°C on Si substrate with room temperature, or (c) 25°C on Si substrate with high temperature of 78°C, under a RF power of 400 W and system pressure of 13 Pa.

At  $60 \pm 3^\circ\text{C}$ , the mean diameter and SD were increased to 96 and 11 nm, respectively. Increasing the monomer temperature showed similar effects as that of lowering the system pressure. More investigations on different temperatures showed similar results. It is because that higher temperature leads to higher evaporation rate of the monomer, and subsequently results in higher monomer concentration and lower plasma energy in the reaction chamber. Thus, for the high monomer temperature of  $60^\circ\text{C}$ , the particles formed are highly mono-dispersed and bigger than these at  $25^\circ\text{C}$ .

#### **4) Effect of Substrate Temperature**

Further experimental results revealed that for plasma polymerization and deposition of thin nanostructured fluoropolymer nanofilms on a substrate with high temperature of more than  $70^\circ\text{C}$ , the deposited species have greater surface mobility and diffusion length, which cannot lead to fluoropolymer films with nanospheres. For instance, the FESEM image of Figure 3.3(c) depicts pp-Zonyl<sup>TM</sup> film (without nanospheres containing) prepared on a Si substrate with  $78^\circ\text{C}$ . The used substrate and parameters of plasma polymerization was same as that of nanosphere film shown in Figure 3.3(a).

#### **3.3.2 Deposition Rate of the Plasma Polymerized Films**

For the plasma polymerization of three unsaturated monomers (HFB, PFS, and Zonyl<sup>TM</sup>), the data in Table 3.2 show that the size of nanospheres in the pp-PFS films is the largest. It is approximately 5 times larger than those particles in pp-Zonyl<sup>TM</sup> films. Hence, the deposition rate for PFS is the highest (about  $3.3 \mu\text{m}/\text{min}$ ), followed by HFB ( $\sim 3.0 \mu\text{m}/\text{min}$ ), and the lowest is Zonyl<sup>TM</sup> ( $\sim 1.5 \text{ nm}/\text{min}$ ). The difference in chemical structure of the monomers determines the different deposition rates for the polymers. PFS is the

monomer with the highest degree of unsaturation. It contains the unsaturated C=C moiety and big aromatic ring. HFB possesses one big aromatic ring while Zonyl<sup>TM</sup> shows one unsaturation C=C moiety. During plasma polymerization, unsaturated C=C groups are more easily broken than saturated C-C groups and unsaturated aromatic ring by the plasma energy, hence comparing with HFB and Zonyl<sup>TM</sup> monomers, PFS monomer (possessing both unsaturation C=C moiety and big aromatic ring) has the highest deposition rate in comparison to pp-HFB and pp-Zonyl<sup>TM</sup> polymers.

Even though the deposition rate is usually lower for a saturated monomer when compared to unsaturated monomers, PFH possesses a linear saturated structure and the deposition rate of pp-PFH film is greater than that of pp-Zonyl<sup>TM</sup> film. It is because the PFH monomer has a lower boiling point (82 – 84°C, depicted in Table 3.1) than that of Zonyl<sup>TM</sup> (210 – 350°C), thus PFH has a higher evaporation rate than Zonyl<sup>TM</sup> under same system pressure. In addition, when plasma polymerization is carried out at the same power and flow-rate, the composite parameter (W/FM) ratio changes inversely with the M (molecular weight) of the monomer used [Inagaki, 1996; Yasuda, 2003]. The average M of PFH and Zonyl<sup>TM</sup> is 388 and 534, respectively. Thus, the higher deposition rate of pp-PFH film compared to pp-Zonyl<sup>TM</sup> film can also be attributed to its high W/FM value, which means a higher concentration of activated species is generated from PFH monomer in the plasma polymerization.

### 3.3.3 Chemical Structures of the Plasma Polymerized Fluoropolymer Films

The FTIR spectra for pp-PFS and pp-Zonyl<sup>TM</sup> films are shown in Figures 3.4(a) and 3.4(b), respectively. Due to the difference in bond scission mechanism at different power

[Inagaki, 1996; Dai, 1997], the input power has a marked effect on the chemical structure of the plasma-polymerized films. When a C=C bond is present in the monomer, only a low RF power is required to make the C=C bond open. From the plasma polymerization at low RF power, a deposition of homopolymer film is created and the polymer molecules have similar structures as that of the monomer [Fonash, 1999]. But high RF powers always bring about more severe scissions and opening of the C=C bond as well as the scissions of other C-C or C-O and C-F bonds for the monomer molecules [Inagaki, 1996], which results in polymers of quite different molecular structures in comparison to the monomer molecules. Therefore, even using the same monomer, different input powers result in different chemical structures of the deposited polymers.

The FTIR spectra of pp-PFS films (shown in Figure 3.4(a)) display a progressive decrease in the absorption bands at 1525, 1500, and 980  $\text{cm}^{-1}$  as the RF power employed is increased during deposition. The bands at 1525 and 1500  $\text{cm}^{-1}$  correspond to the vibration of fluorinated ring, while the band at 980  $\text{cm}^{-1}$  arises from C-F (aromatic) stretching frequency [Yasuda, 1984; Zhang et al., 2000; Fu et al, 2003]. The spectra indicate that with the increasing discharge power, a reduction in the amount of fluorinated aromatic ring in the polymeric film occurred. It is due to some scissions of C-F bonds on the aromatic rings or the opening of a few aromatic rings.

The FTIR spectra of pp-Zonyl<sup>TM</sup> (Figure 3.4(b)) show an increase in the absorption intensity at band of 1110 and 613  $\text{cm}^{-1}$  with the increasing of RF power used for the plasma polymerization. It indicates more vibration of aliphatic monofluorinated groups after some C-F deformation. The absence of the characteristic absorption bands of C=C at

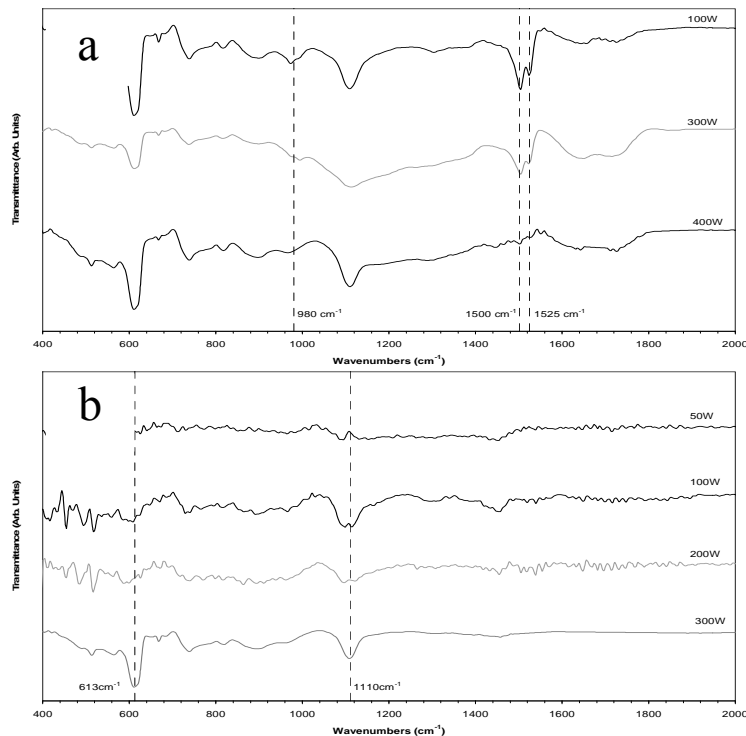


**Figure 3.4** FTIR reflectance spectra of (a) pp-PFS and (b) pp-Zonyl<sup>TM</sup> films deposited at 80 Pa. The RF powers for pp-PFS are 100, 300, and 400 W while for pp-Zonyl<sup>TM</sup> 50, 100, 200, and 400 W.

1680  $\text{cm}^{-1}$  suggests that opening of C=C bonds occur readily as it has lower bond energy in comparison to C-C.

### 3.3.4 Hydrophobic Nature of the Plasma Polymerized Fluoropolymer Films

For hydrophobicity, Cassie and Baxter derived an equation for relating surface roughness to the water contact angle of a sessile drop (in equilibrium to the surface) [Choi et al., 2009]. The Cassie–Baxter equation to Wenzel transition is:

$$\cos \theta = (\varphi - 1)/(r - \varphi) \quad (3.1)$$

where  $\theta$  is the critical contact angle of a liquid on a solid surface,  $\varphi$  is the fraction of solid/liquid interface where drop is in contact with surface, and  $r$  is the solid roughness

(for a completely flat surface,  $r = 1$ ) [Inagaki, 1996; Zhang et al., 2002]. The surface wettability is proportional to the cosine of the contact angle. Contact angles from  $0^\circ$  to  $90^\circ$  indicate spontaneous wetting of the surface, while those from  $90^\circ$  to  $180^\circ$  indicate non-wetting. As such, higher water contact angles imply greater hydrophobicity of the polymers. It refers to the polymer possessing the best anti-humidity property when using as coating layers for microelectronics devices. The hydrophobicity of the surface can be enhanced by increasing the surface roughness of the deposited film.

The water contact angles of the 4 fluoropolymer films obtained under different RF powers are summarized in Table 3.3. Since most water contact angles of the polymers are nearly about or bigger than 90 degree, it indicates that the surfaces of 4 fluoropolymers (especially from the plasma polymerization of PFH and PFS) display a high degree of hydrophobicity. Comparing the data in Table 3.2 and 3.3, it appears that water contact angles did not increase proportionally with the increase in the surface roughness of the pp-PFH films. It is because the surface roughness of the polymer film is not the only factor that governs the water contact angle. The surface composition and surface energy also determine the hydrophobicity, although these two factors are not studied in greater detail in this experiment. Previous studies show that when a high RF power is applied, the deposited film has a higher surface energy than the film deposited from a low RF power [Nguyen et al., 1999; Han et al., 2000; Fu et al., 2004]. In addition, the water contact angle is larger with higher [F]/[C] ratio in the polymers [Shi, 1996]. Since the extent of defluorination is higher at higher RF power due to the scission of C-F bonds [Fu et al., 2004], there is a decrease in water contact angle for the as-polymerized film.



**Table 3.3** Water contact angles for the 4 fluoropolymer surfaces

Deposition Parameters		pp-PFH	pp-HFB	pp-PFS	pp-Zonyl™
Pressure (Pa)	Power (W)	$\theta^*$ (deg)	$\theta$ (deg)	$\theta$ (deg)	$\theta$ (deg)
13	100	70	-	-	58
	400	165	100	160	101
27	100	152	-	-	75
	400	146	102	156	99
80	100	139	112	136	78
	400	123	94	109	97
107	100	116	-	-	86
	400	105	66	99	96

\*  $\theta$  (water contact angle) is the average of  $\theta_A$  (advancing contact angle) and  $\theta_R$  (receding contact angle).

Therefore, by considering different effects of the affecting factors, higher water contact angle or hydrophobic property of the as-synthesized fluoropolymer films can only be achieved by optimizing the RF power and other polymerization parameters for fluoromonomers with different molecular structures.

### 3.3.5 Potential Applications of the Plasma Polymerized Fluoropolymer Films

The hydrophobic nature of the as-synthesized fluoropolymer films makes them suitable to be used as barriers and passivation layers for bio-medical and other technological devices. In addition, fluoropolymers reduce moisture absorption due to the non-polar character of fluorocarbon groups, which reduces their  $\kappa$  value. Thus, these fluoropolymers can potentially be used as low dielectric constant materials.

### 3.4 Conclusions

In summary, fluoropolymers are prepared from the plasma polymerizations of hexafluorobenzene, pentafluorostyrene, perfluoroheptane, and Zonyl<sup>TM</sup> fluoromonomers. By changing the parameters of the polymerization, different physicochemical properties and deposition rates for the as-synthesized polymers can be achieved. These as-prepared fluoropolymers can potentially be used in current microelectronic devices as interlayer or surface coating since most of them have highly hydrophobic property as well as possible low dielectric constant.

**CHAPTER 4**

**POROUS FLUOROPOLYMER NANOSPHERES AND THIN  
FILM PREPARED VIA PLASMA POLYMERIZATION**

**4.1 Introduction**

Porous nanospheres play an important role in the present-day technologies [Tsapis et al., 1997; Singer, 1999; El-Zahab et al., 2004]. They are being used on living beings as effective transportation tools for bio-medicines and enzymes. First of all, porous fine nanospheres are small enough to be introduced into human body to enable controlled release of drugs. Secondly, as a delivery tool of bio-medicine or enzyme, the surface area per unit weight of porous nanospheres is much larger than that of bulk spheres. Hence in comparison to bulk particles, porous particles make bio-medicines and enzymes more effective or active [Van Roon et al., 2005]. Nanoporous nanoparticles are also superior fillers used in encapsulates for weapons [Borini et al., 2003].

Nowadays, only inorganic porous nanoparticles are commercially available and used in bio-sensors, photo-catalytic reactors, unique molecular sieves, and other advanced technologies [Lau et al., 2003; Che et al., 2004; Zhang et al., 2005]. Although organic porous nanospheres are different from inorganic particles in terms of their chemical properties, they have the potential to be used in current and future technologies due to their special characteristics. For instance, fluoropolymer nanospheres have low dielectric constant since fluoropolymer materials possess the lowest  $\kappa$  in all bulk materials. Porous fluoropolymer nanospheres prepared via plasma polymerization always exhibit excellent physicochemical properties, such as low dissipation factor, large hydrophobicity, and good chemical and thermal stability [Liu, et al., 2003]. These advantages of porous fluoropolymer nanospheres indicate their great potential to be used in nano-/micro-scale electronic or biomedical devices. However, currently porous organic nanospheres are

only being developed due to the difficulty in synthesis via conventional polymerization techniques. Accordingly, there is a pressing need to develop porous polymer nanospheres.

In this chapter, a novel approach to the preparation of optically transparent nanoporous fluoropolymer nanospheres via carefully controlled plasma polymerization is described. The synthesized porous nanospheres have a series of diameters, which can be down to ~18 nm with a pore size of 2-6 nm. They are configured by uniform fine nanoparticles, which size is decreased with the increase of system pressure during the plasma polymerization and the minimum size could be down to ~9 nm (related to the system pressure of 13 Pa). The size of the porous nanosphere can be increased with longer plasma-glow-discharge time or lower system pressure. With these porous nanospheres, ultra-thin porous nanosphere films with a thickness ranging from 20 to 100 nm are also prepared. The highly porous films possessed a very low  $\kappa$  value of down to 1.7.

## 4.2 Experimental Section

### 4.2.1 Materials

3,3,4,4,5,5,6,6,7,7,8,8,9,9,10,10,10-Heptafluorodecyl acrylate monomer (97%,  $\text{H}_2\text{C}=\text{CHCOOCH}_2(\text{CF}_2)_7\text{CF}_3$  or HDFA, Sigma-Aldrich Company, St. Louis, MO) was used for the plasma polymerization. The polymerized HDFA polymers (pp-HDFA) were deposited on clean Si wafers or Cu plates.

### 4.2.2 Plasma Polymerization and Characterization of pp-HDFA Polymers

The procedures of plasma polymerization and characterization of pp-HDFA polymers are similar to those described in Section 3.2.2 and 3.2.3. The pore size of pp-HDFA nanospheres was determined from high resolution FESEM (JSM 7401 F or JEOL 6320, JEOL Asia, Japan) images obtained at accelerating voltage of 1 - 10 kV and a pressure of  $\leq 2.8 \times 10^{-4}$  Pa were used. The chemical composition of porous pp-HDFA polymers was analyzed by time-of-flight secondary ion mass spectrometry (ToF-SIMS) and X-ray photoelectron spectroscopy (XPS). The ToF-SIMS measurements were carried on an ION-ToF spectrometer (ION-ToF, GmbH, Münster, Germany). The primary ion beam (10 keV  $\text{Ar}^+$ ) with a spot size of  $\sim 50 \mu\text{m}$  was rastered over an area of  $500 \times 500 \mu\text{m}^2$  while keeping the total dose under  $10^{13}$  ions/ $\text{cm}^2$ . The water contact angles were measured at 25°C and 50% relative humidity on a telescopic goniometer (Rame-Hart, model 100-00 (230), Mountain Lake, NJ). The telescope with a magnification of 23 $\times$  was equipped with a protractor of 1° graduation. The measurement of resist adhesion was carried out on an Instron 5544 Uniaxial Tension System (High Wycombe, U. K). The measurement speed was 10 mm  $\text{min}^{-1}$ . The dielectric constants of pp-HDFA films deposited on copper substrates under similar glow discharge conditions as those on Si

wafers were measured on a RF impedance/capacitance materials analyzer (Hewlett Packard model 4291B) at a frequency of 1 MHz. As shown in following equation, the dielectric constant  $\kappa$  was derived from the measured film capacitance ( $C$ ) between 2 conductive parallel copper plates, which have an area of  $A$  with a gap of  $d$ .

$$C = \kappa \epsilon_0 A / d \quad (4.1)$$

where  $\epsilon_0$  is the permittivity of vacuum ( $8.85 \times 10^{-12}$  F/m). A low- $\kappa$  dielectric has a low permittivity, or low ability to polarize and hold charge. Hence it is a very good insulator for isolating signal-carrying conductors from each other and a necessity in very dense multi-layered IC chips, wherein coupling between very close metal lines need to be suppressed to prevent degradation in device performance.

### 4.3 Results and Discussion

#### 4.3.1 Synthesis of Porous Nanospheres

Porous pp-HDFA nanospheres were prepared via high energy plasma polymerization. From a geometrical perspective, small uniform nanoparticles allow the configuration of larger porous nanospheres or films as there are interstitial spaces among the agglomerated small particles. The configuration scheme is illustrated in Figure 4.1. For the fabrication of porous nanospheres or highly porous films, there are two challenges: (i) the requirement to synthesize fine organic nanoparticles of uniform sizes, and (ii) the aggregation of small nanoparticles into large nanospheres. Although conventional chemical polymerization provides an easy way to prepare small organic nanoparticles, it is difficult to synthesize porous nanospheres via the agglomeration of smaller porous nanoparticles. Hence plasma polymerization was used to achieve this goal. In plasma polymerization, the preparation of uniform small nanoparticles is the basis to achieve porous nanospheres and highly porous films.

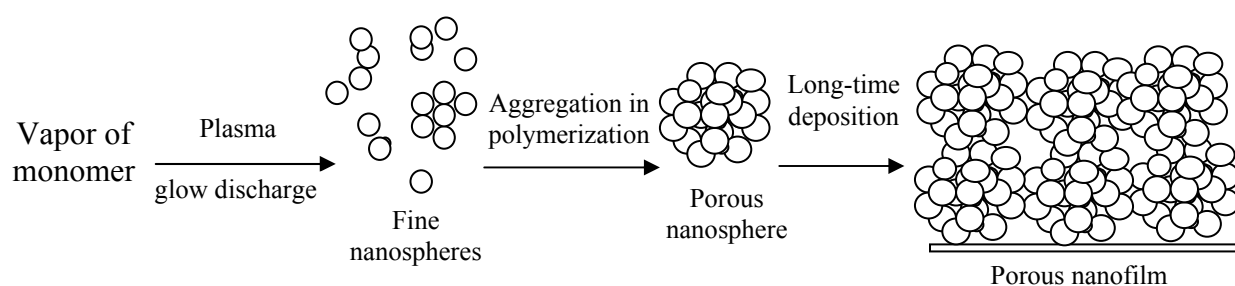


**Figure 4.1** Scheme for the fabrication of porous polymer nanospheres and film via plasma polymerization and deposition.



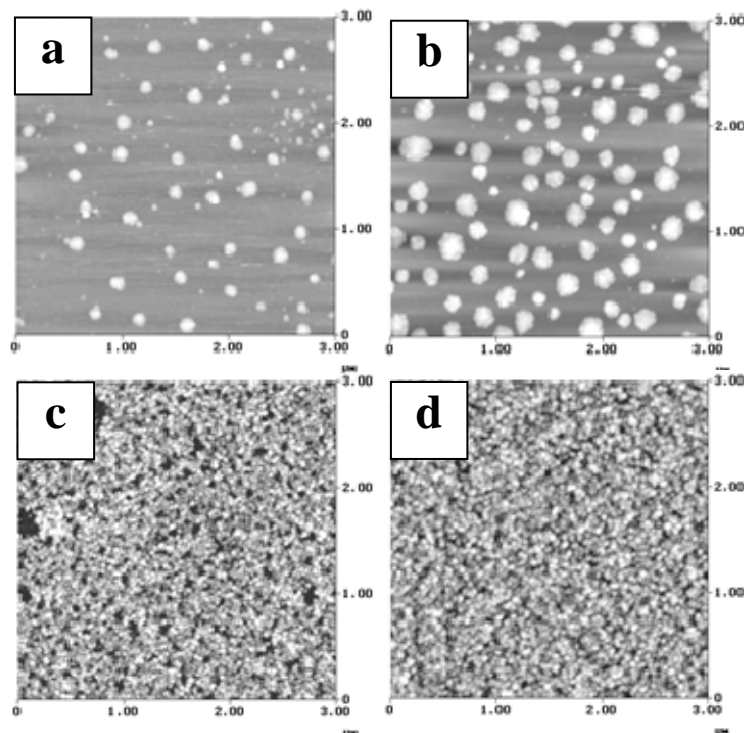


**Figure 4.2**  $3 \times 3 \mu\text{m}$  2D AFM images of pp-HDFA nanospheres deposited at a system pressure of 7 Pa with various glow discharge duration: (a) 3, (b) 10, (c) 20, and (d) 30 s.

The synthesis of nanoporous fluoropolymer nanospheres was based on the finding that for high energy plasma polymerization (e.g., high input RF power of 500 W), the particle size and the size distribution of the fluoropolymer nanoparticles were highly dependent on the glow discharge duration in a specific manner: with the glow discharge duration increasing from a few seconds to several tens of seconds, there was always a large and quick decrease in particle size, which was from the maximum to minimum size, at the low system pressures of  $\leq 13$  Pa. Beyond this atomization period, the generated fine particles became uniform in size distribution and they began to agglomerate into larger porous nanospheres with further increase in the glow discharge duration. The rate of increase in nanosphere size was low. For example, Figure 4.2(a-d) shows the surface

morphologies of fluoropolymer nanospheres generated under RF power of 500 W and a system pressure of 7 Pa at a series of glow discharge durations of 3, 10, 20, and 30 s, respectively. During the initial stage of particle formation ( $\leq 10$  s), the generated particles increased from 88 nm (for 3 s) to 178 nm (for 10 s) in average diameter at a fast growth rate of about 13 nm/s, while the particle SD increased from 24 to 70 nm. The particle distribution was not uniform and the density was low, as shown in Figure 4.2(a) and 4.2(b). The particles formed in the initial stage were generally round with pronounced rough surfaces.

After the initial stage, further growth of the particles under longer glow discharge duration was inhibited due to high energy per unit monomer molecules. Inversely, the largest particles were broken into the finest uniform nanoparticles when the glow discharge duration was increased to 20 s. As a result, there was a large increase in particle density. Figures 4.2(b) and 4.2(c) show the change that with the glow discharge duration increasing from 10 to 20 s, the size of the nanoparticles decreased drastically from 178 to 18 nm in average diameter while the SD of the particle size decreased from 70 to 3 nm. Further investigations showed that the initial atomization time for the largest particles and the size of the finest particles atomized were related to the system pressure. Higher pressure led to delayed atomization of large particles and smaller atomized nanoparticles. For example, the atomization period happened during the glow-discharging time from 20 to 30 s at 13 Pa, leading to the finest particle sizes of  $\sim 9$  nm, which is shown in Figure 4.3 (c) and 4.3(d). The smaller fine particles from 13 Pa as compared to those from 7 Pa at the same power is because higher system pressure always leads to smaller particles [Fu et al., 2003].

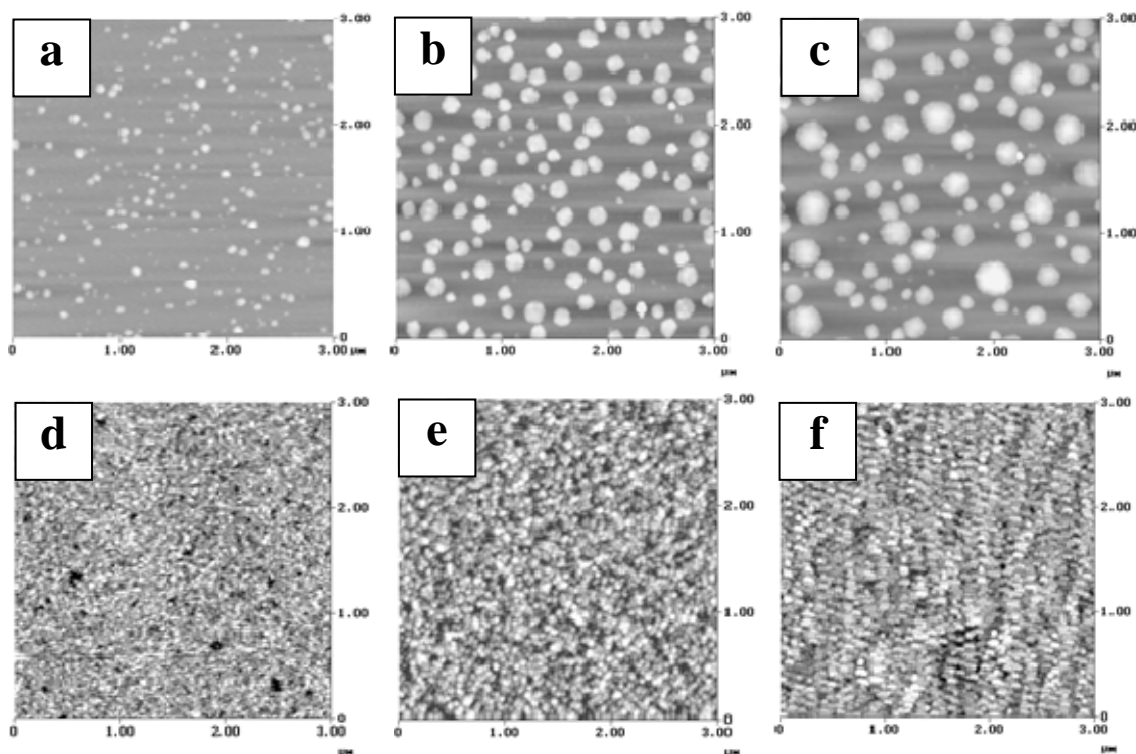


**Figure 4.3**  $3 \times 3 \mu\text{m}$  2D AFM images of pp-HDFA nanoparticles polymerized at a system pressure of 13 Pa with various glow discharge duration. (a)-(f) stands for 3, 10, 20, 30, 60, and 120 s, respectively.

When the glow discharge duration was further lengthened after the atomization period under the same system pressure of 7 Pa, the particle size increased again. However, the growth rate of the sphere size decreased to 1.3 nm/s. This value was much lower than that of the initial stage (13 nm/s). The rate of increase in the SD of particle size was only 0.3 nm/s. In this range of glow discharge, the polymerization process appeared to be homogeneous and more well-defined sphere size distributions were obtained. Thus, uniform pp-HDFA nanospheres of increasing size were synthesized with the increasing glow discharge duration. Figure 4.2(d) shows the 2D AFM image of uniform

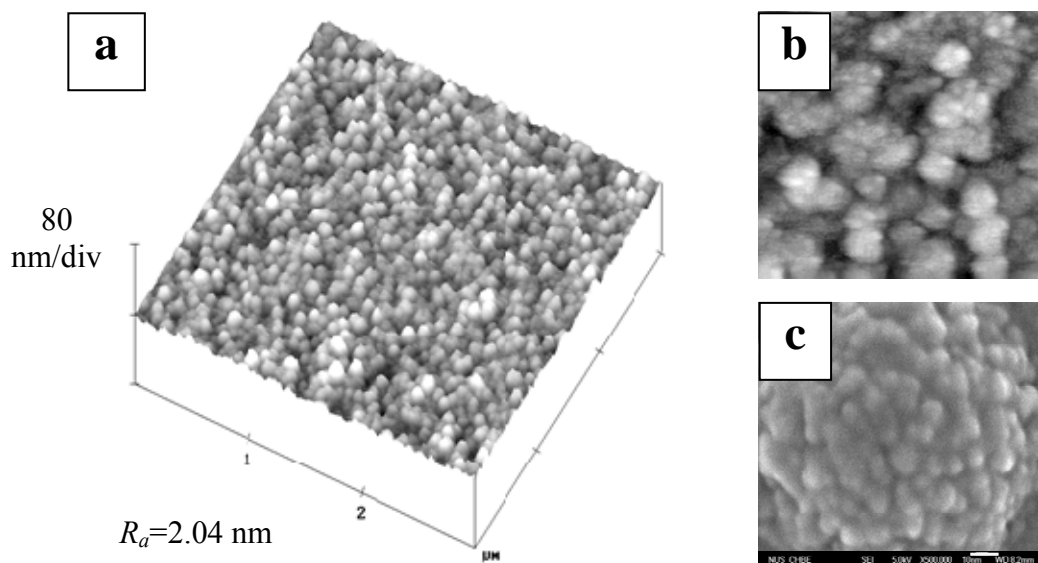


**Figure 4.4** pp-HDFA nanospheres polymerized under RF power of 500 W at a system pressure of 7 Pa by plasma-glow discharge of 55 s. (a)  $3 \times 3 \mu\text{m}$  AFM 3D image and (b)  $0.5 \times 0.5 \mu\text{m}$  2D AFM topographical image. (c) FESEM image (scale bar: 10 nm) of one big nanosphere in (b).

fluoropolymer nanospheres ( $\sim 30$  nm) deposited with a glow discharge duration of 30 s. The high resolution FESEM image showed that these nanospheres were porous in nature. All test results at different system pressures ( $\leq 13$  Pa) under high energy polymerization (RF power = 500 W) showed that except for the initial stage of polymerization, the trends of changes in particle sizes and their distributions against the discharge duration were different from the low energy polymerization (RF < 100 W) of pyrrole and silane monomers, which were reported by two other groups [Boufendi et. al., 1992; Hosono et. al., 2004]. The reasons are given below.

The 3-dimensional AFM image in Figure 4.4(a) shows that nanospheres of  $\sim 80$  nm in average size were prepared at glow discharge duration of 60 s and the system pressure of 7 Pa. The  $0.5 \times 0.5 \mu\text{m}$  2D AFM image in Figure 4.4(b) (from the focused image in

Figure 4.4(a)) clearly shows that these spheres were aggregated with fine nanoparticles. When FESEM is used to enlarge one of big nanospheres (~100 nm) in Figure 4.4(b), the resulting image in Figure 4.4(c) shows that this nanosphere has an average pore size of ~5 nm, configured by the ~15 nm fine nanoparticles, which is similar to the fine particles of Figure 4.2(c).

Since the size of the atomized finest particles generated at high pressure is always smaller than that at low pressure, the agglomerated nanosphere size at high system pressure (such as 13 Pa) is also smaller than that at low system pressure (such as 7 Pa) with the same glow discharge duration after the atomization period. Thus, the smallest porous nanospheres of ~ 18 nm were prepared at 13 Pa with a glow discharge of 38 s at the same RF power of 500 W. Since different sizes of fine nanoparticles will configure different pore sizes, by applying different system pressure, different pore sizes of nanospheres were achieved. For example, the pore size generated in the nanospheres was about 2 - 5 nm at 13 Pa while 3 - 6 nm pores were obtained at 7 Pa (shown in Figure 4.4(c)).

### **4.3.2 Formation Mechanism of Porous pp-HDFA Nanospheres**

The chemical composition and structure of the pp-HDFA nanospheres were characterized by ToF-SIMS and XPS. HDFA monomer has the chemical formula of  $\text{H}_2\text{C}=\text{CHCOOCH}_2(\text{CF}_2)_7\text{CF}_3$  and a molecular weight of 504. For PP-HDFA nanospheres deposited under high RF power of 500 W, the assignment of positive ion fragments in the ToF-SIM spectrum is given in Table 4.1. Different energy and parameter used in plasma polymerization will lead to different concentrations of radical ions for the same monomer. In addition, different monomers have different chemical components and

**Table 4.1** Assignments of positive ions in the ToF-SIM spectra of the pp-HDFA nanospheres

m/z	Proposed structure	m/z	Proposed structure
27	$\text{H}_2\text{C}=\text{CH}^+$	83	$\text{CF}_3-\text{CH}_2^+$
29	$\text{H}_3\text{C}-\text{CH}_2^+$	85	$\text{CH}_3-(\text{CH}_2)_3-\text{CO}^+$
33	$\text{CH}_2\text{F}^+$	127	$\text{CF}_3-\text{CF}^+-\text{CH}=\text{CH}_2$
41	$\text{CH}_2=\text{CH}-\text{CH}_2^+$	177	$\text{CF}_3-\text{CF}_2-\text{CF}^+-\text{CH}=\text{CH}_2$
43	$\text{CH}_3-\text{CH}_2-\text{CH}_2^+$ , $\text{CH}_3-\text{CO}^+$	202	$\text{CF}_3-\text{CF}_2-\text{CH}^+-(\text{CH}_2)_3-\text{CH}=\text{CH}_2$
51	$\text{CHF}_2^+$	257	$\text{CF}_3-(\text{CF}_2)_4-\text{CH}_2-\text{CH}_2^+$
55	$\text{CH}_2=\text{CH}-\text{CH}_2-\text{CH}_2^+$	283	$\text{CF}_3-(\text{CF}_2)_4-\text{CH}_2^+$
57	$\text{CH}_3-(\text{CH}_2)_2-\text{CH}_2^+$ , $\text{CH}_3-\text{CH}_2-\text{CO}^+$	327	$\text{CF}_3-(\text{CF}_2)_4-\text{CF}^+-\text{CH}=\text{CH}_2$
69	$\text{CF}_3^+$	383	$\text{CF}_3-(\text{CF}_2)_6-\text{CH}_2^+$
71	$\text{CH}_3-(\text{CH}_2)_2-\text{CO}^+$	463	$\text{CH}_3-(\text{CH}_2)_7-(\text{CF}_2)_6-\text{CF}_2^+$
77	$\text{CH}_2=\text{CH}-\text{CF}_2^+$		

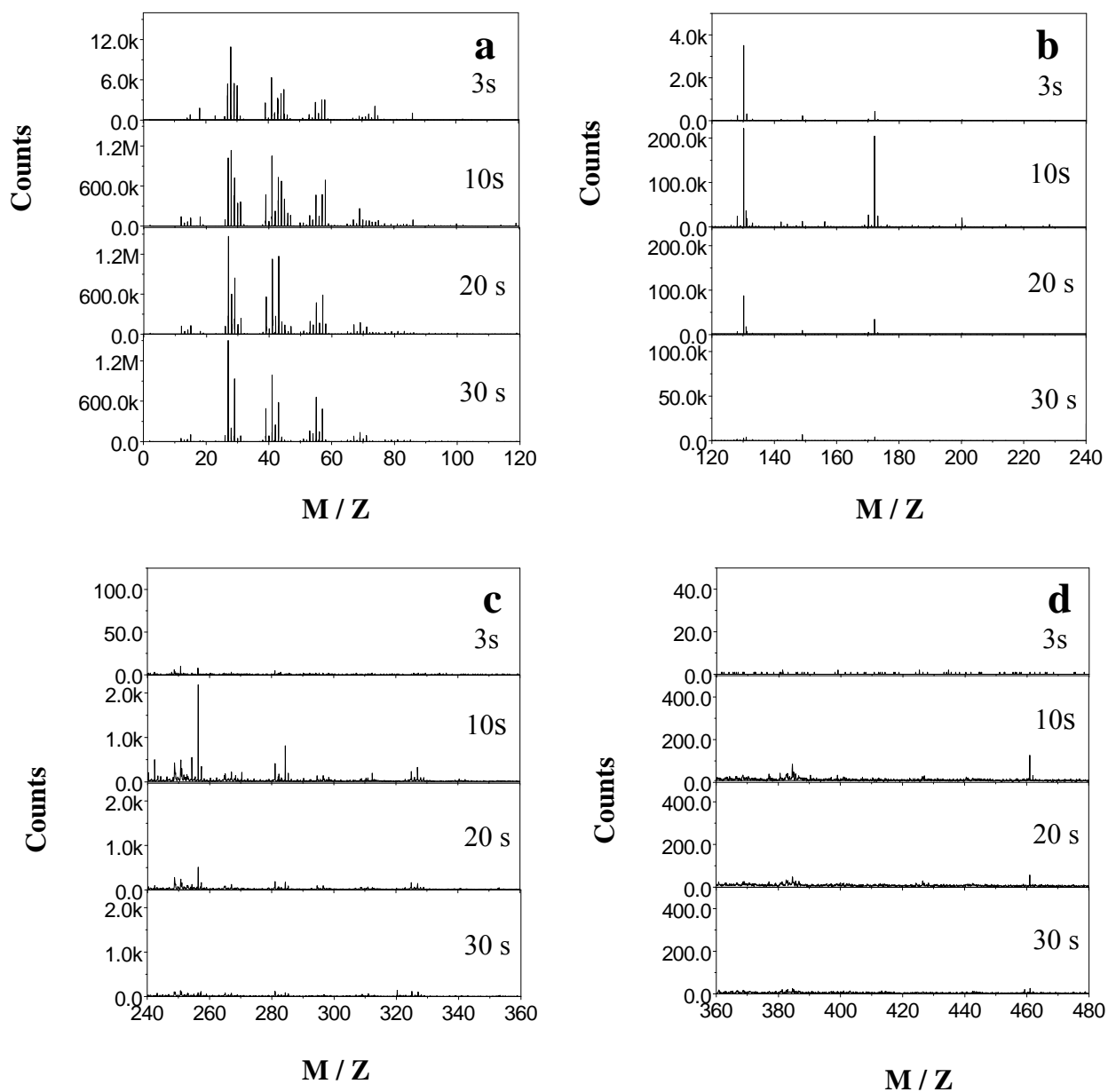
structures, which may lead to different ion fragments during polymerization. Thus, different monomers or same monomer at different energy polymerization may result in different morphologies of the as-polymerized polymers. That is why the changing trends of the particle size and the particle density with the glow discharge duration in the high energy of HDFA polymerization reported here are different from those from the reported low energy polymerization (RF < 100 W) of pyrrole and silane monomers.

Figure 4.5 shows ToF-SIMS spectra of the pp-HDFA nanospheres (shown in Figures 4.2(a-d)), which were prepared with the glow discharge duration of 3, 10, 20, and 30 s, respectively, at the system pressure of 7 Pa. The peak intensities of the fragments reveal that in the initial polymerization stage ( $\leq 10$  s), the large particles, which were polymerized at 3 and 10 s, contain more long chain molecules. After the atomization period, the structures of the fine pp-HDFA nanoparticles (Figure 4.2(c)) and nanoporous nanospheres (Figure 4.2(d)), which were generated at 20 and 30 s, respectively, comprised mainly short chain molecules under the plasma polymerization of longer glow discharge. Thus, these short chain molecules formed the uniform fine nanoparticles and porous nanospheres.

The changes in chemical composition of the pp-HDFA nanoparticles were also examined with XPS analysis, which showed that pp-HDFA fine nanoparticles (depicted in Figure 4.2(c)) and nanoporous nanospheres (as shown in Figure 4.2(d)) have similar chemical compositions: the ratio of C : F : O in both is about 50 : 45 : 5. From this point, the results of XPS and ToF-SIMS are consistent.

### **4.3.3 Synthesis of Ultra-Thin Porous Films with Different Thicknesses via Aggregation of Porous Nanospheres**

The synthesized porous pp-HDFA nanospheres are so small that they can be configured into ultra-thin porous films. It is known that in the fabrication of electronic nano-device or IC chip packaging, ultra-thin low  $\kappa$  films of various thicknesses are urgently needed [Sermon et al., 2001]. Since the sizes of porous nanospheres were found



**Figure 4.5** ToF-SIMS spectra of the pp-HDFA nanospheres deposited at a system pressure of 7 Pa with various glow discharge durations.

to increase with the glow discharge duration or decreasing system pressure after the atomization periods, by choosing appropriate plasma polymerization parameters and procedures, a series of ultra-thin pp-HDFA porous films (18 - 100 nm) with designed sphere sizes or pore sizes were fabricated from single- or multiple-rounds of pulse plasma



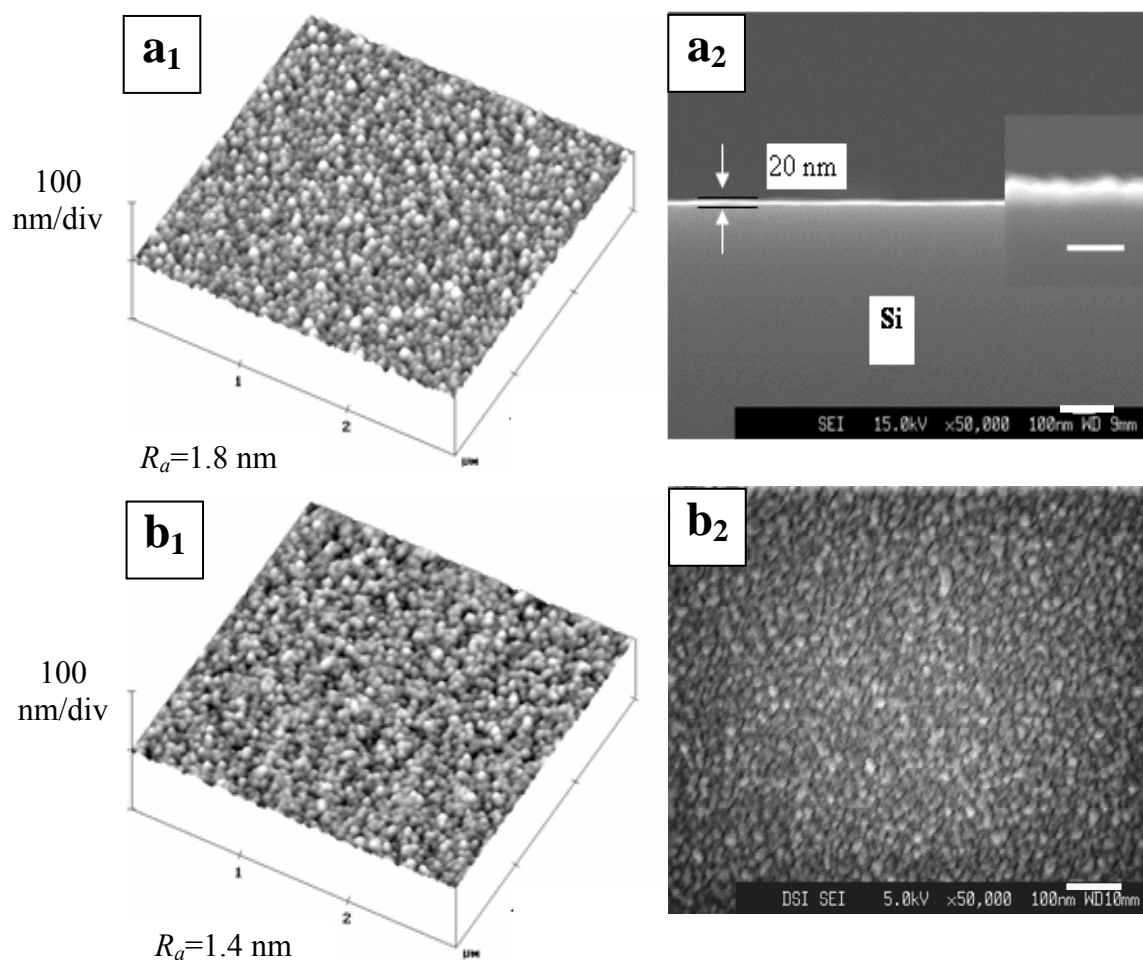


**Figure 4.6** (a<sub>1</sub>) and (b<sub>1</sub>) are  $3 \times 3 \mu\text{m}$  3D AFM images of porous pp-HDFA films polymerized under RF power of 500 W at a system pressure of 13 Pa by plasma-glow discharge of 38 s for one and four rounds, respectively. (a<sub>2</sub>) FESEM lateral view image of (a<sub>1</sub>) porous film on Si wafer. The inset is a high magnification FESEM image at a magnification of 250,000 $\times$  (scale bar = 30 nm). (b<sub>2</sub>) FESEM image of a porous pp-HDFA film via multiple depositions. The scale bar is 100 nm.

polymerizations and depositions. For example, a porous film of  $\sim 20$  nm was polymerized at a 13 Pa system pressure and glow discharge of 38 s in single deposition. Figure 4.6(a<sub>1</sub>) shows the 3D AFM image of the as-prepared porous film. Figure 4.6(a<sub>2</sub>) shows the cross-sectional view of the film, which indicates that the film has a thickness of about 20 nm with particle-like rough surface.

After 4 rounds of glow discharge deposition of 38 s, the thickness of the film increased to 35 nm. Figure 4.6(b<sub>1</sub>) shows the 3D AFM image of the film. The high resolution FESEM image in Figure 4.6(b<sub>2</sub>) shows the pores among the agglomerated porous nanospheres in this type of multi-deposited films can be down to ~10 nm in size. These pores are bigger than the pores in porous pp-HDFA nanospheres (2 – 6 nm). Both films from single and multiple depositions are optically transparent due to the thinness of the film and the intrinsic property of pp-HDFA polymer. The two AFM images of Figures 4.6(a<sub>1</sub>) and 4.6(b<sub>1</sub>) show that the particles and pores in both films are similar in sizes.

#### **4.3.4 Properties of Ultra-Thin Porous Films of Nanospheres**

After the synthesis, the highly porous pp-HDFA films of nanospheres were characterized to explore their potential applications. Table 4.2 shows the physical characteristics of the porous nanosphere films prepared at system pressures of 7 and 13 Pa and RF power of 500 W. The data show that for the plasma polymerization and deposition, the increase in film thickness, water contact-angle, adhesion strength, and pore size in the porous pp-HDFA nanosphere films is proportional to the glow discharge duration. The water contact angles of the films are all larger than 90°, which indicates that these films have excellent hydrophobic properties.

Highly porous polymers are potentially low  $\kappa$  materials due to the extensive built-in air gaps and pores. Air, similar as vacuum, has a lowest  $\kappa$  of about 1. The higher pore ratio in the polymer leads to a lower  $\kappa$  value. Due to the fact that in the ultra-thin nanosphere pp-HDFA films, the nanospheres are porous since they are from the aggregation of fine uniform nanoparticles. The nanospheres also entrap air gaps among them while forming

**Table 4.2** Physical properties of the transparent porous pp-HDFA films deposited via polymerization and deposition at input RF power of 500 W

System pressure (Pa)	7		13	
Glow discharge duration (s)	20	60	30	140
Film thickness* (nm)	20 ± 3	70 ± 5	12 ± 2	61 ± 4
Pore size in film (nm)	4 ± 2	22 ± 4	3 ± 1	18 ± 3
Surface roughness $R_a^*$ (nm)	1	3	1	2
Water contact-angle*				
Advancing $\theta_A$	95 ± 3°	102 ± 4°	93 ± 3°	100 ± 3°
Receding $\theta_R$	93 ± 2°	100 ± 3°	91 ± 2°	97 ± 3°
Adhesion* (N/cm)	1.1 ~ 1.2	1.3 ~ 1.5	1.3 ~ 1.4	1.5 ~ 1.7
Dielectric constant $\kappa^*$	1.9 ± 0.3	1.8 ± 0.2	2.2 ± 0.3	1.7 ± 0.2

\* The results are the average value of 4 samples.

the thin films. Furthermore, fluoropolymers have the lowest  $\kappa$  of all bulk materials. Therefore, the as-synthesized ultra-thin pp-HDFA fluoro-nanofilms are highly porous with possibly very low  $\kappa$  value. The measurement results (shown in Table 4.2) verified that they possess very low  $\kappa$  value of down to 1.7.

The data in Table 4.2 also show that the highly porous ultra-thin films prepared from both system pressures have good adhesions to Si substrates. Essentially, the nanostructured porous fluoropolymers produced by plasma polymerization usually provide additional

features which cannot be attained by conventional chemical polymerization, such as high corrosion resistance and other properties stated previously [Yasuda, 1990; Biederman,1992]. All properties of these porous pp-HDFA films show that the films have potential applications as low  $\kappa$  fillers, hosts for optically active compounds, electronic and in semiconductor packaging.

### 4.4 Conclusions

In summary, an interesting relationship between particle size and glow discharge duration during high energy of plasma polymerization for HDFA monomer was deduced. Based on this finding, by carefully assigning the system pressure and glow discharge duration, porous nanospheres agglomerated of uniform fine nanoparticles were synthesized. With these porous nanospheres, a series of ultra-thin ( $< 100$  nm) low  $\kappa$  nanoporous films were obtained. These ultra-thin low  $\kappa$  nanoporous films, which are readily deposited at room temperature and dry ambience, may be very suitable for the packaging of semiconductor and electronic nanodevices.

**CHAPTER 5**

**MAGNETIC MESOPOROUS FLUOROPOLYMER  
NANOSPHERES FROM PLASMA POLYMERIZATION AND  
SURFACE-INITIALIZING ADSORPTION OF MAGNETIC  
NANOPARTICLES**

**5.1 Introduction**

Small porous spheres have very large surface area per unit mass or volume. This characteristic allows them to achieve high surface loading when they act as absorbents, inhalers or target carriers [Fruchtel et al., 2001; Jia et al., 2003]. Hence, they play an important role in the transport of enzymes and biomolecules, delivery of drugs, synthesis of fine organics, and as supports for catalysts [Suresh et al., 1998; Ryan et al., 2000; Rana et al., 2000; Früchtel et al., 2001]. Most enzymes and biomolecules are known to be macromolecules with sizes ranging from several to tens of nanometers [Jia et al., 2003]. The mesopores, of dimensions ranging from 2 to 50 nm, are thus ideal for loading of these materials. They also permit the ingress of molecules and fine catalysts that are physically excluded from microporous materials [Ryan et al., 2000]. Thus, mesoporous nanospheres exhibit the largest area per unit mass in the packing of macromolecules and fine catalyst particles, compared to other porous particles with larger pore sizes. In comparison to porous inorganic spheres, polymer porous spheres are essential for some special cases because they are easier to be doped or immobilized with magnetic particles or components [Øye et al., 2003]. Hence small organic mesoporous spheres are potentially useful for a wide range of applications, which are not limited in the area for inorganic porous nanoparticles. However, current achievements in the fabrication of porous organic materials are still in macro-size scale. It is due, in part, to limitations in available fabrication methods for organic porous spheres [Hamada et al., 1996; Steen et al., 1999; Øye et al., 2003]. Accordingly, simple approaches for the syntheses of mesoporous organic nanospheres remain of great interest.

In this work, we present a simple and convenient way for the preparation of mesoporous fluoropolymer nanospheres and films via direct plasma polymerization and deposition of the fluoromonomer, 2,3,4,5,6-pentafluorostyrene (PTFS) in dry ambience. The AFM, FESEM, and TEM results showed that the prepared nanosphere size is around 300 nm, with a pore size of around 25 nm. The films from the plasma polymerized PTFS (pp-PTFS) nanospheres exhibited a very low dielectric constant and good hydrophobicity. Furthermore, the mesoporous nanospheres were successfully imparted with magnetic properties via surface-initiated adsorption and thermal-decomposition of pentacarbonyl iron ( $\text{Fe}(\text{CO})_5$ ).



## **5.2 Experimental Section**

### **5.2.1 Plasma Polymerization**

For the preparation of mesoporous pp-PTFS nanospheres and films, plasma polymerization was conducted at room temperature using the Plasma 80 Plus system. A high input RF power of  $\geq 400$  W was chosen to generate high energy plasma during the polymerization. Prior to each plasma polymerization, the plasma chamber was filled with the monomer for 30 s. The detail procedure of polymerization is illustrated in Section 3.2.2.

### **5.2.2 Production of Magnetic Mesoporous Nanospheres**

The as-synthesized pp-PTFS nanospheres on Si(100) wafers were immersed in an 1 : 1 (V/V) mixed solution of oleic acid and oleyl amine for 2 h for functionalization of surface with surfactants. Initially, the reaction mixture was put into an ultrasonic bath for 20 s to expel air out of the pores of the nanospheres and to wet the pore surfaces. The treated sample was dried under reduced pressure. Then the mesoporous pp-PTFS nanospheres with surfactant-functionalized surfaces on the Si substrate were immersed in liquid  $\text{Fe}(\text{CO})_5$  at room temperature for 10 min. During the initial 30 s, the reaction mixture was sonicated to allow  $\text{Fe}(\text{CO})_5$  to penetrate and adsorbed into the pores of the nanospheres. The sample was dried in air and subsequently heated at 200°C for 3 h in an oil bath to decompose the adsorbed  $\text{Fe}(\text{CO})_5$  into iron oxide.

After the treatment, the composite nanospheres were washed with a 5N aqueous HCl solution and water. Finally, the nanospheres were dried under reduced pressure. The synthesis route is shown schematically in Figure 5.1.

**5.2.3 Characterization of the pp-PTFS Polymers**

The characterization methods of the pp-PTFS polymers are similar to those stated in Sections 3.2.2 and 4.2.2. The chemical compositions of the mesoporous pp-PTFS polymers were analyzed by using XPS, ToF-SIMS, and energy dispersive X-ray (EDX, attached to the JEOL 6320 FESEM). Magnetic measurements of the mesoporous pp-PTFS nanospheres were carried out using a vibrating sample magnetometer (VSM, Lake Shore 735, Inc. Ohio, USA).

### **5.3 Results and Discussion**

#### **5.3.1 Synthesis of Mesoporous Nanospheres**

The films of mesoporous pp-PTFS nanospheres were deposited via plasma polymerization at high RF power. From the organic molecular structure and geometry perspectives, highly cross-linked polymer molecules are more likely to form uniform hollow nanoporous structures, in comparison to their linear chain counterparts. This is because linear chain molecules or radicals cannot self-assemble into ordered hollow pores in the absence of cross-linked groups to join them, whereas cross-linked molecules can lead to uniform porous polymers by means of conventional polymerization of organic agents, and almost all the reported porous polymer materials were prepared from the cross-linking polymerization [Liu et al., 1999; Lemieux et al., 2003].

However, plasma polymerization differs from conventional polymerization because in conventional polymerization, the chemical structures of the starting monomers are retained and the chemical composition of the resulting polymer can be predicted. In contrast to the conventional chemical polymerization, plasma polymerization is not restricted to a monomer with a double bond or an unsaturated bond. Unlike the polymer from conventional polymerization, plasma polymerized polymers do not contain regularly repeating molecular units, and are characterized by a three-dimensional structure rather than a one-dimensional chain structure [Han et al., 2000]. The initial molecular structure of the monomer is destroyed to some extent depending on the glow discharge energy during plasma polymerization. Thus, it is impossible to accurately predict the chemical structure of the resultant polymer from that of the initial monomer

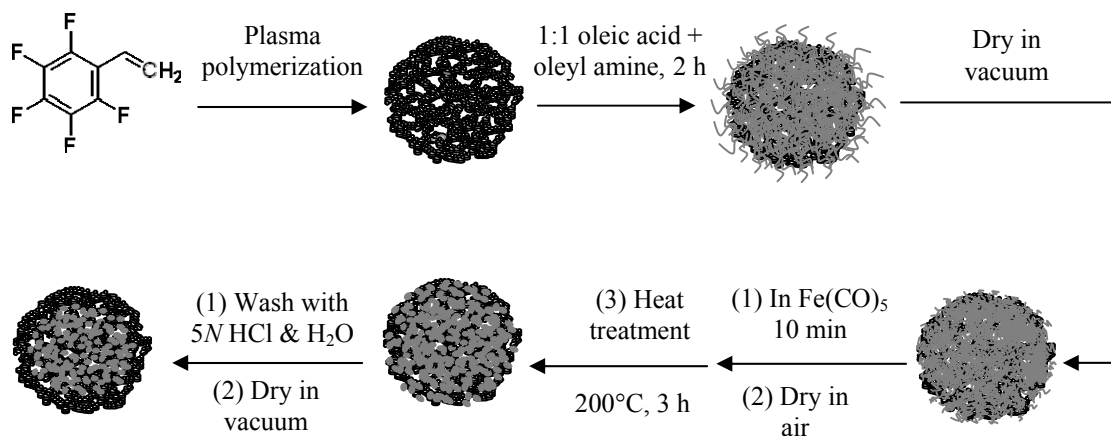


**Figure 5.1** Fabrication scheme of magnetic porous polymer nanospheres via plasma polymerization, surfactant-initiated surface adsorption, and thermal decomposition.

because of the cross-linking, rearrangement of the molecules, and only partial preservation of the chemical structures of monomer structures in the plasma polymerized polymer.

Even though the chemical structures of the polymers plasma-polymerized cannot be predictable, previous studies have shown that in plasma polymerization, low plasma glow discharge energy (corresponding to low power input) always results in solid films or big solid particles. Relatively linear chain segments with a high degree of the monomer structure were also retained in the resultant polymers [Calderon and Timmons, 1997; Han et al., 1998]. An example in this study is the polymerization at low RF power ( $\leq 200$  W), in which only pp-PTFS solid particles were produced. Figure 5.2(a) shows that the solid particles have a size of  $\sim 1.7$   $\mu\text{m}$  when PTFS was polymerized under a low RF power of 200 W with a system pressure of 27 Pa. The results are consistent with these from a previous study by Han's group [Han et al., 1998].

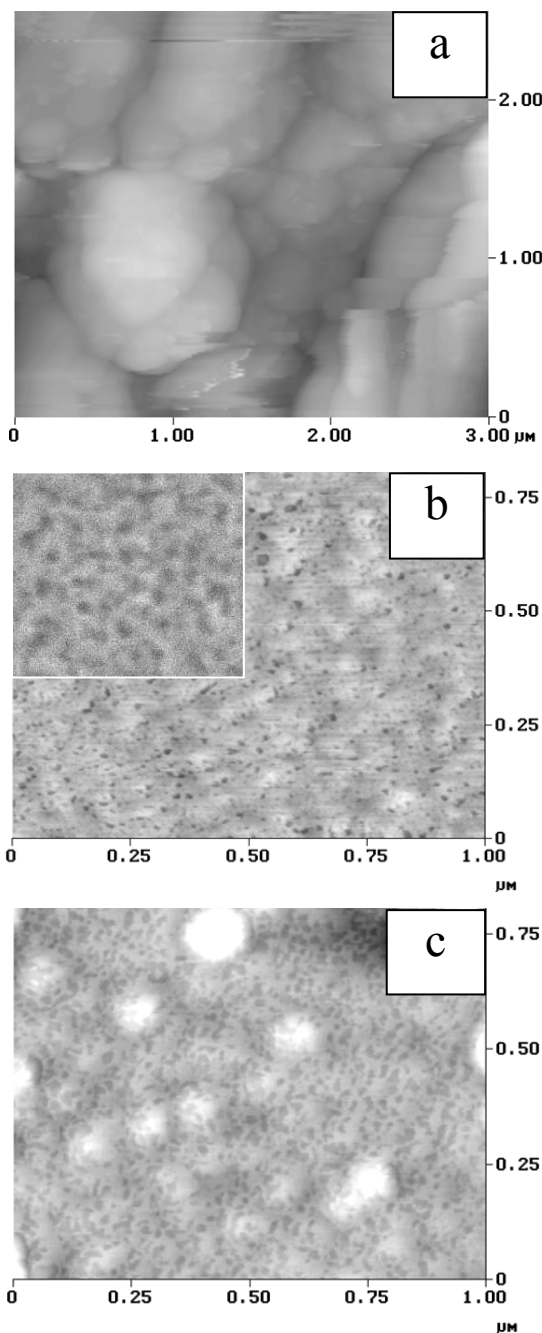


**Figure 5.2** AFM image of pp-PTFS (a) solid particles prepared under a system pressure of 27 Pa and RF power of 200 W with a plasma discharge duration of 60 s. (b) Mesoporous films prepared under a system pressure of 13 Pa and glow discharge power of 500 W with a glow discharge time of 20 s. The inset in (b) is a 200 × 200 nm FESEM image. (c) Mesoporous films compiled nanospheres synthesized under a system pressure of 13 Pa and glow discharge power of 400 W with a plasma discharge duration of 60 s.

On the other hand, glow discharge with high energy that corresponds to high power input condition always leads to small spheres, which contain a high degree of crossing-linkage

molecules [Yasuda, 1985]. The molecule chains are branched and randomly terminated with a high degree of cross-linkage. A monomer with unsaturated carbon bonds and benzene groups can enhance the high 3D cross-linkage by encouraging some chain cross-linking in the radicals and molecules through the retained C=C bonds or benzene groups. These molecules and radicals may configure into very fine uniform nanopores in the resultant polymer films. The pore ratio in the polymer will be increased when nanosphere film is prepared. It is because apart from the smaller fine pores configured by the cross-linking molecules, there are also some bigger pores formed among the nanospheres.

Figure 5.2(b) shows that a porous film was successfully synthesized when plasma polymerization was conducted at very high input power of 500 W under a system pressure of 13 Pa after a glow discharge time of 20 s. The inset FESEM image shows that the porous film has a pore size of about 10 nm (at mesoporous scale). This result suggests that there is a possibility to prepare porous spheres via plasma polymerization.

Thus, another investigation was carried out with an input power of 400 W. Figure 5.2(c) shows a porous film compiled nanospheres (30 ~ 50 nm in size) has been prepared at 400 W under the system of 13 Pa and a glow discharge time of 60 s. Further experiments show that when the RF power was decreased to be < 400 W, there are only bulk nanospheres synthesized. It is because lower RF power leads to bigger molecules and fragments with less cross-linkage chains.

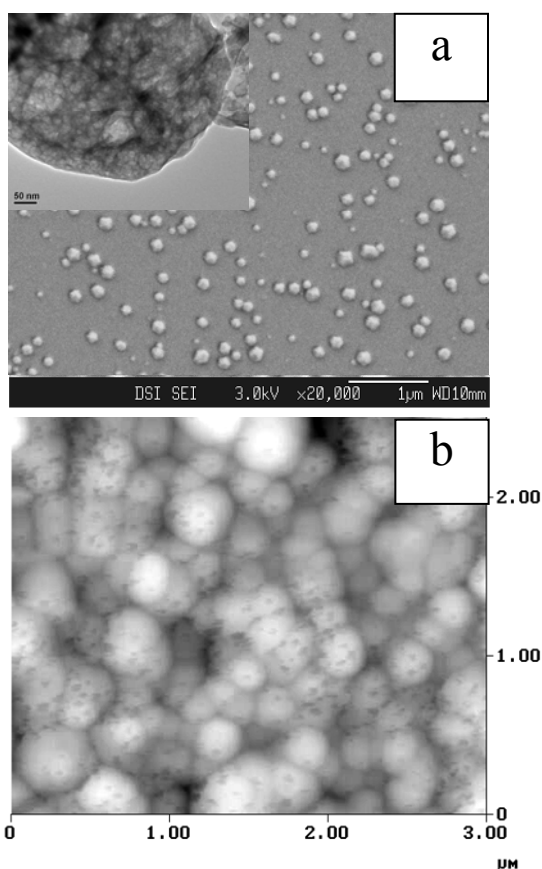


**Figure 5.3** (a) FESEM image of pp-PTFS porous nanospheres prepared under a system pressure of 27 Pa and RF power of 400 W with glow discharge time of 20 s. The inset is a TEM image focusing on a nanosphere. The scale bar is 50 nm. (b) AFM image of pp-PTFS mesoporous nanosphere film deposited via 4 rounds of multi-plasma polymerization under the same polymerization parameters as (a).

Since a high power of 400 W leads to porous film compiled nanospheres, whereas lower input RF power ( $< 400$  W) resulted in bulk nanospheres, after careful selection of the parameters of plasma polymerization, Figure 5.3(a) shows that loosely distributed porous nanospheres ( $\sim 300$  nm) have been successfully prepared. It is based on the synthesis parameters of the porous film compiled nanospheres (depicted in Figure 5.2(c)), and achieved by keeping high plasma energy while reducing the quantity of molecules,

radicals, and fragments produced during plasma polymerization. Namely, fixing RF power at 400 W, while increasing the system pressure from 13 to 27 Pa and shortening the glow discharge time from 60 to 20 s. The TEM image (inset of Figure 5.3(a)) shows that the mesoporous nanospheres have an average size of ~300 nm with the pore size of ~20 nm. After performing pulse-plasma polymerization for 4 rounds under the same conditions, Figure 5.3(b) shows that many more ordered mesoporous nanospheres with sizes ranging from 200 to 400 nm have been deposited. Among the porous nanospheres, there are also bigger pores of 40 – 50 nm in dimension configured (as shown in the figure).

### 5.3.2 Confirmation of the pp-PTFS Molecular Chain Structures

The physicochemical properties (depicted in Table 5.1), chemical compositions, and molecular structures of the plasma polymerized polymers were analyzed when the polymer morphology changed from solid particles (prepared at low energy polymerization) to porous nanostructured spheres and films (synthesized by high energy polymerization). The characterization results show that with the change in polymer morphology, many more radicals or molecules with short cross-linked chains were produced under the increased plasma energy.

First, the high resolution of C 1s XPS spectra in Figure 5.4 were deconvoluted into seven different types of carbon environments. The peaks at 284.6, 285.2, 287.2, 288.0, 290.1, and 292.1 eV are assigned to the  $\underline{\text{C}}-\underline{\text{C}}/\underline{\text{C}}-\underline{\text{H}}$ ,  $\underline{\text{C}}-\underline{\text{C}}\text{F}_x$ ,  $\underline{\text{C}}-\underline{\text{F}}$  (aromatic),  $\underline{\text{C}}-\underline{\text{F}}$  (nonaromatic),  $\underline{\text{C}}\underline{\text{F}}_2$ , and  $\underline{\text{C}}\underline{\text{F}}_3$  species, respectively [Clark and Shuttleword, 1980; Beamson and Briggs, 1993; Han et al., 1998]. The broad peak extending from 291 to 296 eV is the  $\pi$ -bond of



**Table 5.1** Property comparisons of the pp-PTFS polymers deposited at different plasma (RF) energy

Nanostructure type	Solid particles	Porous nanospheres	Porous sphere and film	Porous film
Sample	Fig. 5.2(a)	Fig. 5.3(b)	Fig. 5.2(c)	Fig. 5.2(b)
Glow discharge power (W)	200	400	400	500
Glow discharge pressure (Pa)	27	27	13	13
Glow discharge time (s)	60	20	60	20
Particle size <sup>a</sup> (nm)	1700 ± 600	285 ± 95	60 ± 25	—
Surface roughness $R_a$ (nm) <sup>b</sup>	95	22	2	~0
F/C ratio	0.55	0.50	0.47	0.43
Water contact-angle (°) <sup>c</sup>	111	103	100	99
Dielectric constant ( $\kappa$ )	2.3	1.7	1.9	2.0

<sup>a)</sup> Average of 50 particles on the surface.

<sup>b)</sup> Surface roughness value was obtained from the roughness profile of 1 × 1 μm AFM image.

<sup>c)</sup> Average value of advancing and receding contact angles for 3 samples.

shake-up satellite structure, reflecting the presence of aromatic rings in the synthesized polymers. The spectra of Figure 5.4(a-c) were from the obtained solid particles (Figure 5.2(a)), porous spheres (Figure 5.3(b)), and porous film (Figure 5.2(b)), respectively. From Figures 5.4(a) to 5.4(b), then to 5.4(c), the plasma polymerization energy was increased due to the increased input RF power (from 200 to 400, then to 500 W), or decreased system pressure (from 27 to 13 Pa). It is known that a lower system pressure leads to fewer monomer molecules in the chamber [Beamson and Briggs, 1993], which results in higher energy per monomer molecule even at same RF power.

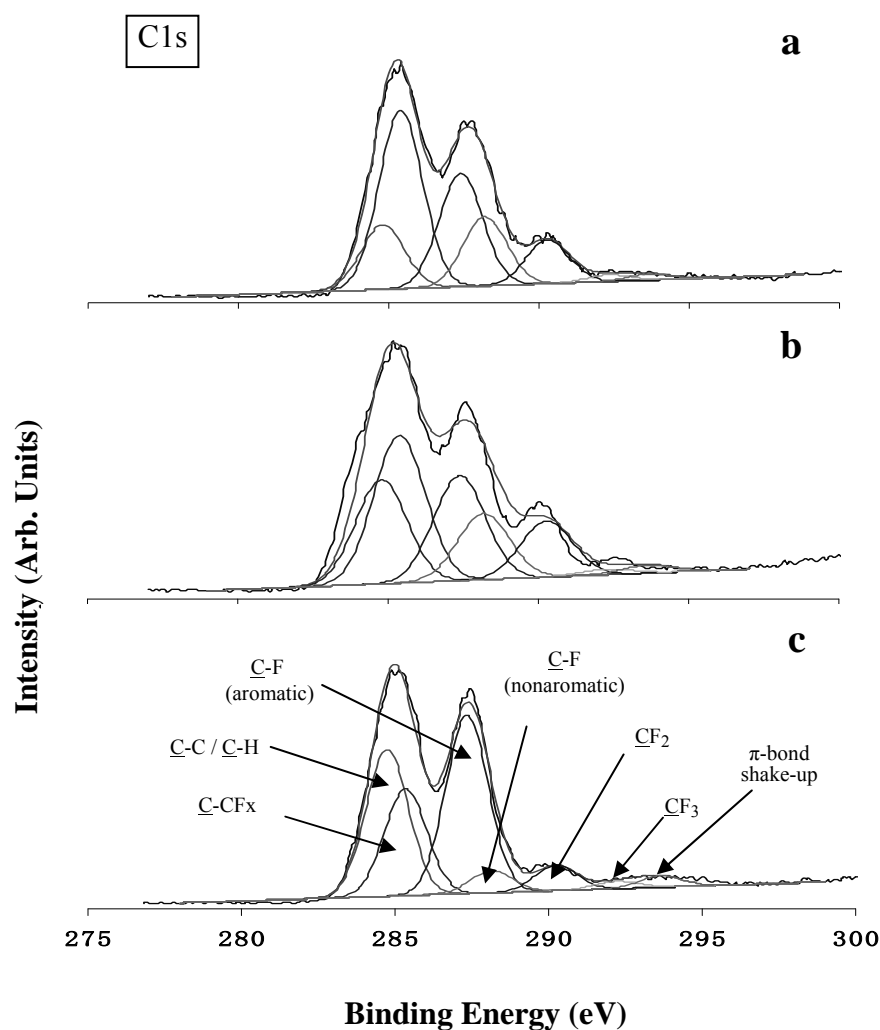


**Figure 5.4** High-resolution XPS C 1s core-level spectra of pp-PTFS nanostructured polymers deposited under different polymerized parameters. (a) solid particles, (b) porous nanospheres, (c) porous film.

Under the high input RF power of  $\geq 400$  W, the  $\underline{\text{C}}\text{-C}$  (instead of  $\underline{\text{C}}\text{-H}$ ) contribution increased significantly, especially for the highest polymerization energy at 500 W (as shown in Figure 5.4(c)). It is noted that  $\underline{\text{C}}\text{-H}$  contribution was only from the reaction monomer and it always decreased when small fragments  $\text{CH}_x$  and H were swept away by the carrier Ar gas stream during and after the high energy of plasma polymerization. Conversely, the peak intensity of fluorine containing groups such as  $\underline{\text{C}}\text{-CF}_x$ ,  $\underline{\text{C}}\text{-F}$  (

**Table 5.2** Assignments of positive ions and ToF-SIMS spectra of pp-PTFS structures

m/z	Proposed structure	m/z	Proposed structure
15	$\text{CH}_3^+$	193	$\text{CF}_3\text{—CF}_2\text{—CH}^+\text{—CHF—CH}_2\text{—CH}_3$
33	$\text{CH}_2\text{F}^+$	209	$\text{CF}_3\text{—CF}_2\text{—CH}^+\text{—CF}_2\text{—CH=CH}_2$
43	$\text{CH}_3\text{—CH}^+\text{—CH}_3$	223	$\text{CHF}_2\text{—(CF}_2)_2\text{—CHF—CH=CH—CH}_2^+$
47	$\text{CH}_2\text{F—CH}_2^+$	Spectra of ToF-SIMS* 	
51	$\text{CHF}_2^+$		
57	$\text{C(CH}_3)_3^+$		
69	$\text{CF}_3^+$		
74	$\text{CHF}^+\text{C(CH}_3)_2$		
77	$\text{CH}_2\text{=CH—CF}_2^+$		
79	$\text{CH}_3\text{—CH}^+\text{—CHF}_2$		
83	$\text{CH}_2\text{=CH—C(CH}_3)_2\text{CH}_2^+$		
83	$\text{CF}_3\text{—CH}_2^+$		
85	$\text{CH}_3\text{—CH}^+\text{—C(CH}_3)_3$		
96	$\text{CHF=CH—CHF}_2^+$		
127	$\text{CF}_3\text{—CF}^+\text{—CH=CH}_2$		
145	$\text{CF}_3\text{—CF}^+\text{—CF=CH}_2$		
147	$\text{CF}_3\text{—CF}^+\text{—CHF—CH}_3$		
177	$\text{CF}_3\text{—CF}_2\text{—CF}^+\text{—CH=CH}_2$		
179	$\text{CF}_3\text{—CF}_2\text{—CF}^+\text{—CH}_2\text{—CH}_3$		
183	$\text{CF}_3\text{—CF}_2\text{—CF}^+\text{—CH}_2\text{F}$		

\* (a) solid particles in Figure 5.2(a), (b) porous spheres in Figure 5.3(b), (c) porous film in Figure 5.2(b).

nonaromatic), and  $\underline{C}F_2$  decreased. It indicates that with the decomposition of some benzene groups and defluorination of the monomer molecules under high energy, more C-C bonds and fewer  $CF_x$  ( $x = 1, 2, \text{ or } 3$ ) bonds are generated. It can be inferred that more cross-linked  $-C(-C-)_2$  and  $-C(-C-)_3$  groups in the molecules are produced.

Secondly, the ToF-SIMS results (shown in Table 5.2) showed that in comparison with the fragmentation of long chain molecules, short chain molecules and fragments, of which MW is in the range of 20 to 80, have stronger peak intensity for the polymerized porous nanospheres and films. For these short chain molecules, their positive radicals consist of  $CH_2F^+$ ,  $CH_3-CH^+-CH_3$ ,  $CH_2F-CH_2^+$ ,  $C(CH_3)_3^+$ ,  $CHF_2^+$ ,  $CF_3^+$ ,  $CHF^+C(CH_3)_2$ ,  $CH_2=CH-C(CH_3)_2CH_2^+$ ,  $CH_2=CH-CF_2^+$ ,  $CH_3-CH^+-C(CH_3)_3$ ,  $CH_3-CH^+-CHF_2$ , etc [Han et al., 1998]. Hence, most of them (especially are of non-fluorine containing groups) are of cross-linked chain radicals, e. g.,  $CH_3-CH^+-CH_3$ ,  $C(CH_3)_3^+$ ,  $CHF^+C(CH_3)_2$ ,  $CH_2=CH-C(CH_3)_2CH_2^+$ ,  $CH_3-CH^+-C(CH_3)_3$ ,  $CH_3-CH^+-CHF_2$ . In contrast, solid particles produced at the low power of 200 W have higher peak intensity ratio of long chain ( $MW > 100$ ) to short chain, in comparison to the porous polymers. Therefore, after considering all the variation in the XPS and ToF-SIMS results at different input RF powers, the mesoporous pp-PTFS polymers produced under high energy polymerization probably contain a substantial amount of radicals or fragments with highly 3D cross-linked chains.

### 5.3.3 Potential Applications of the Mesoporous pp-PTFS Polymers

The so-prepared porous films and nanospheres were further characterized to explore their potential applications. For comparison purpose, the properties of the plasma polymerized

polymers (including solid particles) are listed in Table 5.1. The results show that after plasma polymerization, the [F]/[C] ratio (from XPS analysis) is 0.55 for the solid particles (Figure 5.2(a)) produced at low power of 200 W, and 0.43 – 0.50 for the porous nanospheres (Figure 5.3(b)) and porous film (Figure 5.2(b)) produced at high RF power of  $\geq 400$  W. It is noted that the [F]/[C] ratio of PTFS monomer is 0.625. Hence, the mesoporous nanostructure polymers still contain a high ratio of fluorine, although defluorination has occurred to some extent at high energy polymerization. The water contact angles of the porous nanostructured polymers reach about 100 degrees because of the high fluorine content, suggesting that the porous pp-PTFS polymers are highly hydrophobic with potential for anti-humidity applications.

In particular, porous fluoropolymer particles are expected to have very low dielectric constant because fluoropolymers possess the lowest  $\kappa$  values ( $\leq 2.2$ ) among all of bulk materials [Singer, 1996], and the incorporation of air reduces the  $\kappa$  value of the resulting polymer further [Ramos, 1997; Yang et al., 2003] due to the fact that the dielectric constant of air is about 1. Since these mesoporous fluoropolymers have a large porous volume, their effective  $\kappa$  value is reduced to 1.7 (Table 5.1). The fluoropolymer nanospheres prepared via plasma polymerization are known to possess good physico-chemical properties, such as low dissipation factor, good chemical stability, large hydrophobicity, and good thermal stability [Liu et al., 2004]. These advantages allow the porous fluoropolymer nanospheres to be used in various areas, such as in low  $\kappa$  fillers, pigments, and as hosts for optically active compounds [Ozin, 1992; Huo et al., 1997].

Furthermore, if these fluoropolymer nanospheres can be imparted with magnetic properties, their applications will be enhanced since magnetic nanoporous nanospheres are important in delivery and controlled release of drugs [El-Kareh et al., 1997]. As a delivery tool, their behaviors can then be controlled with an external applied magnetic field. In addition, the surface-adsorbed magnetic nanoparticles on the mesoporous pp-PTFS nanospheres are potentially useful as catalysts in bio-engineering and specialty chemical technologies [Bronstein et al., 2001; van Roon et al., 2005]. Thus, further functionalization of the present mesoporous pp-PTFS nanospheres to achieve magnetic porous nanospheres was carried out via surface adsorption and thermal decomposition of  $\text{Fe}(\text{CO})_5$  into magnetic iron oxide nanoparticles.

Although  $\text{Fe}(\text{CO})_5$  can be adsorbed on the fluoropolymer surface, the adsorbed layer was found to be unstable due to the easy evaporation of the adsorbed  $\text{Fe}(\text{CO})_5$ . Hence oleic acid and oleyl amine were used as initiator and stabilizer in the adsorption process. The two chemical agents are well known to be good surfactants when used together, as they contain hydrophilic amine and lipophilic oleic groups. As such,  $\text{Fe}(\text{CO})_5$  can be adsorbed or attached to the hydrophobic organic materials through the surfactant. Since the plasma polymerized fluoropolymers are highly hydrophobic [Liu et al., 2004], the mesoporous pp-PTFS nanospheres were surface-functionalized with the surfactants before adsorption of  $\text{Fe}(\text{CO})_5$ . In addition,  $\text{Fe}(\text{CO})_5$  is well known to be easily decomposed into magnetic iron oxides at high temperature [Huang et al., 1996]. Therefore, the mesoporous pp-PTFS nanospheres can become magnetic porous nanospheres after immobilization of the iron oxide nanoparticles from the thermal decomposition of adsorbed  $\text{Fe}(\text{CO})_5$ , as depicted in Figure 5.1.

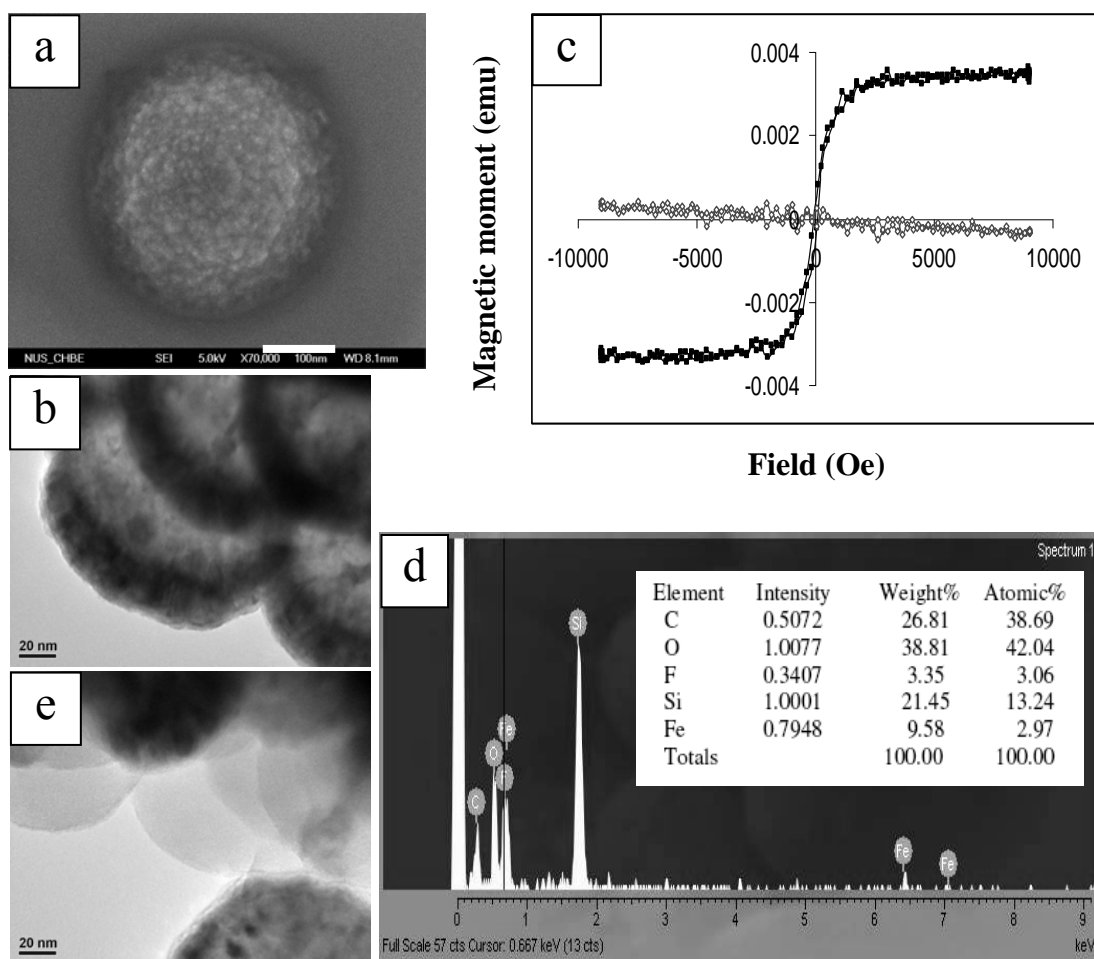


**Figure 5.5** (a) FESEM images of one porous pp-PTFS nanosphere with immobilized iron oxide nanoparticles. (b) TEM image of one part of ~300 nm pp-PTFS nanosphere loaded with iron oxide nanoparticles. The scale bars of (a) and (b) are 100 and 20 nm, respectively. (c) and (d) are the respective VSM and EDX analysis results of the magnetic nanospheres on a  $10 \times 8$  mm Si substrate. In (c), the open symbol (-◇-) and solid symbol (-■-) stand for the magnetic moment of the mesoporous pp-PTFS nanospheres prior to and after immobilization of the iron oxide nanoparticles, respectively. (e) TEM image of one part of a magnetic pp-PTFS nanosphere after HCl washing.

Figure 5.5(a) shows a FESEM image of one ~300 nm magnetic mesoporous pp-PTFS nanosphere obtained from the nanosphere of Figure 5.3(a) via the synthesis route in Figure 5.1. Under ultrasonic agitation and through the function of oleic acid and oleyl

amine surfactants,  $\text{Fe}(\text{CO})_5$  can be evenly adsorbed onto the hydrophobic surfaces and pores of nanoporous pp-PTFS nanospheres. Thus, the magnetic iron oxide nanoparticles are uniformly distributed on the surface of the nanospheres after  $\text{Fe}(\text{CO})_5$  decomposition. The TEM image in Figure 5.5(b) also shows the evenly adsorbed iron oxide nanoparticles inside the surfaces and pores of the  $\sim 300$  nm pp-PTFS nanosphere. From a comparison of the VSM measurements (as shown in Figure 5.5(c)) prior to and after the immobilization of iron oxide nanoparticles on the mesoporous pp-PTFS nanospheres, it is obvious that there is no magnetic response for the mesoporous pp-PTFS nanospheres prior to the immobilization of the magnetic nanoparticles. After the functionalization, the porous fluoropolymer nanospheres possess a normal magnetization-hysteresis ( $M-H$ ) loop, which indicates that the adsorbed iron oxide components are ferromagnetic materials and their magnetization domain directions can be changed under the induction of an applied magnetic field. The magnetic moment of the monodispersed nanospheres is about 0.0036 emu for an area of  $10 \times 8 \text{ mm}^2$  over which the nanospheres spread. The EDX analysis results in Figure 5.5(d) clearly show that iron oxide was present in the mesoporous pp-PTFS nanospheres. Therefore, the EDX results are consistent with the VSM results. The TEM image in Figure 5.5(e) shows that after etching by 5N HCl and rinsing by water, some iron oxide nanoparticles, which were on the outer surface and pores of one  $\sim 300$  nm porous pp-PTFS nanosphere, were removed. Hence, the process allows more effective outer surface in the nanosphere for other molecular adsorption and targeting.



### 5.4 Conclusions

In summation, a methodology for the preparation of mesoporous fluoropolymer nanospheres and films by means of plasma polymerization of pentafluorostyrene under suitable high RF power is demonstrated. The mesoporous nanospheres can be readily converted to magnetic porous nanospheres with more functions via chemical adsorption and thermal-decomposition. The present simple strategy has potential to be extended to other monomers to prepare similar novel porous nanostructures.

**CHAPTER 6**

**MAGNETIC MESOPOROUS FLUOROPOLYMER  
NANOSPHERES FROM PLASMA POLYMERIZATION /  
ETCHING AND ADSORPTION OF SURFACE-  
FUNCTIONALIZED MAGNETIC NANOPARTICLES**

## 6.1 Introduction

Porous particles play an important role in present-day technologies, such as catalysis, enzyme adsorption, drug delivery, and biomolecular transportation [El-Kareh and Bronner, 1997; Martin et al., 2000; Maier, 2001]. Organic porous particles possess unique characteristics differing from those of inorganic porous particles. For example, porous fluoropolymers have very low dielectric constants and good chemical resistance [Teare et al., 2002; Fu et al., 2004]. Hence, organic porous particles are of great interest and increasing demand [Ozin, 1992]. However, unlike the widely available inorganic porous particles (such as porous silica and zeolite), only a few types of porous organic particles are commercially available. The as-synthesized porous organic particles are usually in the micrometer-scale [Hamada et al., 1996; Øye et al., 2003]. The limited availability of organic particles of different dimension and pore size is due, in part, to limitations in available fabrication methods. In addition, the preparation of porous organic particles usually involves multi-component processes and complex procedures in fluid phases [Steen et al., 2001]. Accordingly, simple approaches for the preparation of nanoporous organic nanospheres remain of great interest.

The work described in this chapter involves a ‘dry’ and simple approach for preparing mesoporous fluoropolymer nanospheres via direct plasma polymerization and dry etching. The porous nanospheres were about 200 to 300 nm in diameter, with pore sizes of 5 – 20 nm. These porous polymer nanospheres allowed the adsorption of other surface-functionalized inorganic nanoparticles. Thus, surface-functionalized super-paramagnetic nanoparticles of PtFe of about 3 nm in size were adsorbed in the pores and on the

surfaces of the as-synthesized mesoporous fluoropolymer nanospheres to produce the magnetic porous nanospheres.

## 6.2 Experimental Section

### 6.2.1 Preparation of Porous Nanospheres

The monomer, 3,3,4,4,5,5,6,6,7,7,8,8,9,9,10,10,10-heptafluorodecyl acrylate or HDFA was also used for the plasma polymerization and deposition of solid spheres on cleaned Si(100) wafers. Each plasma polymerization was initiated at a pre-determined system pressure after 1 min of monomer flow. The detailed procedure of polymerization is similar to that described in Section 3.2.2.

After deposition of the pp-HDFA solid nanospheres on the Si(100) substrates, argon (Ar) plasma etching was subsequently carried out. The synthesis procedure and the expected particle morphologies are shown schematically in Figure 6.1(a). Prior to and after Ar plasma dry etching, the deposition chamber was purged with argon under a system pressure of 80 Pa for 2 and 5 min, respectively, to remove the residual reactants and intermediate species. The chamber temperature was maintained at around room temperature during the plasma etching process.

### 6.2.2 Synthesis of Magnetic PtFe Nanoparticles

Permanent magnetic PtFe nanoparticles of good chemical stability were chosen to be adsorbed in the pores and on the surfaces of mesoporous pp-HDFA nanospheres in this work. They were prepared via the reduction of  $\text{Pt}(\text{acac})_2$  (acac = acetylacetonate,  $\text{CH}_3\text{COCHCOCH}_3$ ) by 1,2-hexadecanediol and thermal decomposition of  $\text{Fe}(\text{CO})_5$  in a high-temperature ( $\sim 300^\circ\text{C}$ ) solution of dioctylether under an Ar atmosphere on a vacuum line. An  $\text{Fe}(\text{CO})_5$  to  $\text{Pt}(\text{acac})_2$  molar feed ratio of 4 : 1 was used. A combination of oleic acid and oleyl amine was used as the stabilizer. From this process, super-paramagnetic

nanoparticles (~3 nm in size) in colloidal form and with an approximate formula of  $\text{Fe}_{68}\text{Pt}_{32}$  were produced. The synthesis route is shown schematically in Figure 6.1(b) and more details are available in the literature [Sun et al., 1989].

### **6.2.3 Adsorption of Magnetic PtFe Nanospheres onto the Porous pp-HDFA Nanospheres**

The as-synthesized PtFe nanoparticles were collected by centrifugation and then dispersed in deionized water at a concentration of ~1 mg per 10 ml in an ultrasonic bath. The Si substrate with deposited mesoporous pp-HDFA nanospheres was immersed in the colloidal solution of the magnetic nanoparticles in an ultrasonic bath for 30 s. The nanosphere layer was subsequently dried in a gentle stream of  $\text{N}_2$  gas at  $50 \pm 5$  °C. The preparation procedure is shown schematically in Figure 6.1(c).

### **6.2.4 Characterization of the pp-HDFA Nanospheres**

The procedures of characterization of the pp-HDFA nanospheres are similar to those illustrated in Sections 3.2.2, 4.2.2, and 5.2.3.

## 6.3 Results and Discussion

### 6.3.1 Synthesis of Mesoporous Nanospheres

The mesoporous nanospheres were prepared by plasma polymerization and deposition, followed by Ar plasma dry etching of the deposited solid particles, as illustrated schematically in Figure 6.1(a). It is known that solid polymer nano-/micro-particles of various sizes can be prepared via plasma polymerization and deposition under controlled glow discharge conditions [Han and Timmons, 2000; Hadjadj et al., 2001; Takahashi et al., 2003; Chen et al., 2004]. Most of these particles are composed of short and long chain molecules, radicals, and molecular fragments. Figure 6.2(a) shows the FESEM image of the solid pp-HDFA spheres under an input RF power of 200 W, system pressure of 40 Pa, and plasma glow discharge time of 40 s. The sizes of the nanospheres range from 200 to 300 nm.

It is well known that a plasma system can perform two entirely different functions. One involves plasma polymerization when there is existing monomer or organic molecules in the plasma chamber. Another function involves etching when there is only an inert gas, such as Ar, CF<sub>4</sub>, and N<sub>2</sub>, present in the reaction chamber. During plasma etching, it is supposed that when the plasma etching time is controlled properly, small fragments, radicals, and molecules will be etched away preferentially, leaving behind long chain radicals and macromolecules. The plasma etched solid particles will eventually assume a hollow structure. Our experimental result verified this suggestion. Figure 6.2(b) shows that the FESEM image of the porous nanospheres generated from the solid nanospheres (shown in Figure 6.2(a)) after etching for 5 s by Ar plasma at RF power of 200 W and a

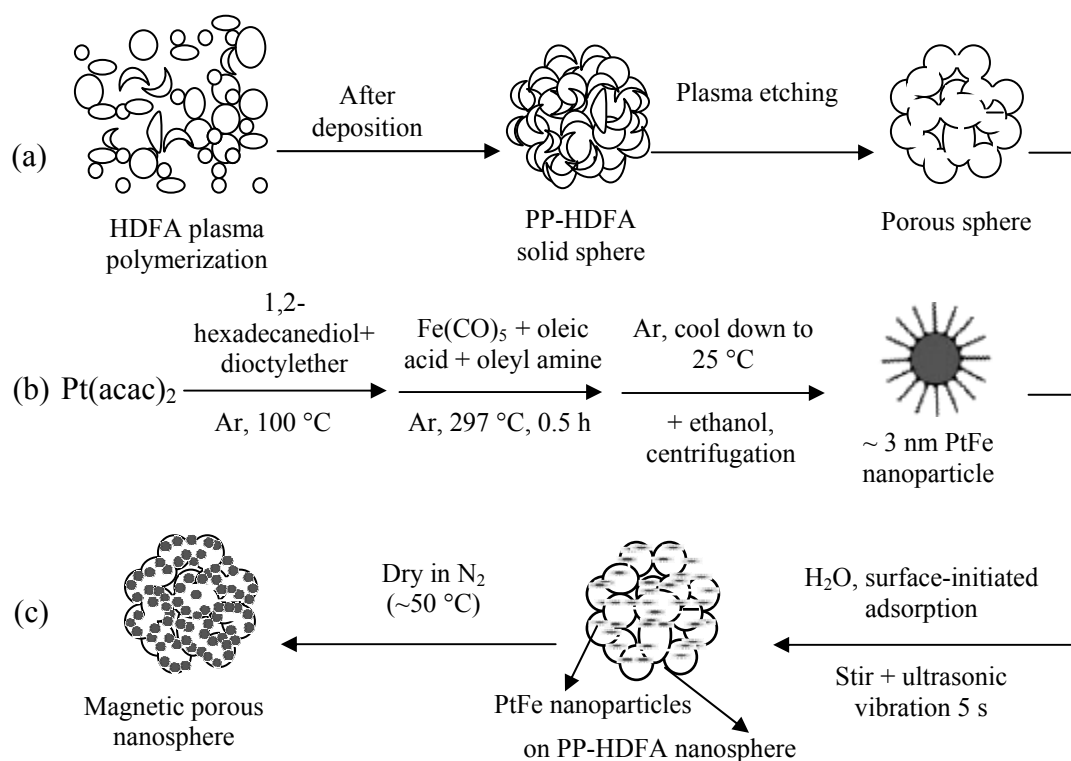


**Figure 6.1** Scheme illustrating (a) the preparation of mesoporous fluoropolymer nanospheres via plasma polymerization and plasma etching, (b) the preparation of surface-functionalized PtFe nanoparticles, and (c) the adsorption of magnetic PtFe nanoparticles on the porous polymer nanospheres.

system pressure of 40 Pa. The plasma conditions used for etching were similar to those used for the plasma polymerization of solid nanospheres. The sizes of the porous nanospheres remain in the range of 200 – 300 nm. The pores in the spheres are about 5 – 15 nm. The pore size is dependent on the etching time. With prolonged etching, more and larger molecular fragments and radicals are etched away, leaving behind larger pores. For example, the pore size of the spheres in Figure 6.2(b) increased to about 8 – 20 nm when the etching time was prolonged to 8 s. However, Figure 6.2(c) further shows that when Ar plasma-etching time was increased to 22 s, of, the porous spheres have become much smaller. The pore size has increased significantly and some of the porous nanospheres



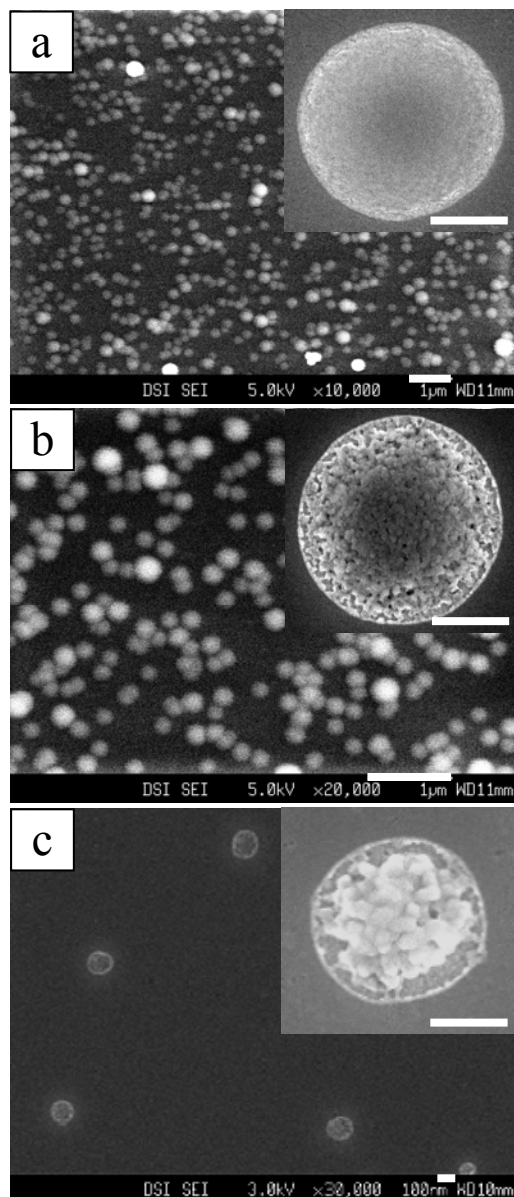


**Figure 6.2** FESEM images of (a) solid pp-HDHF particles polymerized under an input RF power of 200 W, system pressure of 40 Pa and glow discharge time of 45 s, and the solid particles after (b) 5 s and (c) 22 s of Ar plasma etching under the same RF power and system pressure. The scale bars in the images of parts (a) and (b) are 1 μm, and of part (c) is 100 nm, while the scale bars for the 3 insets are 100 nm.

may have been blown away during etching and subsequent argon purging. Thus, the etching time was controlled at a duration shorter than 25% of the plasma polymerization time in order to avoid excessive degradation and loss of the porous spheres.

Further investigations showed that during plasma etching, the input RF power should be controlled at the same or lower level than that used for the plasma polymerization. Otherwise, the long chain macromolecules, which form the cores, will be similarly etched away, resulting in the absence of pores or formation of poorly-defined shallow pores. Thus, the extent of plasma etching should be controlled to within a certain range of RF power (less than that used for polymerization) [Yasuda, 1984; Jeong et al., 1999] and duration (less than 25% of the polymerization time), when the other parameters are fixed.

**6.3.2 Chemical Composition of the Porous Nanospheres.** In order to verify that shorter chain fragments were preferentially etched away over longer chain molecules to form the porous spheres, the chemical structures of the plasma polymerized spheres before and after Ar plasma etching were analyzed by ToF-SIMS. The HDFA monomer has a molecular weight of 504 and a chemical structure of  $\text{H}_2\text{C}=\text{CHCOOCH}_2(\text{CF}_2)_7\text{CF}_3$ . The assignments of the positive ion fragments in the ToF-SIMS spectrum of the plasma polymerized pp-HDFA nanospheres are shown in Table 6.1 [Teare et al., 2002]. There is a higher F content for the long chain fragments ( $\text{MW} > 120$ ) than for the short chain fragments ( $\text{MW} \leq 50$ ).

Figures 6.3(a) and 6.3(b) show the ToF-SIMS spectra of the solid pp-HDFA nanospheres (described in Figure 6.2(a)) before and after 8 s of Ar plasma etching, respectively. After Ar plasma etching of the porous structure, the relative peak intensities of short chain fragments decrease substantially while those of the long chain fragments increase significantly. The results indicate that short chain molecules and radicals have been preferentially removed during plasma dry etching. Thus, the ToF-SIMS results verified

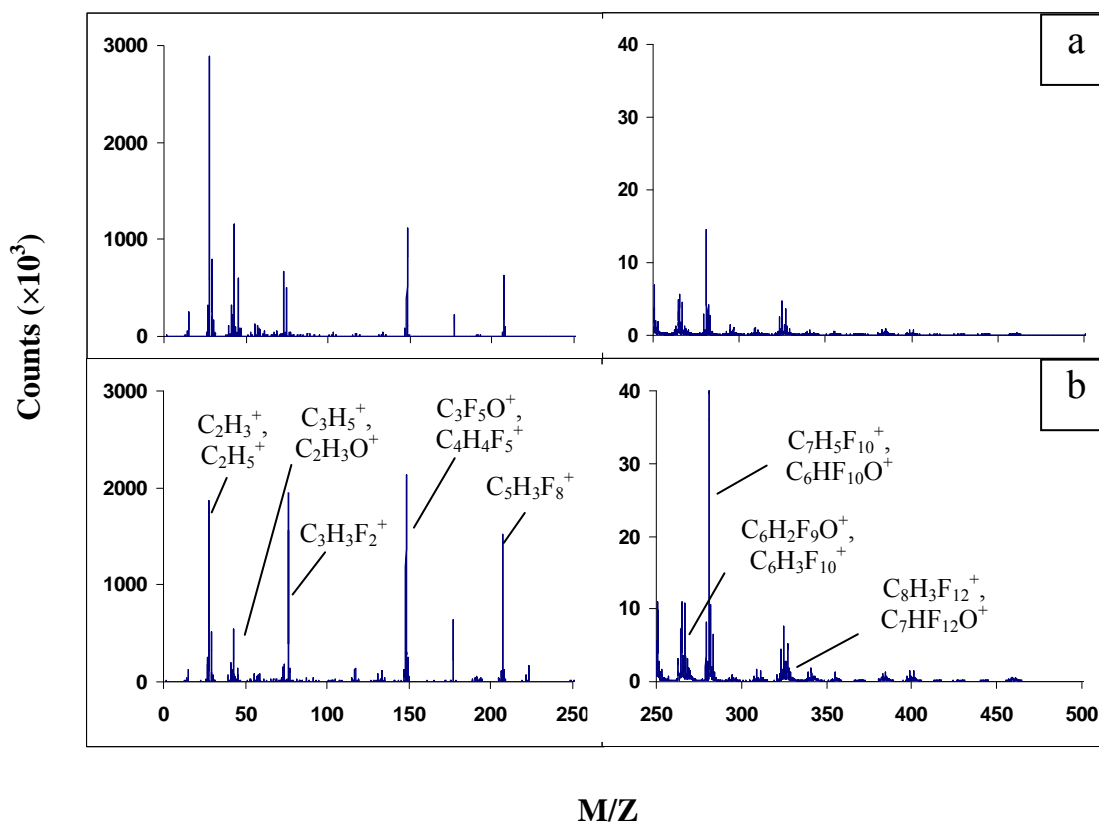


**Figure 6.3** ToF-SIMS spectra of the pp-HDFA spheres (a) before and (b) after 8 s of plasma etching.

that as a consequence of plasma dry etching, the porous nanospheres consist of longer chain molecular fragments and large molecules compared to the original solid nanospheres.

The changes in chemical composition of the nanospheres before and after Ar plasma etching were investigated by XPS. The results are shown in Figure 6.4 and Table 6.2. The XPS wide scan spectrum (Figure 6.4(a)) of the solid pp-HDFA nanospheres (described in Figure 6.2(a)) shows the respective binding energies (BEs) of Si 2p and Si 2s at about

**Table 6.1** Assignments of the positive ion fragments in the ToF-SIMS spectra of pp-HDFA nanospheres

m/z	Proposed structure	m/z	Proposed structure
27	$\text{H}_2\text{C}=\text{CH}^+$	127	$\text{CF}_3-\text{CF}^+-\text{CH}=\text{CH}_2$
29	$\text{H}_3\text{C}-\text{CH}_2^+$	147	$\text{CF}_3-\text{CF}_2-\text{CO}^+$ , $\text{CF}_3-\text{CF}_2-\text{CH}^+-\text{CH}_3$
41	$\text{CH}_2=\text{CH}-\text{CH}_2^+$	149	$\text{CH}_3-(\text{CH}_2)_6-\text{CF}_2^+$
43	$\text{CH}_3-\text{CH}_2-\text{CH}_2^+$ , $\text{CH}_3-\text{CO}^+$	215	$\text{CF}_3-(\text{CF}_2)_2-\text{CF}^+-\text{CH}_3$
47	$\text{H}_3\text{C}-\text{CHF}^+$	261	$\text{CF}_3-(\text{CF}_2)_3-(\text{CH}_2)_2-\text{CH}_2^+$ , $\text{CF}_3-(\text{CF}_2)_3-\text{CH}_2-\text{CO}^+$
55	$\text{CH}_2=\text{CH}-\text{CH}_2-\text{CH}_2^+$	265	$\text{CF}_3-(\text{CF}_2)_3-\text{CF}^+-\text{CH}_3$
57	$\text{CH}_3-(\text{CH}_2)_2-\text{CH}_2^+$ , $\text{CH}_3-\text{CH}_2-\text{CO}^+$	279	$\text{CF}_3-(\text{CF}_2)_3-\text{CF}^+-\text{CH}_2-\text{CH}_3$ , $\text{CF}_3-(\text{CF}_2)_3-\text{CHF}-\text{CO}^+$
69	$\text{CF}_3^+$	283	$\text{CF}_3-(\text{CF}_2)_4-\text{CH}_2^+$
71	$\text{CH}_3-(\text{CH}_2)_2-\text{CO}^+$	327	$\text{CF}_3-(\text{CF}_2)_4-\text{CF}^+-\text{CH}=\text{CH}_2$
77	$\text{CH}_2=\text{CH}-\text{CF}_2^+$	329	$\text{CF}_3-(\text{CF}_2)_4-\text{CHF}-\text{CO}^+$
83	$\text{CF}_3-\text{CH}_2^+$	383	$\text{CF}_3-(\text{CF}_2)_6-\text{CH}_2^+$
85	$\text{CH}_3-(\text{CH}_2)_3-\text{CO}^+$	401	$\text{CF}_3-(\text{CF}_2)_6-\text{CHF}^+$

100 and 151 eV, C 1s at about 285 eV, O 1s at about 531 eV, and F 1s at about 685 eV. It is known that high plasma energies can lead to the deposition of small particles [Øye et al., 2003; Fu et al., 2003]. Hence, a moderate RF power of 200 W was chosen for the preparation of pp-HDFA nanospheres. Nevertheless, this level of plasma energy still led

to a considerable extent of defluorination in the deposited spheres. As a result, although the as-deposited solid nanospheres still retain a significant fluorine content (a [F]/[C] ratio of about 0.52), their fluorine content is much lower than that of the starting monomer molecules (the theoretical [F]/[C] ratio for HDFA is 1.3). The C 1s core-level spectrum (Figure 6.4(b)) can be curve-fitted with seven different carbon environments:  $\underline{\text{C}}\text{-C}/\underline{\text{C}}\text{-H}$  (hydrocarbon) at 284.6 eV,  $\underline{\text{C}}\text{-CF}_x$  (hydrocarbon adjacent to a fluorocarbon group) at 285.0 eV,  $\underline{\text{C}}\text{-O}$  at 286.2 eV,  $\underline{\text{C}}\text{=O}$  at 287.4 eV,  $\underline{\text{C}}\text{F}/\text{O}=\underline{\text{C}}\text{-O}$  at 288.5 eV,  $\underline{\text{C}}\text{F}_2$  at 291.1 eV, and  $\underline{\text{C}}\text{F}_3$  at 293.0 eV. The  $[\underline{\text{C}}\text{-O}] : [\text{O}=\underline{\text{C}}\text{-O}]$  and  $[\underline{\text{C}}\text{-O}] : [\underline{\text{C}}\text{-C}/\underline{\text{C}}\text{-H}]$  ratio of the deposited nanospheres are substantially higher than 1:1 and 1:2, respectively, for the acrylate polymer, suggesting a substantial extent of post-polymerization oxidation of the sample.

Differing from the plasma polymerization process, the subsequent Ar plasma etching enhances the fluorine content. Figures 6.4(c) and 6.4(e) show the wide scan spectra of the pp-HDFA solid nanospheres (described in Figure 6.2(a)) after Ar plasma etching for 5 and 8 s, respectively. The intensity ratio of the F 1s component to C 1s component increases with the increase in plasma etching time of the solid pp-HDFA nanospheres. The C 1s core-level spectral line shapes of the as-deposited, and 5 s and 8 s Ar plasma etched pp-HDFA nanospheres (shown in Figures 6.4(b), 6.4(d) and 6.4(f), respectively, as well as in Table 6.2) also indicate that with the increase in Ar plasma etching time, the relative intensities of the  $\underline{\text{C}}\text{F}_2$  and  $\underline{\text{C}}\text{F}_3$  components increase while those of the  $\underline{\text{C}}\text{-C}/\underline{\text{C}}\text{-H}$  groups decrease. The overall elemental [F]/[C] ratio, determined from the F 1s and C 1s spectral area ratio, increases from 0.52 for the solid nanospheres to 0.75 and 0.86,

**Table 6.2** XPS results of pp-HDFA nanospheres before and after Ar plasma etching

		Binding energy	Spectrum area (%)		
		(eV)	pp-HDFA	5 s Etching	8 s Etching
XPS Assignment	<u>C</u> -C/ <u>C</u> -H	284.6	20.7	14.5	9.2
	<u>C</u> -CF <sub>x</sub>	285.0	24.6	25.5	26.2
	<u>C</u> -O	286.2	17.0	9.6	9.2
	<u>C</u> =O	287.4	5.7	10.4	10.5
	<u>C</u> -F/ <u>C</u> OO	288.5	15.8	16.0	17.0
	<u>C</u> F <sub>2</sub>	291.1	11.3	12.4	14.0
	<u>C</u> F <sub>3</sub>	293.0	4.9	11.6	13.9
C (%)		--	56.8	51.0	48.3
F (%)		--	29.8	38.3	41.7
O (%)		--	13.4	10.7	10.0
F/C ratio		--	0.52	0.75	0.86

respectively, for the porous spheres from 5 and 8 s of Ar plasma etching. These elemental [F]/[C] ratios are in good agreement with those derived from CF<sub>x</sub> components in the high resolution C 1s core-level spectra (Table 6.2). The results are consistent with the fact that smaller hydrocarbon molecules were etched away preferentially to give rise to the increase in the [F]/[C] ratio of the resulting porous nanospheres. Thus, the XPS results are also consistent with the ToF-SIMS results.

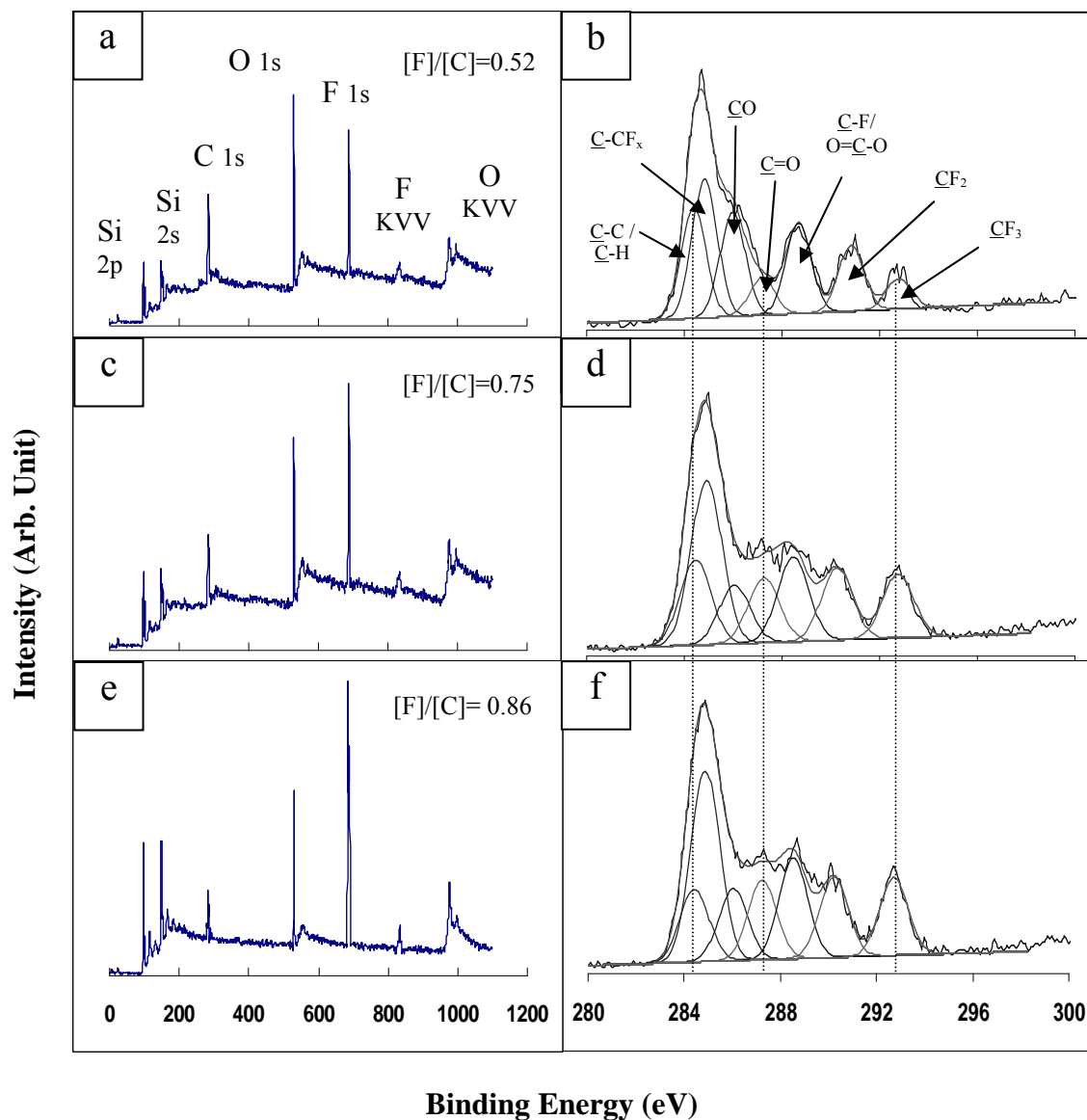


**Figure 6.4** XPS wide scan spectra and C 1s core-level spectra of the pp-HDFA spheres before etching (a, b) and after 5 s (c, d) and 8 s (e, f) of plasma etching.

### 6.3.3 Functionalization of the Mesoporous pp-HDFA Nanospheres

Since the mesoporous pp-HDFA nanospheres have an extensive network of nanopores and high fluorine content, the dielectric constant  $\kappa$ , of these porous nanospheres is expected to be low (air has the lowest  $\kappa$ ,  $\sim 1.0$ , among all materials). For the films of

assembled porous nanospheres deposited on copper substrates (instead of the Si(100) substrates to facilitate  $\kappa$  measurements) under conditions similar to those used for the deposition of porous nanospheres shown in Figure 6.2(b), the  $\kappa$  value is 1.7, in comparison to 2.0 for the film of assembled solid nanospheres. Furthermore, fluoropolymer nanospheres prepared via plasma polymerization always possess excellent physicochemical properties, such as low dissipation factor, good chemical stability, good hydrophobicity, and high thermal stability [Liu et al., 2004]. Hence these mesoporous pp-HDFA spheres are potentially useful for the controlled release of drugs, in the adsorption of chemical and biological catalysts, as ultra-low  $\kappa$  materials and fillers, and as optically active components. Thus, further functionalization of the present mesoporous nanospheres was carried out via adsorption of surfactant-modified super-paramagnetic PtFe nanoparticles into the pores and onto the surfaces of the mesoporous pp-HDFA nanospheres.

The super-paramagnetic PtFe nanoparticles were synthesized in the presence of oleic and oleyl amine surfactants [Sun et al., 2000]. Hence, the as-prepared PtFe nanoparticles from this procedure are colloid particles with surface-functionized hydrophilic amine and lipophilic alkyl oleic bifunctional groups. These metallic nanoparticles can be readily adsorbed onto other hydrophobic organic materials via the alkyl oleic ends. The affinity of lipophilic functional groups of the colloidal nanoparticles for the highly hydrophobic fluoropolymer spheres [Liu et al., 2004] is further enhanced in an aqueous dispersion. As a result, the PtFe colloid nanoparticles are expected to be adsorbed on the mesoporous pp-HDFA nanospheres to produce the porous magnetic nanospheres, as depicted in Figure 6.1(c).



**Table 6.3** EDX analysis results of magnetized pp-HDFA nanospheres

Element	KeV	Mass (%)	At (%)
C	0.277	34.65	46.73
O	0.525	38.00	38.47
F	0.677	15.10	12.88
Fe	6.398	4.36	1.27
Pt	2.048	7.89	0.66
Total	--	100.00	100.00

Under vigorous stirring and ultrasonic agitation, the PtFe nanoparticles became dispersed in deionized water to form a colloidal suspension. Thus, they can be evenly adsorbed in the pores and on the surfaces of the mesoporous pp-HDFA nanospheres. Figure 6.5(a) shows the FESEM image of the magnetic mesoporous pp-HDFA nanospheres obtained from the corresponding porous nanospheres (described in Figure 6.2(b)). The TEM image of Figure 6.5(b) shows the PtFe nanoparticles evenly adsorbed inside the pores of the pp-HDFA nanosphere. The PtFe nanoparticles are about 3 nm in size. Comparison of the VSM results of the mesoporous pp-HDFA nanospheres prior to and after adsorption of the PtFe nanoparticles (as shown in Figure 6.6) reveals that there is no magnetic response from the mesoporous pp-HDFA nanospheres prior to adsorption of the PtFe nanoparticles. After magnetization, the porous fluoropolymer nanospheres exhibit a normal  $M-H$  loop, indicating that the magnetization direction of the adsorbed PtFe domains can be reversed through induction by the applied magnetic field direction. The magnetic moment of a 250-nm thick layer of nearly monodispersed nanospheres in an

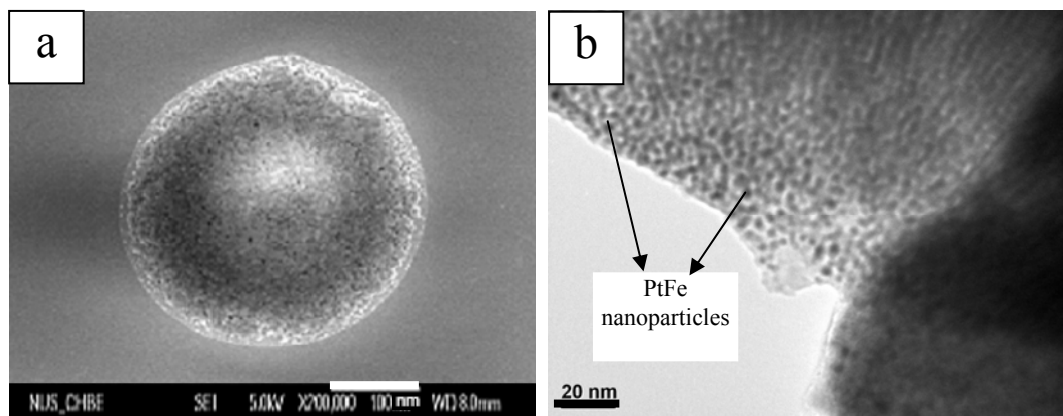


**Figure 6.5** Images of a porous pp-HDFA nanosphere (from 5 s of plasma etching of the solid nanosphere) with adsorbed magnetic PtFe nanoparticles: (a) FESEM image, (b) TEM image. The scale bars in (a) and (b) are 100 and 20 nm, respectively.

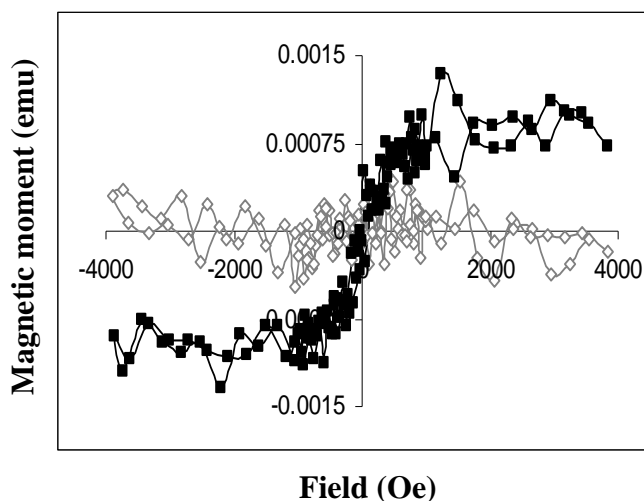


**Figure 6.6** VSM analysis results of a 250-nm thick layer of the magnetized pp-HDFA nanospheres on a  $5 \times 3 \text{ mm}^2$  Si substrate. The open symbol (-◇-) and solid symbol (-■-) stand for the magnetization of the mesoporous pp-HDFA nanospheres prior to and after adsorption of the PtFe nanoparticles, respectively.

area of  $5 \times 3 \text{ mm}^2$  on the Si substrate is about 0.001 emu. The EDX analysis results in

Table 6.3 clearly show that both Fe and Pt are present in the mesoporous pp-HDFA

nanospheres. Therefore, the EDX results are consistent with the VSM and XPS results. It is noted that the [F]/[C] ratio and oxygen content from the EDX results differ somewhat from those determined by XPS. The discrepancies can probably be attributed to the difference in sampling depth of the two techniques and some effects of the surfactants, which adsorbed on PtFe nanospheres, onto the porous pp-HDFA nanospheres. The magnetic nanoporous nanospheres are of importance in targeting, delivery and controlled release of drugs [Ozin, 1992; Huo et al., 1997], while the surface-adsorbed PtFe nanoparticles on the mesoporous pp-HDFA nanospheres are potentially useful as catalytic systems [Steen et al., 2001; Van Roon et al., 2005].

**6.4 Conclusions**

A controlled approach to the preparation of mesoporous fluoropolymer nanospheres via one-pot plasma polymerization and dry etching was described. The porosity and pore size of nanostructured polymer nanospheres could be controlled by the duration of Ar plasma etching and plasma RF power. The dielectric constant of films of these assembled mesoporous fluoropolymer nanospheres is as low as 1.7. Surface-modified magnetic nanoparticles of about 3 nm in size could be adsorbed on the mesoporous fluoropolymer nanospheres to produce the magnetic porous nanospheres. The present strategy of one-pot plasma polymerization and etching for the preparation of porous fluoropolymer particles can be extended to other monomers to produce a variety of functional nanoporous polymer nano-/microspheres and films.

**CHAPTER 7**

**STERICALLY ALIGNED FLUOROPOLYMER  
NANOSPHERES FROM SELF-ASSEMBLY DURING PLASMA  
POLYMERIZATION**

## 7.1 Introduction

Organic nanostructures play an important role in emerging and advanced technologies [Verveer et al., 2000; Takizawa et al., 2000; Valsesia et al., 2004; Ibn-Eihaj et al., 2001]. Self-assembly arising from non-covalent molecular interactions is a powerful tool for obtaining well-defined organic nanostructures [Lehn, 2001; Boal et al., 2000; Rosei et al., 2002; Percec et al., 1998]. Self-assembly offers two distinctive advantages: process simplicity and potential to overcome fundamental and economic limitations of conventional lithography-based fabrication [Park et al., 1997; Lammertink et al., 2000]. So far, the fabrication of regular organic nanostructures by self-assembly has been achieved mainly in two ways: generation in the liquid phase [Yao et al., 2004; Zhang et al., 2004; Serizawa et al., 2004; Böltau et al., 1998] and synthesis via liquid phase transfer [Schäffer et al., 2000; Yin et al., 2001]. It is known that in the liquid phase, some fabricating processes are not feasible. On the other hand, the method of liquid phase transfer may require a temperature which is higher than the glass transition temperature ( $T_g$ ) of the material [Liu et al., 2002]. Therefore, there is a need to find a simple method for creating organic nanostructures by self-assembly in a dry phase ambience and at low temperature ( $< 50^\circ\text{C}$ ). Self-assembly in a dry phase ambience is also a useful tool to elucidate the interactions among organic molecules because of the absence of solvent effects. However, in a dry process at low temperature, it is difficult to control the self-assembly of organic molecules due to the fact that the effect of gravity is usually much larger than the interactive force among molecules.

In this work, we present a general self-assembly strategy for depositing sterically aligned fluoropolymer nanospheres and nanopatterns from the vapor ambience during plasma

polymerization. Not only does the self-assembly process meet the requirements of a dry process at a low temperature, it can also be extended to other polymer systems and nano-/microstructures. When plasma polymerizations were carried out under high glow discharge power ( $\geq 400$  W), the morphology of the deposited fluoropolymer films could be varied from self-assembled 2D nanoparticle chains and nanoparticle bars, to self-assembled 3D nanoparticle pyramids, through decreasing the initial monomer concentration in the plasma chamber and adjusting the glow discharge time. The sizes of nanoparticles in the nanostructures ranged from 15 to 40 nm. These nanostructures possess some special properties, such as abilities to behave as substrates in the adsorption of CO<sub>2</sub>, O<sub>2</sub>, etc.

## **7.2 Experimental Section**

### **7.2.1 Materials and Process**

Although plasma polymerization is currently limited to the fabrication of condensed or porous polymer films, it possesses the basic requirements for fabricating regular and nanostructured materials via self-assembly of the deposited polymers. In the process of plasma polymerization, there are radicals, cations, and anions produced at same time. The electric field present can act as an induction field, which can be used to reduce the effect of gravity, for example. In order to generate very light nanoparticles via high plasma energy per unit monomer molecules, a high RF power of no less than 400 W was applied during each plasma polymerization. The monomer 3,3,4,4,5,5,6,6,7,7,8,8,9,9,10,10,10-heptafluorodecyl acrylate or HDFFA was also chosen for plasma polymerization due to its high boiling point (90°C/4 mmHg, a high boiling point monomer with its low vapor pressure under ambient condition was expected to produce a low monomer concentration in the plasma chamber at room temperature). Hydrogen-terminated Si or H-Si wafers were chosen to act as the crystal induction substrates because the H-Si bonds on the substrate surface are aligned along the crystal epitaxis line of the Si (100) wafer.

### **7.2.2 Preparation of H-Si Wafers**

Si(100) wafers were cut into chips of 15 × 20 mm in size, with the sides parallel to the crystal epitaxis line of the Si(100) substrate. The Si chips were immersed in a 10% HF solution for 5 min, followed by rinsing with distilled water and then dried in a stream of purified argon.



### **7.2.3 Plasma Polymerization and Characterization of pp-HDFA Polymers**

The methods and procedures of plasma polymerizations and characterization of pp-HDFA polymers are similar to those stated in Sections 3.2.2, 3.2.3, and 4.2.2.

## 7.3 Results and Discussion

### 7.3.1 Three Scenarios of Plasma Deposition

Plasma polymerization is a well-known mean for depositing bulk polymer films. The three scenarios associated with the present approach to deposit self-assembled nanostructures during plasma polymerizations are shown schematically in Figure 7.1. Depending on the plasma density (viz., the concentration of macromolecular ions, radicals and fragments) in the glow discharge, there are three scenarios under which depositions can result in distinctly different film morphologies during the polymerization and deposition process carried out with the H-Si wafer surfaces. When the flow-rate of carrier gas (thus, the monomer flow-rate) and the plasma parameters are fixed, the plasma density is determined by the initial monomer concentration fed into the glow discharge. From the investigation of HDFA polymerization, changing the initial monomer charging time prior to plasma ignition was found to be effective in controlling the monomer concentration, in comparison to changing the system pressure and other parameters. Thus, the three scenarios were achieved mainly by varying the initial monomer charging time, and to a lesser extent the plasma parameters.

**A. Deposition of Bulk or Porous Films.** In the first scenario of the deposition process in Figure 7.1, a high concentration of fragments, radicals and ions is produced when the initial amount of monomer charged into the system is in excess of the amount to be completely polymerized. Energy per unit monomer molecule under a given RF power is low. Prior to deposition on the substrate, some of the fragments aggregate to form larger particles, partially through post polymerization by the residual radicals.

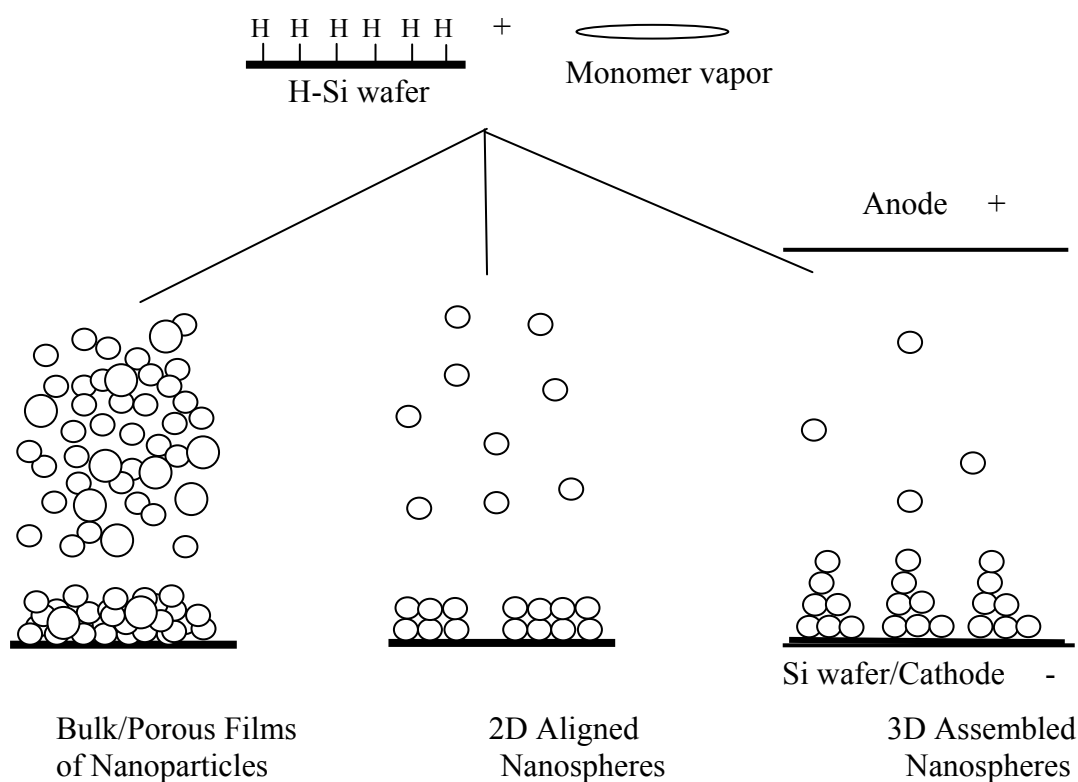


**Figure 7.1** Schematic of illustration of plasma deposition under different glow discharge conditions.

The particles can further combine and absorb other smaller fragments or un-reacted monomer molecules to form even larger and coarser particles. Some of the fragments and ions are deposited directly on the wafer surface as well. The deposited polymer films usually comprise less well-defined micro-/nano-structures of different sizes. The majority of the reported films from plasma polymerizations and deposition are of this nature. In this work, when the concentration of HDFFA monomer was at a high level by means of maintaining a system pressure of 13 Pa and the carrier gas flow-rate of 30 sccm, and by providing 60 s of monomer feed time prior to the initiation of the glow discharge, non-structured porous pp-HDFFA films (Figure 7.2(a)) were deposited under a plasma

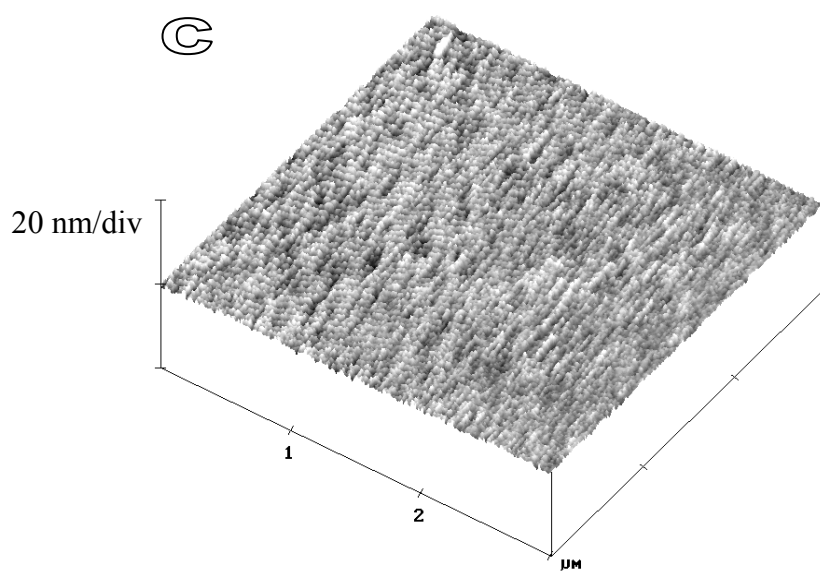
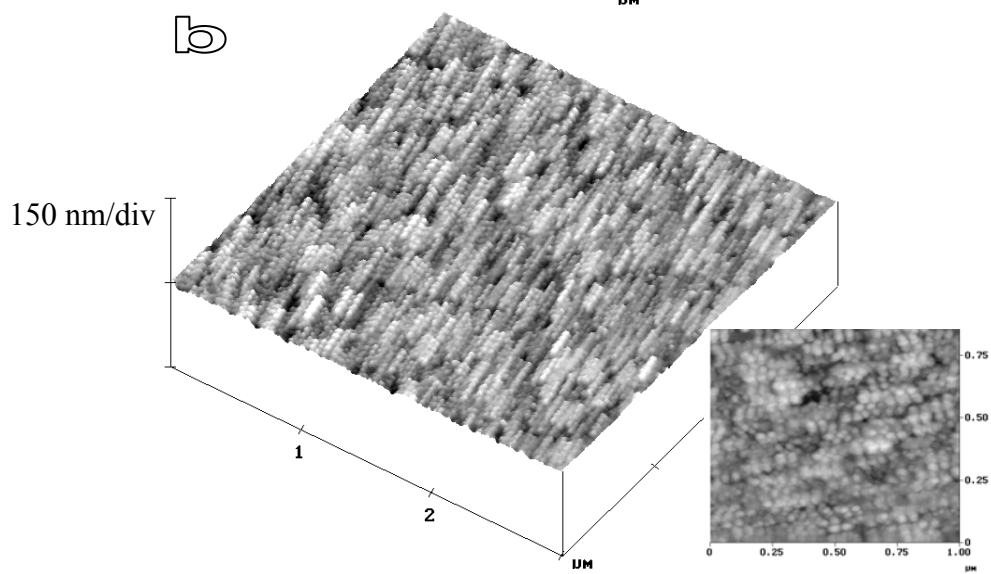
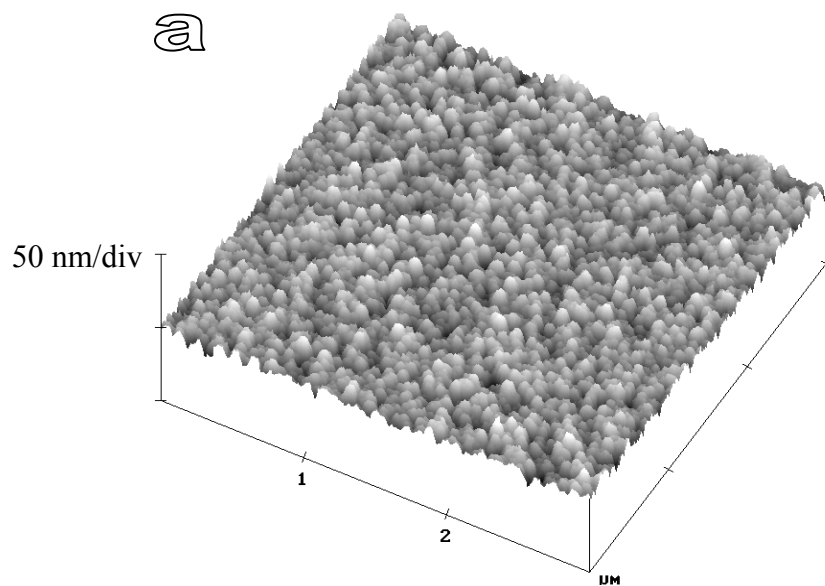


**Figure 7.2**  $3 \times 3 \mu\text{m}$  AFM image of (a) the pp-HDFA porous film deposited under a pressure of 13 Pa, RF power of 400 W, and glow discharge time of 60 s. (b) and (c) 2D (linearly) aligned pp-HDFA nanospheres chains deposited under a pressure of 53 and 107 Pa, respectively, RF power of 400 W, and plasma glow discharge time of 60 s. The plasma chamber was charged with the HDFA monomer for 60, 30, and 30 s for (a), (b), and (c), respectively, prior to plasma polymerization.

polymerization time of 60 s and RF power of 400 W.

**B. Deposition of Planar 2D (Linearly) Aligned Fluoropolymer Nanospheres.** In the second scenario of the deposition process in Figure 7.1, the initial density of active species and fragments in the glow discharge chamber is controlled to be just sufficient to form particles of about the same size. When the particles are eventually deposited on the H-Si surface, the nanoparticles contact the wafer surface and assemble under the induction of H-Si bonds. As the H-Si bonds are arranged along the epitaxial crystal direction of the H-Si(100) wafer, the deposited nanoparticles become linearly aligned. The density of the linearly aligned nanoparticles depends on the instantaneous amount of polymerized particles. Sufficient numbers of particles will form continuous chains of particles across the entire wafer surface and fully cover the wafer surface. The AFM image in Figure 7.2(b) confirms this postulation. Under a system pressure of 53 Pa and RF power of 400 W at room temperature, orderly-aligned particles (particle chains) have been successfully deposited on a clean H-Si wafer surface during the 60 s of plasma glow discharge, after 30 s of initial monomer charging into the plasma chamber. Comparison of the AFM image and the wafer crystal direction indicated that the orientation of particle chains was along the epitaxial crystal direction of the H-Si(100) wafer. Upon varying the scanning angle of the AFM image, the orientation of the particle chains remained

unchanged. Thus, the self-assembled nanoparticle chains were the result of induction by the linear alignment of the H-Si bonds on the wafer surface, instead of the effect of the AFM tip during imaging. The average diameter of the particle size in Figure 7.2(b) is about 30 nm. The particle size in the particle chain varies with the system pressure when other polymerizing parameters are kept constant. It is known that higher system pressure, which results in a lower relative monomer concentration in the chamber, will lead to smaller particle size [Zong et al., 2007]. Linearly aligned nanoparticle chains with an average particle diameter of about 15 nm, as shown in Figure 7.2(c), were obtained on an H-Si wafer when the system pressure was increased to 107 Pa during plasma polymerization.

On the other hand, when the initial monomer concentration in the glow discharge chamber was decreased by reducing the monomer feed time prior to the onset of glow discharge, with the corresponding shortening of the plasma glow discharge time in order to keep the initial energy per unit molecule approximately the same as that used for the deposition of nanoparticles in Figure 7.2(b), the density of the particle chains was reduced. The AFM images in Figures 7.3(a) and 3(b) show that individual 2D linearly assembled nanoparticle bars of 100 – 200 nm in length were generated after 15 s of glow discharge, when the discharge RF power was kept at 400 W, pressure at 53 Pa, and the initial HDFFA monomer charging time prior to the glow discharge was further reduced to 20 and 15 s, respectively. The  $1 \times 1 \mu\text{m}$  AFM image in the inset of Figure 7.3(b) (with the substrate rotated by about  $90^\circ$ ) reveals that the particle bars consist of nanoparticles of about 40 nm in diameter. The aligning direction of the particle bars had changed by  $90^\circ$

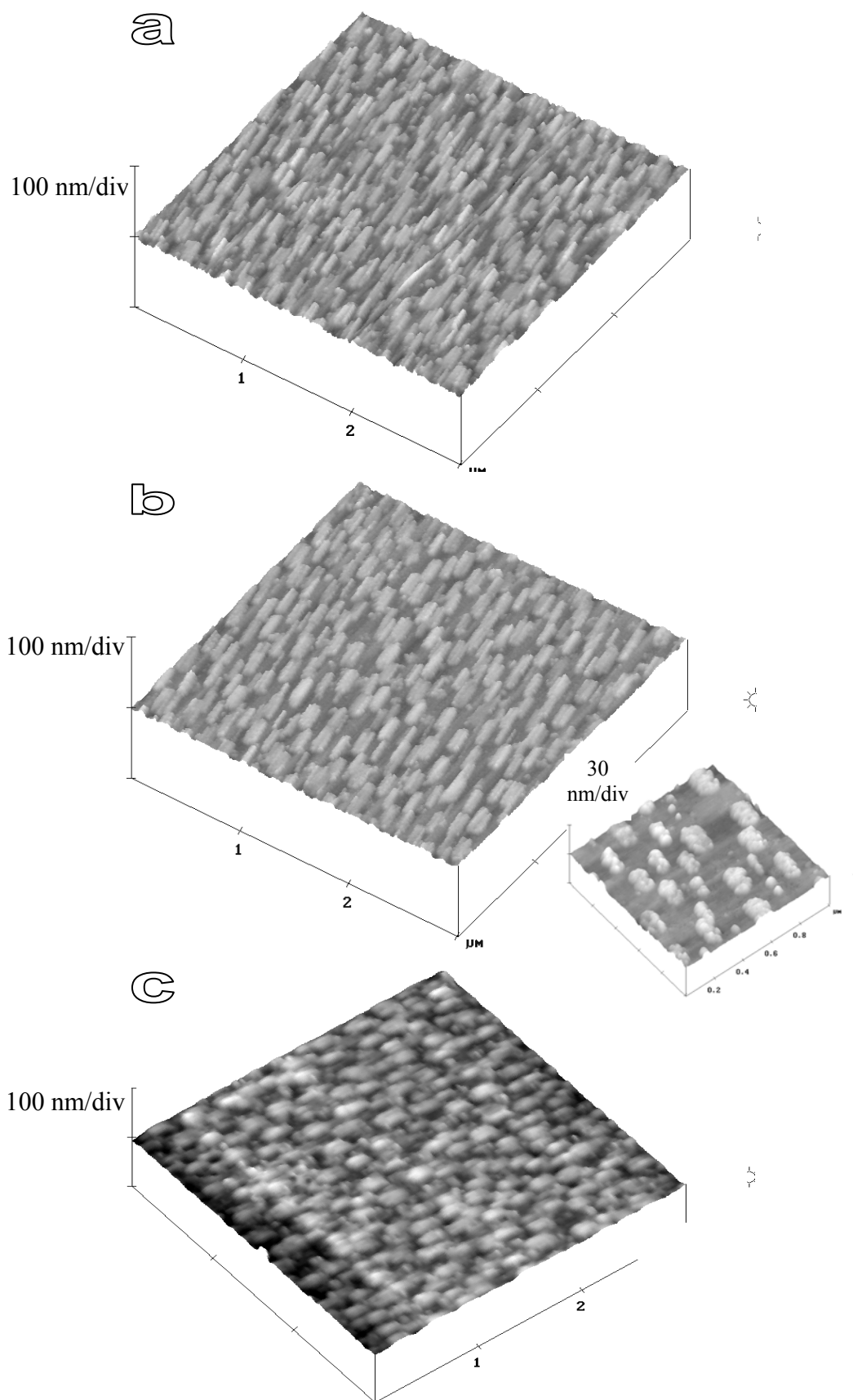


**Figure 7.3**  $3 \times 3 \mu\text{m}$  AFM image of the 2D aligned pp-HDFA particle bars deposited under a pressure of 53 Pa and RF power of 400 W, with glow discharge time of 15 s for (a) and (b) (one round deposition), and (c) (two rounds deposition). The plasma chamber was feed with the monomer for 20, 15, and 15 s, respectively, before polymerization. The inset of (b) is a  $1 \times 1 \mu\text{m}$  AFM image of the wafer rotated by about  $90^\circ$  before scanning while keeping the scanning direction of the tip unchanging.

with the rotated substrate, although the scanning direction of the AFM tip remained unchanged. The density of these particle bars can be improved by repeating plasma polymerization twice while keeping the parameters of plasma polymerization and monomer concentration constant. Figure 7.3(c) shows the AFM image of the particle-bar generated from repeated plasma polymerization and deposition under conditions similar to that used to deposit the particles in Figure 7.3(b).

**C. Deposition of 3D Assembled Pyramids of Nanospheres.** Based on the second scenario, when the plasma density at the onset of polymerization was further reduced to a very low level by further decreasing the initial monomer concentration in the chamber, only sparsely and randomly distributed spherical particles of about the same size were deposited on the H-Si surface initially, as shown in Figure 7.4(a). Under this condition, continuous production and deposition of particles (using the monomer in the carrier gas stream) on the H-Si wafer surface by prolonging the glow discharge time will give rise to the third scenario in Figure 7.1. Because of the small amount of molecules present initially (from the reduction in the initial monomer charging time) and their prolonged exposure to plasma power, high energy per monomer molecule will decompose all the molecules into cation and anion radicals in the glow discharge chamber. The induction effect of the electric field during plasma polymerization becomes important and will



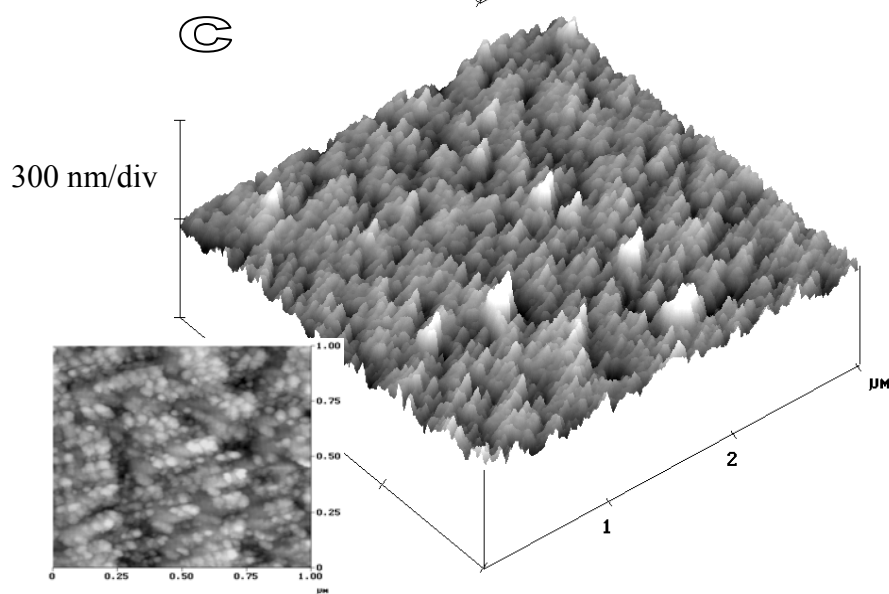
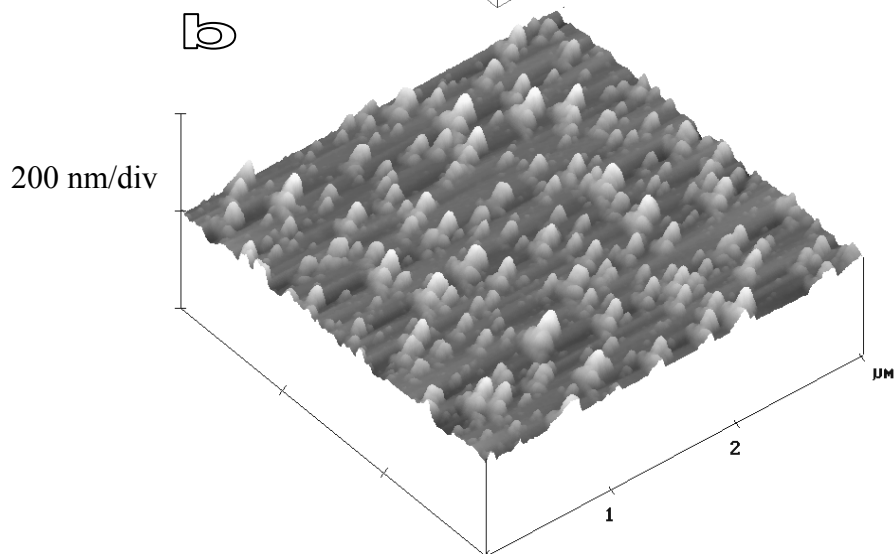
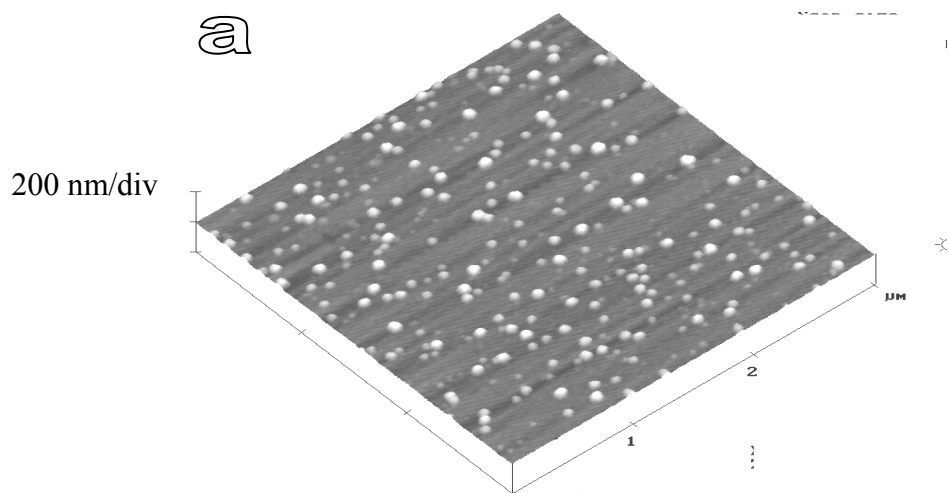


**Figure 7.4**  $3 \times 3 \mu\text{m}$  AFM images of the pp-HDFA particles deposited under a pressure of 53 Pa and RF power of 400 W with glow discharge time of (a) 5, (b) 15, and (c) 40 s, respectively. The plasma chamber was initially charged with the monomer for 5 s. The inset of (c) is a  $1 \times 1 \mu\text{m}$  AFM image, which shows pyramids of  $\sim 50$  nm nanoparticles.

result in oriented particle deposition in the vertical direction. Longer deposition time can generate taller nanostructures in some instances. The particles became charge-free once the RF power was cut off. Nevertheless, self-assembly in the vertical direction along the direction of the electric field must overcome the gravitational effect, which is comparatively less important for self-assembly in the horizontal direction. It is known that even in the liquid phase, it is difficult to form regular organic molecular nanostructures in the vertical direction due to the gravitational effect [Vekilov et al., 1996]. In order to decrease the gravitational effect, the particle size had been reduced to below 60 nm during polymerization, under an ultra-low monomer concentration and the high RF power of  $\geq 400$  W.

Figures 7.4(b) and 7.4(c) show the vertically (3D) assembled nanoparticles prepared under the induction of the electric-field during plasma polymerization and deposition at the pressure of 53 Pa, RF power of 400 W, an initial monomer charging time of only 5 s, and plasma glow discharge time of 15 and 40 s, respectively. In comparison with the previous scenarios, it can be concluded that for plasma polymerization, the initial morphology of the deposits is governed to some extent by the initial monomer concentration in the system. Prolonging the glow discharge time (and thus the monomer feed) led to the growth of 3D nanoparticle pyramids from the sparsely distributed particles. In general, the third scenario of pp-HDFA particle deposition on the H-Si

surface was controlled by a balance in intermolecular force, molecule-substrate interaction [Lopes et al., 2001], electric field and gravitational effect. Molecule-substrate interaction and gravity effect will result in pp-HDFA particles aligning on the planar surface along the epitaxial crystal direction of the H-Si(100) wafer. The combined interactive forces during particle deposition have produced the unique pyramid morphology. The AFM images in Figures 7.4(b) and 7.4(c) show the self-assembled pp-HDFA nanoparticle pyramids. The  $1 \times 1 \mu\text{m}$  AFM image (inset of Figure 7.4(c)) clearly shows that the pyramids originate from piles of nanoparticles with a diameter of  $\sim 50 \text{ nm}$ .

Further investigation showed that the nanoparticle pyramids could also be produced under a higher glow discharge RF power of 500 W, a reduced system pressure of 13 Pa, and a longer monomer charge time of 10 s. The nanoparticle pyramids also grew from an initial few randomly distributed spherical particles, upon prolonging the glow discharge time.

### **7.3.2 Properties and Applications**

It is known that fluoropolymers prepared via plasma polymerization always possess excellent physicochemical properties, such as low dissipation factor, low dielectric constant, good chemical stability, and high thermal stability [Fu et al., 2003]. These advantages allow the fluoropolymers to be used in some specific areas, such as in low  $\kappa$  fillers and pigments, etc [Yang et al., 2003; Zong et al., 2007]. In order to further explore the applications of the self-assembled pp-HDFA fluoropolymer particles, their nanostructures were characterized and further investigated. Table 7.1 shows the characterization results of the three types of pp-HDFA nanostructures, which take the

**Table 7.1** Physicochemical properties of the pp-HDFA nanostructures

Sample	Fig. 7.2(a)	Fig. 7.2(b)	Fig. 7.3(b)	Fig. 7.4(c)
Nanostructure type	Porous film	Particle chains	Particle bars	Particle pyramids
Monomer feed time (s)	60	30	15	5
Glow discharge power (W)	400	400	400	400
Glow discharge pressure (Pa)	13	53	53	53
Glow discharge time (s)	60	60	15	40
Particle size <sup>a)</sup> (nm)	78 ± 5	30 ± 3	33 ± 4	52 ± 5
Surface roughness $R_a$ (nm)	3	1	2	10
Water contact-angle				
Advancing $\theta_A$	70 ± 3°	55 ± 2°	64 ± 2°	75 ± 3°
Receding $\theta_R$	68 ± 3°	52 ± 2°	62 ± 2°	72 ± 3°
[C:F:O] ratio <sup>b)</sup>	0.40 : 0.30 : 0.30	0.41 : 0.27 : 0.32	0.44 : 0.27 : 0.29	0.42 : 0.20 : 0.38
[C:F:O] ratio After 2 days in O <sub>2</sub>	0.39 : 0.26 : 0.35	0.39 : 0.24 : 0.37	0.43 : 0.25 : 0.32	0.40 : 0.15 : 0.45
[C:F:O] ratio After 2 days in CO <sub>2</sub>	0.42 : 0.24 : 0.34	0.42 : 0.24 : 0.34	0.45 : 0.24 : 0.31	0.43 : 0.17 : 0.40

<sup>a)</sup> Average of 100 particles on the surface.

<sup>b)</sup> The theoretical [C : F : O] ratio for the HDFA monomer is 0.39 : 0.55 : 0.06.

shapes of nanoparticle chains, bars, and pyramids. The normal porous pp-HDFA film was also characterized and its properties are also listed in Table 7.1 for comparison. The data in the Table 7.1 show that the diameters of pp-HDFA nanoparticles in the self-assembled nanostructures of particle chains (depicted in Figure 7.2(b)), bars (in Figure 7.3(b)), and pyramids (in Figure 7.4) are from ~30 to 52 nm, which are much smaller than that (~110 nm) of pp-HDFA nanoparticles in the common-deposited porous film (in Figure 7.2(a)).

The water-contact-angles of the nanostructured pp-HDFA are lower than  $90^\circ$ . Hence they can be used as another type of fluoropolymer substrates as compared to the fluoropolymers possessing high water-contact-angle ( $> 90^\circ$ ) [Feldkamp et al., 2006]. The XPS-derived [C:F:O] ratios in the Table 7.1 illustrate that the fluorine ratios in the plasma polymerized pp-HDFA decreased in comparison to original HDFA monomer. It is because some of the HDFA monomer molecules are fragmented into small  $CF_x$  and F fragments, which might be swept away by the carrier Ar gas stream during and after the high energy of plasma polymerization.

The data in Table 7.1 also show the further investigation results on gas adsorption by the as-synthesized pp-HDFA nanostructures. It indicates that these nanostructures are good adsorption materials for  $O_2$  and  $CO_2$ . During the experiments of gas adsorption, the Si wafers with pp-HDFA nanostructures were cut into pieces after the plasma polymerization, then separately stored in  $O_2$ ,  $CO_2$ , air,  $N_2$ , and Ar for 2 days before XPS measurement. Figure 7.5 shows the changes of chemical composition in the 3D particle-pyramid nanostructures shown in Figure 7.4(c) after  $CO_2$  and  $O_2$  gas adsorption. In Figure 7.5(a), the C 1s core-level XPS spectrum of the pristine (as-synthesized) pp-HDFA nanoparticle pyramids is curve-fitted with seven different carbon environments:  $\underline{C}$ -C/  $\underline{C}$ -H (hydrocarbon) at the binding energy of 285.0 eV,  $\underline{C}$ - $CF_x$  (hydrocarbon adjacent to a fluorocarbon group) at 285.4 eV,  $\underline{C}$ -O at 286.6 eV,  $\underline{C}=\underline{O}$  at 287.8 eV,  $\underline{C}F$  or  $O-\underline{C}=\underline{O}$  (ester or carboxylic acid) at 289.4 eV,  $\underline{C}F_2$  at 291.3 eV, and  $\underline{C}F_3$  at 293.4 eV [Beamsom and Briggs, 1992; Teare et al., 2002]. The spectra in Figure 7.5(b) show that for the pyramid sample stored in  $CO_2$ , the  $O-\underline{C}=\underline{O}$  peak intensity increases substantially in comparison to that of original particle pyramid sample of Figure 7.5(a), consistent with

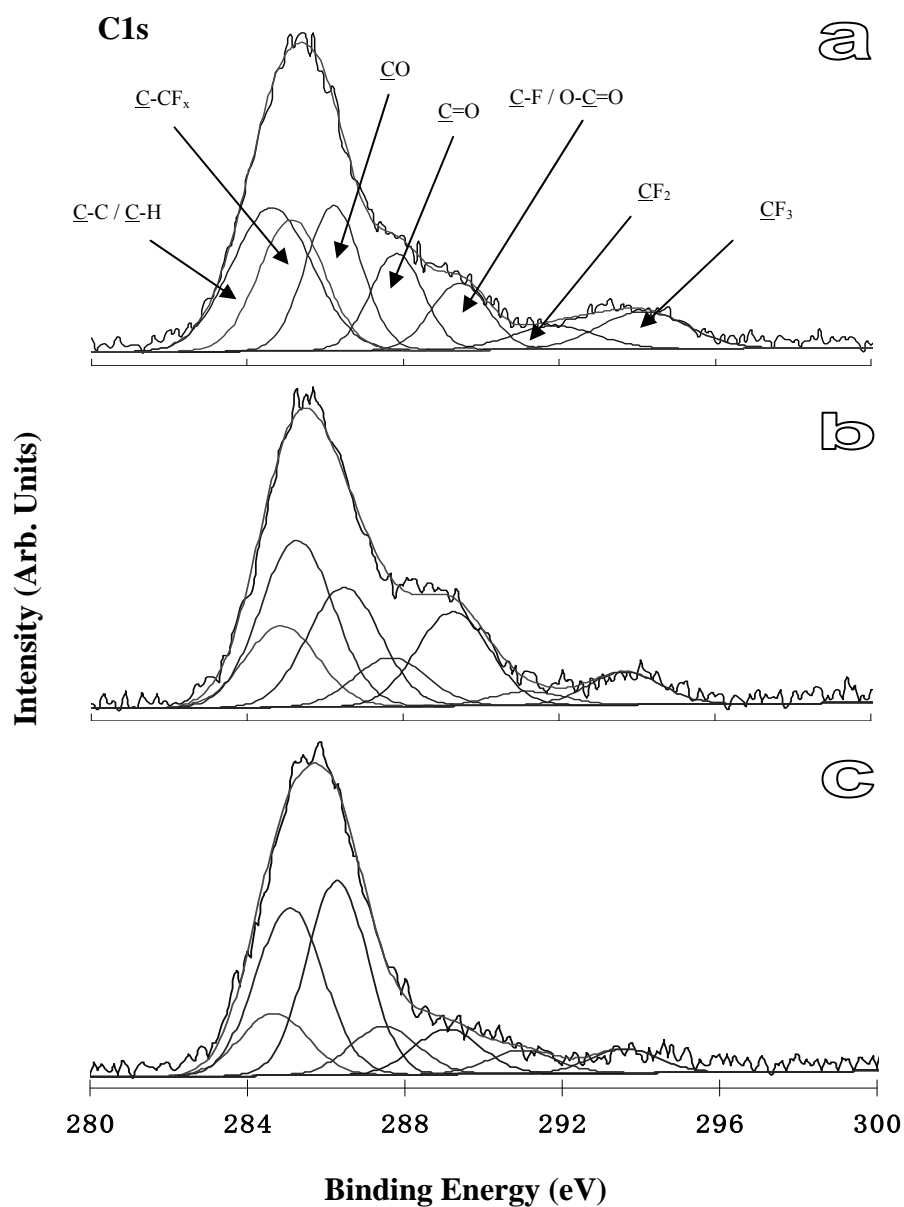


**Figure 7.5** C 1s core-level XPS spectra of the pp-HDFA nanoparticle pyramids (a), and the nanoparticle pyramids after storing in  $\text{CO}_2$  (b) and  $\text{O}_2$  (c), respectively, for two days.

the increase of C and O contents in the polymer (depicted in Table 7.1). For the pyramid sample stored in  $\text{O}_2$ , the C 1s core-level spectra in Figure 7.5(c) shows a significant increase in the  $\underline{\text{C}}\text{-O}$  peak intensity while a decrease is observed for most of the other

group peaks (including  $\underline{\text{C}}=\text{O}$ ,  $\text{O}-\underline{\text{C}}=\text{O}$ , and fluorine-contained groups). As a result, the O content increased, which leads to the decrease in the relative proportion of C and F ratio in the pyramid polymer. The spectrum in Figure 7.5(c) also reveals that the adsorption of  $\text{O}_2$  by the pp-HDFA nanostructures favors the formation of C-O species instead of C=O and O-C=O species. In addition, XPS results also showed that the  $\underline{\text{C}}-\text{O}$  and  $\text{O}-\underline{\text{C}}=\text{O}$  peak intensities increased after the pyramid sample was exposed to air for two days. It is because there are a lot of  $\text{O}_2$  and some  $\text{CO}_2$  existing in the atmosphere. However, further XPS testing results showed that the chemical compositions remained nearly constant for the samples stored in  $\text{N}_2$  and Ar. This implies that there is no adsorption of  $\text{N}_2$  and Ar by the pp-HDFA nanostructures. Based on these results, the pp-HDFA nanostructures synthesized from plasma polymerization can selectively adsorb gases. Further XPS examinations indicated that other pp-HDFA particle nanostructures have similar property as the nanoparticle pyramids in selective gas adsorption, which are shown in Table 7.1 as well.

**7.4 Conclusions**

A controlled methodology for depositing sterically ordered 2D and 3D self-assembled fluoropolymer nanoparticles via plasma polymerization and deposition is described. The well-defined polymer nanospheres were based on the controlled deposition conditions, such as the critical control of the initial plasma density, substrate, and choice of a high input RF power. The self-assembled polymer nanostructures may have numerous applications, such as for in selectively adsorbing gases. Since self-assembly of organic molecules during deposition from a dry vapor ambience can be readily achieved, it is believed that the present strategy has the potential to be used with other monomers for producing more well-defined functional organic nanostructures for nano-level electronics.



**CHAPTER 8**

**0 - 3 DIMENSIONAL CONDUCTIVE AND MAGNETIC  
NANOSTRUCTURES PREPARED FROM COLLOIDAL  
POLYPYRROLE DISPERSIONS**

**8.1 Introduction**

Electroactive polymers have been widely explored for applications in batteries, capacitors, actuators, electrodes, separation membranes, organic light-emitting-devices (OLEDs), printed circuit board (PCB), touch screens, and others [Skotheim et al., 1997; Rupprecht and Epstein, 1999]. In these applications, electroactive polymers of different properties, structures, and morphologies are required [Skotheim et al., 1997; Rupprecht and Epstein, 1999; Heeger, 2001]. Hence simple methods for materials processing and device fabrication will be desirable. Conductive polymers are also potentially useful in the fabrication of nano-devices and in nano bio-technology [Heeger, 2001; Kumar and Sharma, 1998]. In the area of nano-device fabrication, 0 - 3D nanostructures are required as well [Kumar and Sharma, 1998; Winther-Jensen et al., 2002; Kumar and Sharma, 1998]. It is known that polymer solutions and melts can be readily cast or processed into various shapes and sizes, including nanostructures. However, many of the electroactive polymers of importance, such as polypyrrole, polyphenylene, polythiophene, and polyacetylene, are not melt processable and are generally insoluble in common organic solvents [Wessling, 2005]. Therefore, it remains a challenge to prepare stable conductive polymer solutions and melts for device fabrication and feature design [Haba et al., 2000; Pich et al., 2002; Marcilla et al., 2006; Lu et al., 2004; Saravanan et al., 2006].

In comparison to other conductive polymers, polypyrrole possesses some unique properties, such as low toxicity, excellent environment stability, high electrical conductivity, interesting redox property, and ease of preparation [Kang et al., 1987; Qin et al., 2006]. PPY has been widely explored for applications in advanced technologies [Skotheim et al., 1997; Rupprecht and Epstein, 1999; Heeger, 2001; Lu et al., 2004].

Although different features of pyrrole polymers synthesized by chemical or electrochemical oxidative polymerization are largely intractable [Zhang and Wan, 2003; Hulvat and Stupp, 2003], non-aqueous colloidal PPY dispersions and aqueous PPY-magnetite particle dispersions can be prepared by other and our groups [Zhang and Wan, 2003; Grenier and Pisula, 2006; Wuang, et al., 2007].

In this work, we adopt a simple approach to the preparation of relatively much more stable conductive PPY colloidal dispersions. In-situ oxidative polymerization of pyrrole by  $\text{FeCl}_3$  oxidant was carried out in an aqueous solution of sodium dodecyl benzene sulfonate (NaDS) and poly(vinyl alcohol) (PVA) according to a previous method [Wuang et al., 2007] of our group with some modifications. The as-prepared aqueous PPY dispersions can be used to fabricate unique nanostructures, ranging from 0D nanoparticles, 1D nanowires, and 2D nanofilms to 3D nanoflowers, and nanosensors by casting, coating, and spraying of the colloidal PPY dispersion. By coupling the metal-sputtering and solution-treatment processes, conductive nanospheres were converted to conductive PPY core-magnetic CoFe shell nanoparticles, hollow magnetic CoFe nanospheres, and conductive PPY microspheres with magnetic CoFe handles.

## 8.2 Experimental Section

### 8.2.1 Synthesis of Stable Conductive Colloidal PPY Dispersions

Pyrrole monomer (> 98%, C<sub>4</sub>H<sub>5</sub>N, Merck-Schuchardt, Schuchardt, Germany), was used for the preparation of aqueous PPY dispersions via oxidation by FeCl<sub>3</sub>. PVA (average MW 25,000, 88%, Sigma-Aldrich Company, St. Louis, MO) and NaDS (80%, SIGMA Chem. Co., St. Louis, Mo) were used as stabilizer-surfactants in the reaction. In the preparation of PPY colloidal dispersion, a 10 ml of aqueous mixture of pyrrole (0.005 to 0.1 M), NaDS (0.001 to 0.005 M), and PVA (0.001 to 0.015 M) was prepared under vigorous stirring. The reactant mixture was added gradually into 10 ml of 0.3 M (or higher) FeCl<sub>3</sub> aqueous solution in an ice-bath under vigorous stirring. After stirring for 2 h, the mixture was transferred into an ultrasonic bath for 20 min, and was stirred continuously for another 20 h. A dark green PPY dispersion was obtained. The detailed procedure has been illustrated in a previous publication of our group [Wuang et al., 2007]. But in the current work, both PVA and NaDS surfactants were simultaneously used during the synthesis of PPY dispersion and without the presence of Fe<sub>3</sub>O<sub>4</sub> nanoparticles.

### 8.2.2 Conversion of Aqueous Colloidal PPY Dispersion into 0 - 3D Nanostructures

0D nanospheres were prepared by adding the dark green PPY colloidal dispersion dropwise into a ketone solvent, such as acetone, butanone, etc., under stirring in an ice-bath. The black PPY nanospheres were collected by centrifugation at a speed of 9000 rpm for 15 min, followed by acetone-rinsing and drying under reduced pressure. Small nanospheres (down to ~ 20 nm) were prepared by diluting the PPY dispersion with distilled water before addition into acetone under vigorous stirring. 1D nanowires were prepared by casting the PPY dispersion into the nanopores of an alumina membrane filter

(Whatman Anodisc 25, Maidstone, England), or injecting the PPY dispersion through the nanopores of the alumina membrane filter into acetone solution without stirring. The membrane filter has uniform straight-through nanochannels with diameters ranging from 150 to 250 nm and a thickness of 60  $\mu\text{m}$ .

2D PPY porous film was fabricated via sprinkling a mixture of acetone and the PPY dispersion (at a volumetric ratio of 2 : 1, thoroughly mixed by vigorous shaking) onto Si wafer, followed by drying under reduced pressure. 2D planar film on Si was prepared via spin-coating the PPY dispersion on the Si wafer at speeds of 200 ~ 4000 rpm for 30 s, followed by slow drying in air. The thickness of the film was controlled by the spinning speed. 3D nanoflowers were prepared by sprinkling a mixture of PPY dispersion and water (at a volumetric ratio of 1 : 2) onto a Si wafer, followed by cooling in liquid  $\text{N}_2$  and drying under reduced pressure.

### 8.2.3 Fabrication of Nanostructured Magnetic Spheres

*Magnetic CoFe Shell-PPY Core Nanospheres* – The as-synthesized conductive PPY nanospheres were dispersed into acetone under vigorous stirring in an ultrasonic bath. The dispersion was spread onto a clean Si wafer, which was placed on a floating wooden plate in an ultrasonic bath. The nanospheres dispersed into a loose monolayer under ultrasonic agitation after the evaporation of acetone. After further drying of the sample under reduced pressure, the top sides of the nanospheres were sputter-deposited with a thin layer of magnetic CoFe nanofilm (10 ~ 20 nm) in a magnetron sputtering system (ATC model, AJA International, Inc., Scituate, MA) at room temperature. The thickness of CoFe film was controlled by the sputtering time. The magnetic nanospheres were

subsequently lifted up, under an upward magnetic field ( $\sim 300$  Oe), and deposited on the under-side of a Si wafer placed directly above. The bottom parts of the nanospheres were then sputter-deposited with 10 - 20 nm of CoFe film as well.

*Hollow Magnetic CoFe Nanospheres* – The loosely-distributed PPY nanospheres were deposited with a magnetic multilayer film of Au/CoFe/Au ( $\sim 2/7/2$  nm in thickness) via evaporation in a vacuum electron beam evaporator (Edwards Auto 306, Ceramisis Ltd., London, England). Then the magnetic nanospheres were lifted up and deposited on the under-side of another Si wafer under a magnetic field. The structure under magnetic field was transferred into an ultrasonic water bath for 5 h to allow the PPY-surfactant core of the magnetic nanospheres to dissolve into water. Finally, the nanospheres were rinsed with distilled water and dried in a vacuum oven.

*PPY Microspheres with Magnetic Handles* – A suspension of PPY nanospheres in acetone was spread onto a Si wafer by spin-coating at a speed of 100 rpm for 20 s. The PPY nanospheres on the Si wafer were further dried under reduced pressure after the evaporation of acetone. A thin CoFe layer of 15 nm was subsequently sputtered on the top side of the PPY nanospheres. The nanospheres on the Si wafer were immersed into an aqueous solution of isopropanol (IPA) (IPA : H<sub>2</sub>O = 1 : 1, v/v) and put into an ultrasonic bath. Then, an upward weak magnetic field (about 30 Oe) was applied for 2 h. After the solution was drained, the sample was dried under reduced pressure. From this procedure, PPY nanospheres were converted into PPY microspheres with magnetic CoFe handles.

The synthesis procedures which allowed the preparation of various nanostructures from the colloidal PPY dispersion are shown schematically in Figure 8.1.

### **8.2.4 Characterization of the PPY Nanostructures**

The morphology of PPY was studied with the JEOL 6320 FESEM. Conductive colloidal PPY nanospheres were also examined with the JEOL JEM-2010. The operation parameters for the FESEM and TEM measurements are illustrated in Section 3.2.3 and 5.2.3, respectively.

The conductivity and sensory property measurements of the conductive PPY samples were carried out using a Keithley 238 electrometer (containing a 4-probe system) and a D. C. power supply. A constant current of 100 mA was set for the 4-probe conductivity measurements while a constant voltage of 500 mV was assigned for sensory property measurements. The measurement procedure for the liquid PPY dispersion on SiO<sub>2</sub> wafer was same as that of solid PPY film, but the thickness of the liquid film is measured using ellipsometers (WVASE 32 model, Wextech Systems, Inc., Suiter, NY) instead of Surface Profiler (Tencor P-12 model, KLA-Tencor, Milpitas, California) for solid film. The PPY sensor, which was made of a thin layer of porous PPY nanofilm, was configured on a polyethylene terephthalate (PET, 0.05 mm in thickness) film with evaporation deposited Cu films as the electrodes. The dimension of the porous PPY layer was about  $2 \times 6 \text{ mm}^2$  in area and about 300 nm in thickness. Magnetic measurements of the PPY nanostructures were carried out using VSM, detailed procedure is illustrated in Section 5.2.3. The chemical composition of the conductive PPY nanospheres was analyzed by

XPS and EDX. Detailed procedures of the measurements are stated in Sections 4.2.2 and 5.2.3.



### 8.3 Results and Discussion

#### 8.3.1 Preparation of the Stable Aqueous Colloidal PPY Dispersion

The stable aqueous conductive PPY colloidal dispersion was synthesized via direct oxidation of pyrrole using  $\text{FeCl}_3$  as the oxidant in presence of surfactants. In order to achieve finer and uniform PPY nanospheres and improve stability and conductivity of the resulting colloid dispersion, both NaDS and PVA surfactants were used simultaneously as the steric stabilizers in the work, which is different from others and our previous works [Wuang et al., 2007; Xing and Zhao, 2006; Ghosh and Kar, 2004]. Hence the as-synthesized stable aqueous dispersion of PPY is actually a colloidal PPY containing PVA, NaDS,  $\text{FeCl}_3$ , and other products from the reaction. PVA and NaDS surfactants are partially soluble in water and alcohols, such as methanol, ethanol, isopropanol (IPA). Since both PVA and NaDS cannot be dissolved into acetone or butanone, the PPY particles, doped and with surface-adsorbed surfactants, in the aqueous dispersion can be effectively deposited from acetone or butanone. After removal of acetone, the resulting solid PPY-surfactant polymers can be re-dispersed partially or fully into water or alcohols.

In the preparation of the stable aqueous PPY dispersion using both PVA and NaDS as the steric stabilizers, an appropriate concentration of each reactant is required as well. A low molar ratio of pyrrole to the oxidant was used since previous studies have shown that with NaDS as the stabilizer, there is no apparent agglomeration when pyrrole concentration is low [Xing and Zhao, 2006]. Although there were two surfactants, NaDS and PVA, used in this work, our results also revealed that low concentration of pyrrole (< 0.1 M in the total reaction mixture of 20 ml) produced a stable aqueous PPY

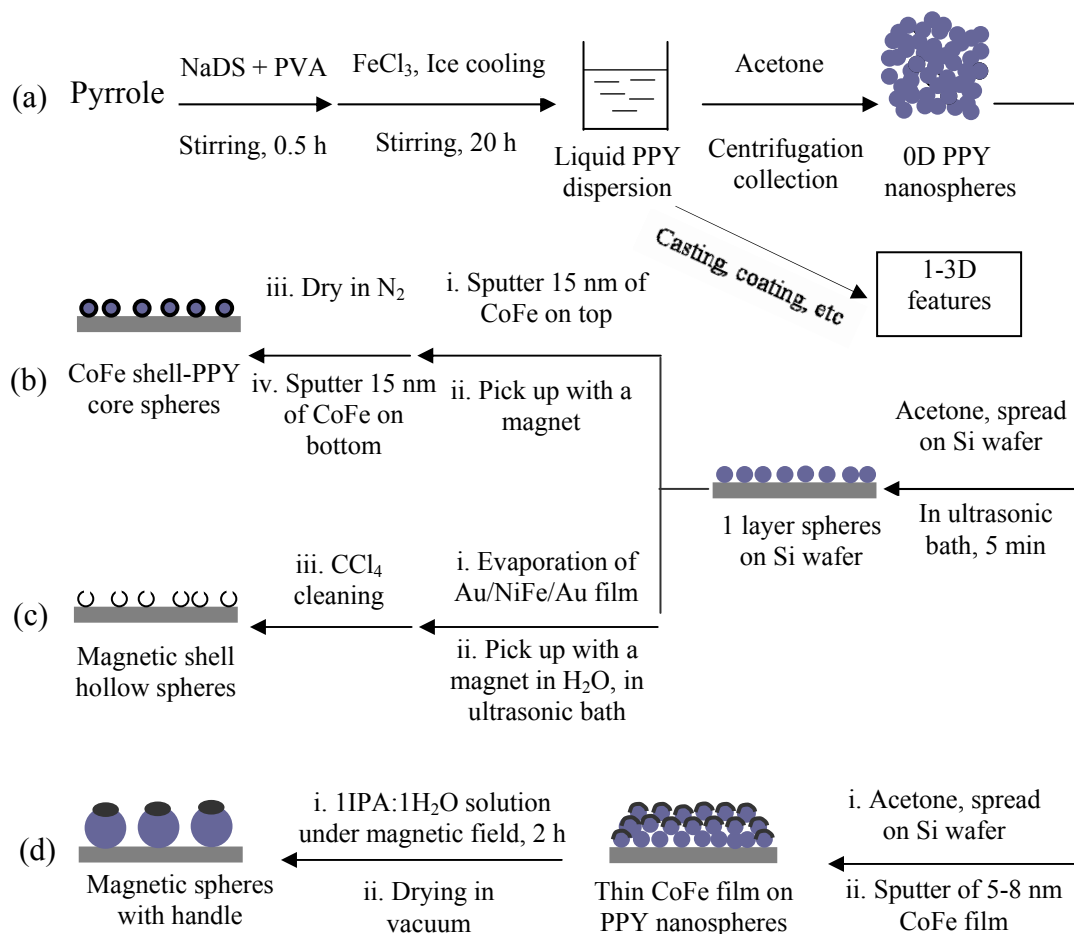


**Figure 8.1** Fabrication schemes of (a) PPY dispersion, 0D solid PPY nanospheres, and 1-3D nanostructures, (b) PPY core-CoFe shell nanospheres, (c) hollow magnetic CoFe shell nanospheres, and (d) magnetic PPY spheres by means of chemical oxidation polymerization, magnetic film sputtering, and solution treatment processes.

dispersion readily, while higher pyrrole concentration ( $> 0.5 M$ ) produced PPY precipitates. Thus, the molar ratio of pyrrole to  $\text{FeCl}_3$  was limited to 0.01 : 1 or lower in the preparation of PPY dispersions.

In this study, a typical aqueous conductive PPY dispersion was synthesized from a 20 ml aqueous mixture of 0.02 M pyrrole, 0.03 M NaDS, 0.01 M PVA, and 0.2 M  $\text{FeCl}_3$  under

vigorous stirring (at speed of 1200 rpm). The as-synthesized aqueous dispersion (colloidal emulsion) is very stable. No precipitation occurred in the dispersion after it had been sealed and stored in a dry box for 3 years.

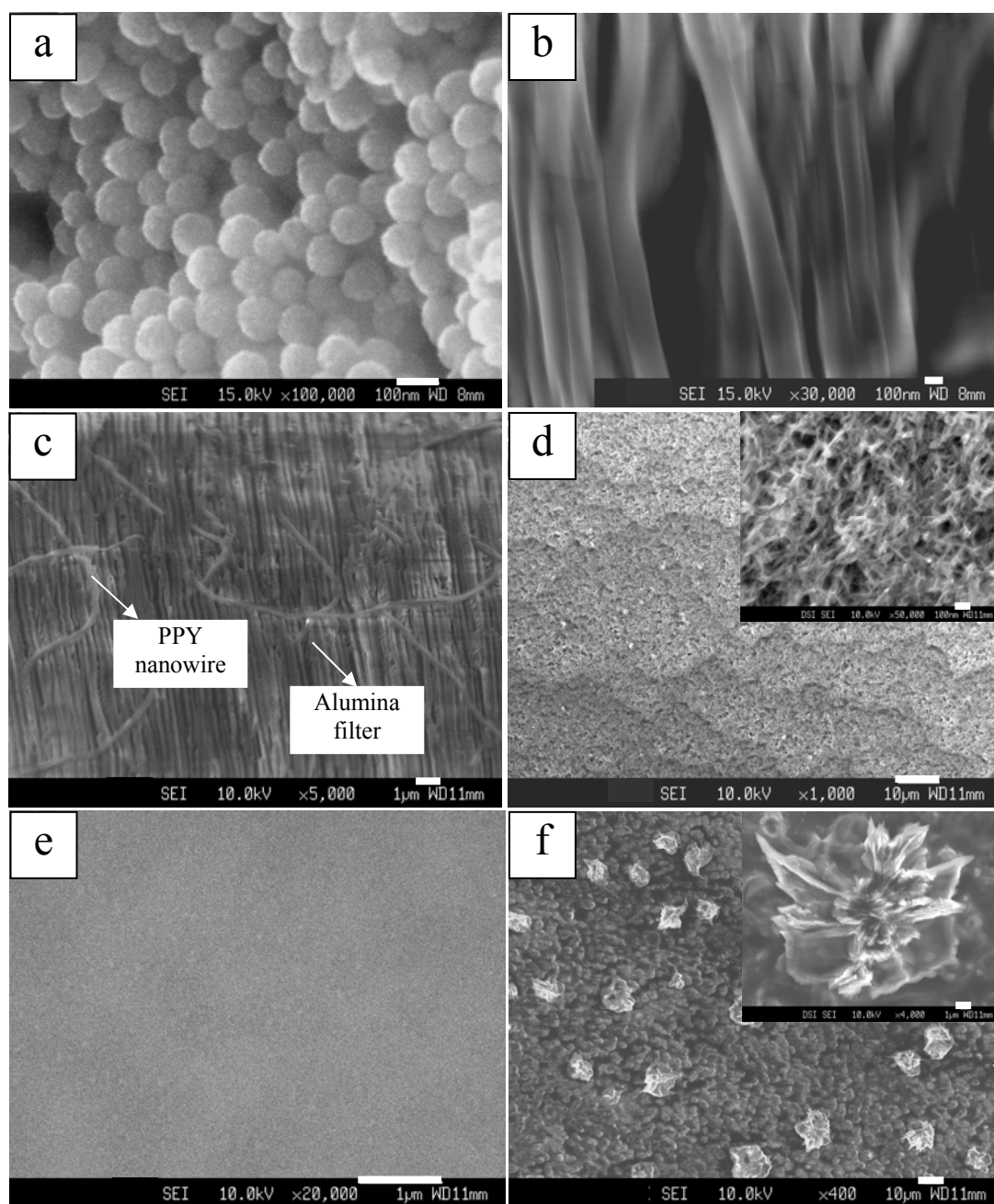
### **8.3.2 Syntheses of 0 - 3D Solid Nanostructures**

There are two approaches for transferring the aqueous PPY dispersion into solid phase, viz. mixing the aqueous PPY dispersion with acetone or butanone and drying the PPY dispersion in air or under reduced pressure. Depending on the method and procedure of phase conversion, different structural features (0 - 3D) and sizes (from several nanometers to microns) of solid polymers can be prepared.

A fast way to convert the aqueous PPY dispersion into solid structures is by mixing. When the aqueous colloidal PPY dispersion is mixed into acetone or butanone, the PPY colloids are precipitated from the solution immediately. The shapes of the PPY nanostructures depend on the mixing procedures. For example, to prepare fine uniform solid conductive nanospheres, the aqueous colloidal PPY dispersion was added drop-wise into acetone or butanone under vigorous stirring. Figure 8.2(a) shows the FESEM image of PPY nanospheres of about 80 nm in size prepared at a mixing-stirring speed of 1000 rpm. The size of the nanospheres can be reduced to about 20 nm by diluting the synthesized aqueous colloidal PPY dispersion with distilled water before adding drop-wise into acetone under higher stirring speed of 1200 rpm in an ice bath. The reduced size of the nanospheres is probably caused by the low concentration of PPY, which allows dispersion of the polymer into finer nanospheres in the aqueous medium at low temperature under vigorous stirring.

Figures 8.2(b) and 8.2(c) show the FESEM images of PPY nanowires with a diameter of 250 and 150 nm, respectively, prepared by casting the aqueous PPY colloidal dispersion into a porous alumina membrane, which has uniform straight-through nano-channels of about 150 - 250 nm. In Figure 8.2(b), the alumina membrane has been etched away by a 1 : 1 (v/v) aqueous mixture of 10% NaOH and acetone after casting the PPY dispersion. In order to improve the strength and resistance of the PPY nanowires to hydrolysis, the cast PPY together with the alumina membrane was kept at 130°C for 20 h in an oven prior to etching by NaOH. To achieve very long PPY nanowires, the aqueous PPY colloidal dispersion can be injected into stationary acetone through the nanoporous alumina membrane. From this procedure, PPY nanowires of millimeters (or longer) in length can be prepared. The FESEM image in Figure 8.2(c) shows the long solid PPY nanowires with a diameter of about 150 nm synthesized by this procedure.

In addition to 0D PPY nanospheres and 1D PPY nanowires, 2D nanofilms can also be prepared from the PPY dispersion via mixing with acetone or butanone. The FESEM image in Figure 8.2(d) shows the 2D porous nanofilm with a thickness of about 3  $\mu\text{m}$  and an average pore size of about 100 nm, prepared via sprinkling the mixture of acetone and PPY dispersion on a Si wafer, followed by drying the mixture under reduced pressure. The pores were formed due to differential evaporation rates between acetone and water from the sprinkled film under reduced pressure. The remaining PPY, with adsorbed PVA and NaDS molecules, forms the porous network structure. Planar solid PPY film can be prepared by using another conversion method, namely spin-coating of the aqueous PPY dispersion on an atomically flat single crystal Si wafer, followed by drying slowly in air.



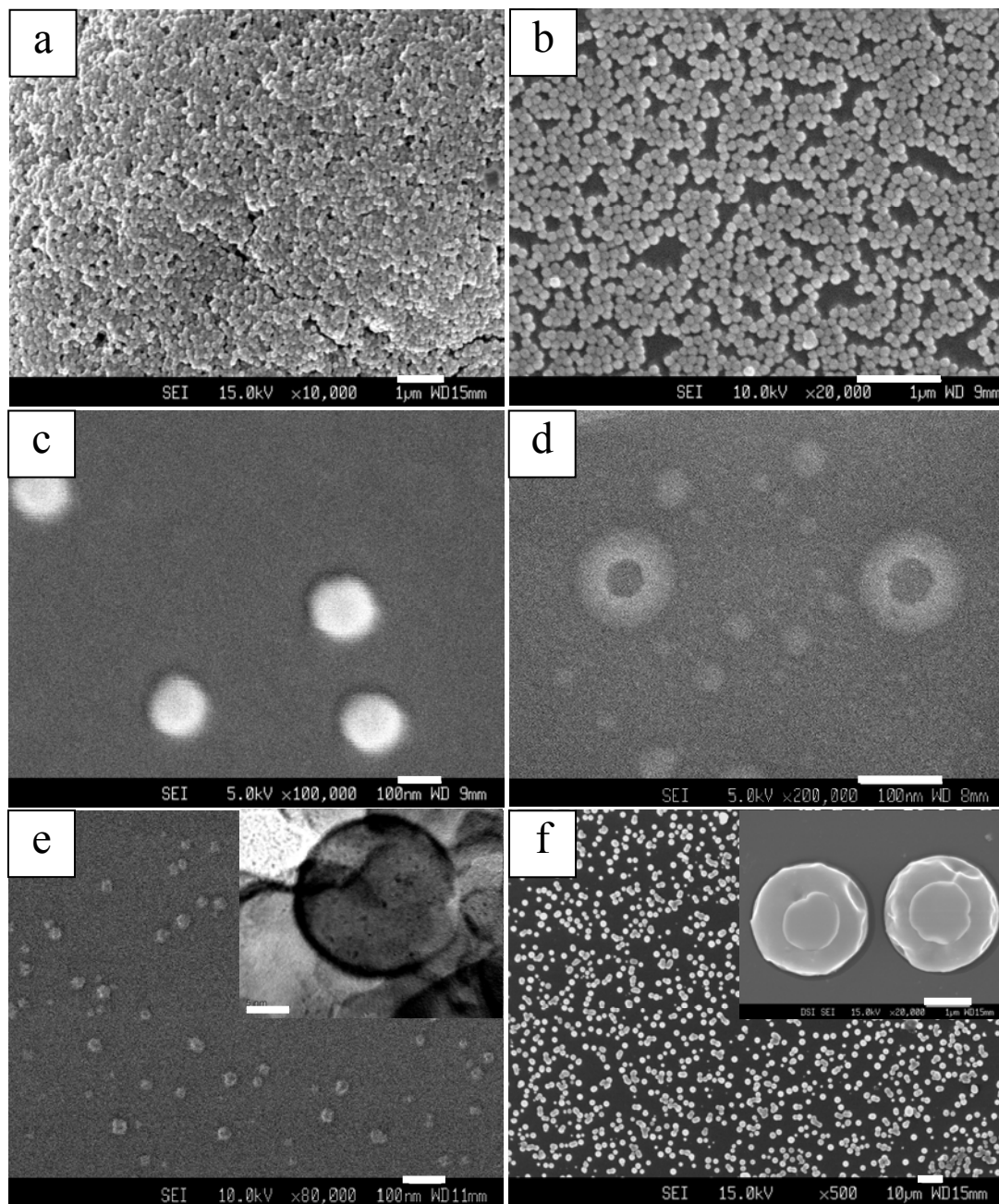
**Figure 8.2** FESEM images of (a) PPY nanospheres synthesized via drop-wise addition of PPY dispersion into acetone under stirring at a speed of 1000 rpm, (b) PPY nanowires prepared via casting PPY dispersion into alumina filter, baking, and dissolving the alumina filter, (c) PPY nanowires synthesized via casting of liquid PPY dispersion into acetone through an alumina filter with a pore size of 150 nm, (d) PPY porous film fabricated via sprinkling PPY and acetone solution onto Si wafer surface and drying under reduced pressure, (e) PPY flat film prepared via spin-coating PPY dispersion on Si wafer and drying in air, and (f) PPY nanoflowers synthesized via sprinkling PPY and H<sub>2</sub>O mixture on Si wafer, followed by cooling in liquid N<sub>2</sub> and drying under reduced pressure. The scale bars in the images of (a) and (b) are 100 nm; (c), (e) and the inset of (f) are 1 μm; (d) and (f) are 10 μm.

Figure 8.2(e) shows a PPY film about 30 nm in thickness, fabricated via spin-coating of PPY dispersion on a Si wafer at speed of 3000 rpm for 20 s, followed by drying in air for 20 h. Besides 0 to 2D nanostructures, 3D nanoflowers (shown in Figure 8.2(f)) can also be prepared by sprinkling a mixture of PPY dispersion and water (1 : 2, v/v) onto a Si wafer, followed by cooling in liquid N<sub>2</sub> and drying under reduced pressure. The nanoflowers have a size of 10 to 30 μm and a leaf thickness of down to about 20 nm (as revealed by FESEM under a high magnification of 100,000×). The FESEM image shows that the 3D nanoflowers are formed individually. It is probably because the polymer in the diluted PPY dispersion shrank and coagulated into 3D aggregates under the cryogenic shock of liquid N<sub>2</sub> and reduced dispersion. From the tilted side-view of the FESEM image, the nanoflower is up to 4 μm in height.

### **8.3.3 Fabrication of Nanostructured Magnetic PPY Nano-/Microspheres**

Other than the 0 to 3D nanostructures, many other types of functional nanostructures can be generated from the as-prepared colloidal PPY dispersion. For instance, magnetic and conductive nanostructured nano-/micro-spheres, which are of current interest and with potential applications in biotechnologies and catalysis [Hao et al., 2004; Cruz-Silva et al., 2008], can be fabricated from the colloidal PPY nanospheres.

*Synthesis of Magnetic CoFe Shell-Conductive PPY Core Nanospheres* – After the PPY nanospheres are prepared by drop-wise addition of PPY dispersion into acetone, PPY nanosphere films of different thickness (after acetone evaporation) can be achieved via spin-coating the mixture on Si wafers by controlling the spinning-speed. Figure 8.3(a) shows a uniform dry film of PPY nanospheres with a thickness of 300 nm formed under a



**Figure 8.3** FESEM images of (a) a thick layer of PPY nanospheres laid on Si wafer surface; (b) one layer of PPY nanospheres on Si wafer surface prepared via spin-coating for 20 s at a speed of 2000 rpm, (c) magnetic CoFe shell/conductive PPY core nanospheres, (d) and (e) hollow magnetic CoFe nanospheres. The inset is a TEM image; (f) magnetic handle microspheres. The scale bars in the FESEM images of (a), (b) and inset of (f) are 1 µm, (c)-(e) are 100 nm while (f) is 10 µm. The scale bars for the TEM image in the inset of (e) is 5 nm.

spin-coating speed of 2000 rpm for 20 s. By using acetone to dilute the mixture three-fold and putting it in an ultrasonic bath, a monolayer of loosely distributed PPY nanospheres on Si wafer can also be generated, as shown in Figure 8.3(b).

After a thin layer of CoFe magnetic film (15 - 25 nm) was sputter-deposited on the self-assembled monolayer of nanospheres, the top surfaces of the nanospheres were covered with a magnetic film. In an ultrasonic bath, the nanospheres can be easily separated from the Si wafer in acetone. It should be noted that if the deposited CoFe film was more than 40 nm, the PPY nanospheres will join together and cannot be lifted off from the Si wafer. After transferring the sputtered PPY nanospheres to another wafer under a 300 Oe magnetic field, a 15 - 25 nm CoFe nanofilm was again sputter-deposited on the exposed under-side of the nanospheres, resulting in the complete coverage of the PPY nanospheres by the CoFe magnetic films. Figure 8.3(c) shows the FESEM image of these core-shell magnetic conductive nanospheres with a size of ~100 nm.

*Synthesis of Magnetic Hollow Nanospheres* – Hollow nanospheres with a magnetic CoFe shell can also be prepared from the PPY nanospheres. After depositing thin layers of Au (1 - 2 nm), CoFe (3 - 15 nm), and Au (1 - 2 nm) on the self-assembled monolayer of nanospheres via the electron-beam-evaporation system under the substrate rotation, almost all surface of the nanospheres was covered by the composite magnetic/metal film. As the bottom of the nanospheres in contact with the Si substrate was not properly coated with the metals, the PPY-surfactant cores can be extracted by water when the nanospheres were lifted up from the Si wafer by a magnetic field in an ultrasonic water bath. The interior and exterior Au films in the multi-layer metal films can prevent the



CoFe nanofilm from corroding in water. Depending on the duration of dissolution, the PPY cores of the magnetic nanospheres can be partially or completely dissolved away. Figure 8.3(d) shows the FESEM image of hollow magnetic CoFe nanospheres (having a size of about 100 nm), which are converted from  $\sim 80$  nm PPY nanospheres. The inset-TEM image of Figure 8.3(e) shows smaller hollow CoFe nanospheres of about 30 nm generated from fine ( $\sim 20$  nm) PPY nanospheres.

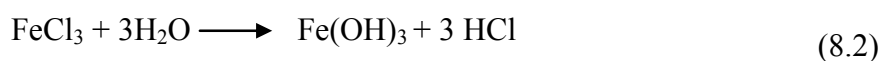
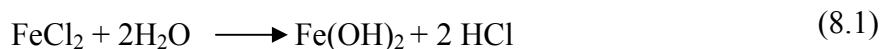
*Fabrication of Conductive Microspheres with A Magnetic Handle* – Since the as-synthesized solid conductive PPY-surfactant nanospheres are soluble in water and alcohols, PPY microspheres with a magnetic CoFe handle can be synthesized from an aqueous alcohol solution under the influence of a magnetic field in an ultrasonic bath. The synthesis route is also shown schematically in Figure 8.1.

Figure 8.3(f) shows the FESEM image of PPY microspheres with magnetic handles. They were fabricated by immersion of a thick layer of PPY nanospheres (about  $1.5 \mu\text{m}$  in thickness, the particle size was same as that in Figure 8.3(a)) covered with a thin layer of CoFe film (about 15 nm). The synthesis was carried out in an aqueous solution of IPA (IPA :  $\text{H}_2\text{O}$  = 1 : 1, v/v) under a weak magnetic field of 30 Oe (in the upward direction) in an ultrasonic bath. Comparing Figure 8.3(f) with Figure 8.3(a), it is clearly shown that the PPY nanospheres swelled from 80 nm to about  $2 \mu\text{m}$  after the treatment of IPA aqueous solution. The reason is probably because the CoFe film, which was deposited on top of PPY nanospheres, disintegrated in IPA aqueous solution during vigorous ultrasonic agitation. Each piece, together with the strongly attached PPY nanospheres, became a nucleus of a big sphere under the effect of magnetic field in the upward direction. By

prolonging the process time, the nuclei grew larger by adsorbing the PPY colloidal particles, which came from the decomposed PPY nanospheres at the underlying layers (without CoFe film covering), through the delivery of IPA aqueous solution in the ultrasonic bath. Finally the spheres swelled from nanospheres to microspheres after 2 h, with a magnetic handle on each of the PPY microspheres. The composition analysis of the microspheres is given below.

### 8.3.4 Properties, Chemical Composition, and Other Applications of the PPY Dispersion and Nanostructures

In order to discover more individual potential applications of the stable aqueous PPY dispersions and conductive PPY nanostructures, the PPY with different phases and shapes were characterized. The results are shown in Table 8.1. PPY has unique properties, such as good conductivity (up to  $10^{-2}$  s.cm<sup>-1</sup> level) of the aqueous dispersion and solid films, high surface area in the porous film compared to the normal flat films. The results of VSM measurements show that the aqueous colloidal PPY dispersion is a magnetic conductive fluid and the solid conductive PPY nanostructures also possess weak magnetism (Table 8.1). The magnetism is due to some FeCl<sub>3</sub> reactant and FeCl<sub>2</sub> reduced, which are retained in the PPY, are converted to magnetic Fe(OH)<sub>3</sub> and Fe(OH)<sub>2</sub> after hydrolysis [Gubbins, 2006]. The chemical reactions are:



The wide-scan XPS spectra in Figure 8.4 exhibit the differences in chemical compositions among the solid PPY in various shapes. As depicted in Figure 8.4(b), the spectra of the porous PPY film (described in Figure 8.2(d)), the Si 2p, Si 2s, S 2p, and Cl 2p components are at the binding energies of about 100, 151, 164, and 198 eV, respectively, while C 1s, N 1s, O 1s, and Fe 2p components are at the BE about 285, 398, 531, and 707 eV, respectively. Thus, the XPS result is consistent with the VSM data that the as-synthesized nanospheres and films possess magnetism. The magnetism of the PPY dispersions can potentially be improved by increasing the composition of Fe compounds via higher FeCl<sub>3</sub> reactant concentration, such as increasing from 0.3 to 0.4 M, in pyrrole polymerization. It will be further investigated.

The EDX results in Figure 8.5 also show the components of the nanostructured nano-/micro-spheres. The result in Figure 8.5(a) illustrates that the nanospheres (depicted in Figure 8.3(a)) are mainly composed of C, O, N, Cl, and Fe, which is consistent with the XPS analysis result (main peak: C, O, N, Cl, and Fe) illustrated in Figure 8.4(a). The EDX result of Figure 8.5(b) illustrates the composition of the hollow CoFe nanospheres (depicted in Figure 8.3(d)). It indicates that there is still some PPY left in the hollow CoFe nanospheres. The analysis results of the handle and bulk of the PPY microsphere (illustrated in Figure 8.5(c)) show that the handle contains much higher CoFe components (total 37 % in atomic ratio) than the bulk (total 8 % in atomic ratio) of the sphere. It implies that the handle of the microsphere has stronger magnetism. The analyses on the top of the 3D flower and the bottom substrate show that the 3D flower contains much higher C, N components (illustrated in Figure 8.5(d)) than the bottom. It reveals that the 3D flowers consist mainly of PPY.

**Table 8.1** Physicochemical properties of the as-synthesized PPY dispersion and nanostructures

	Dissolvable media	Non-dissolvable media	Conductivity $\sigma$ (s.cm <sup>-1</sup> ); Magnetization (emu/mg)	Other properties
Liquid dispersion	H <sub>2</sub> O, alcohol, dimethyl formamide	Acetone, butanone, CCl <sub>4</sub> , CHCl <sub>3</sub> , toluene, ethyl acetate, etc	10 <sup>-2</sup> - 10 <sup>-4</sup> ; 10 <sup>-4</sup> - 10 <sup>-5</sup>	Dark green color, pH 0.5 - 4.5
Flat film			10 <sup>-2</sup> - 10 <sup>-4</sup> ; 10 <sup>-2</sup> - 10 <sup>-3</sup>	Brown color
Nanospherical film			10 <sup>-3</sup> - 10 <sup>-5</sup> ; 10 <sup>-3</sup> - 10 <sup>-4</sup>	Black, sphere size: 20 - 80 nm
Porous film			10 <sup>-3</sup> - 10 <sup>-4</sup> ; 10 <sup>-3</sup> - 10 <sup>-5</sup>	High surface area
Magnetic core-shell or hollow sphere	Acid		~10 <sup>6</sup> ; 10 <sup>3</sup> -1	Size: 30 - 150 nm
Magnetic handle microsphere	Acid, alcohol, H <sub>2</sub> O, dimethyl formamide		10 <sup>-3</sup> - 10 <sup>-4</sup> ; 10 <sup>-1</sup> - 10 <sup>-2</sup>	Size: 0.5 - 2 $\mu$ m

Because the as-synthesized PPY is a conductive, magnetic, and bio-degradable polymer [Li et al., 2005], it should have a number of applications in industries, microelectronics, nano- and bio-technologies. For example, the PPY spheres encapsulated with magnetic films can serve as catalyst centers in bio-technology, tracers in life-science, magnetic

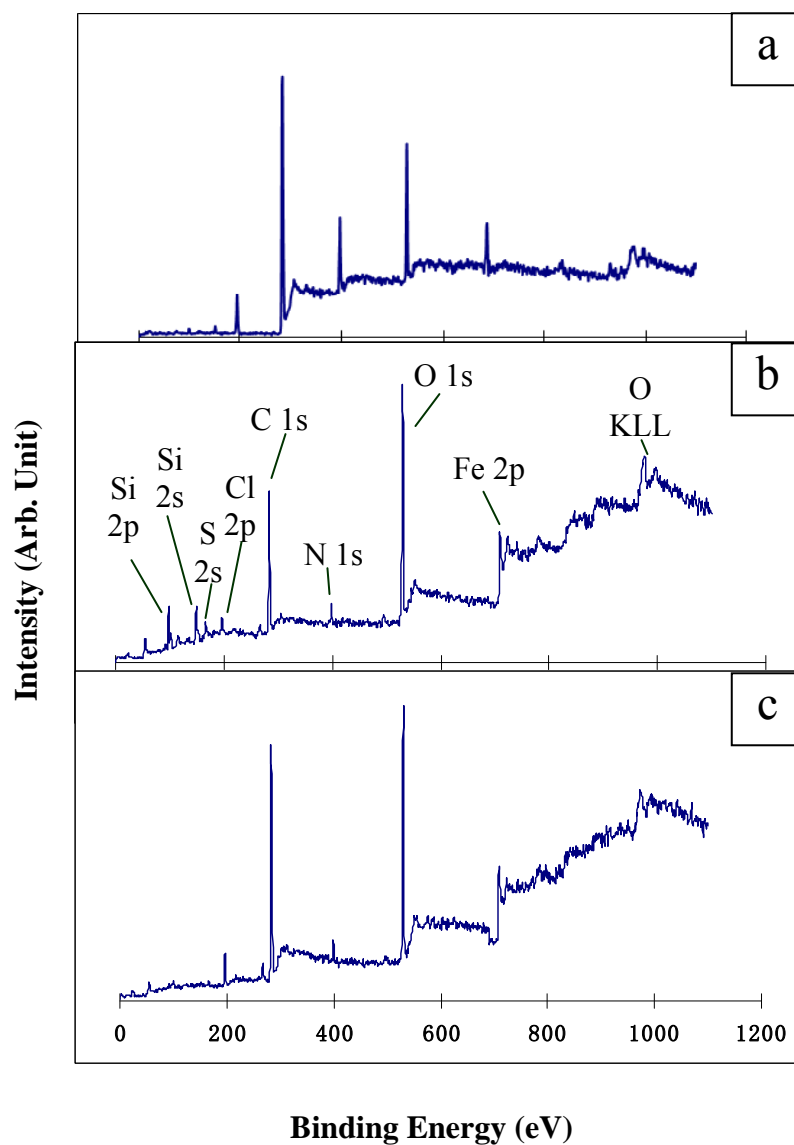


**Figure 8.4** XPS wide scan spectra of the solid conductive PPY nanostructures: (a) planar film from drying PPY dispersion in air, (b) porous film from drying the mixture of PPY dispersion and acetone under reduced pressure, and (c) solid nanospheres from addition of dropwise PPY dispersion into acetone.

alignment tool in nanotechnology, and host for controlled-release of drugs or optically active compounds [Wuang et al., 2007; Xing and Zhao, 2006; Li et al., 2005]. Organic spheres with built-in magnetic handles are potentially used as stimuli-responsive tracers.

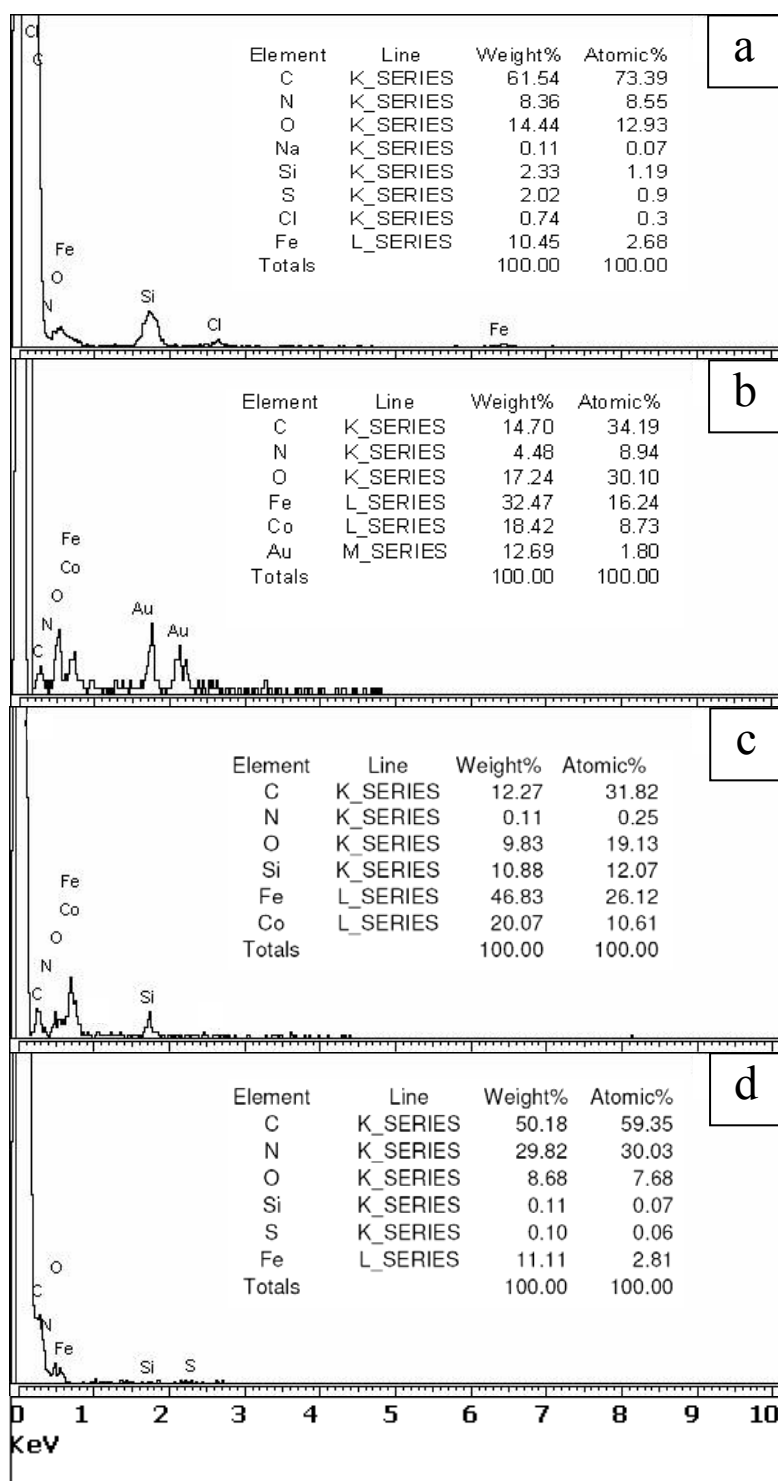


**Figure 8.5** EDX results of (a) PPY nanospheres, (b) hollow magnetic CoFe nanospheres, (c) handle of magnetic PPY microsphere, and (d) 3D PPY nanoflower.

The porous conductive films can be used as electrode-surface coatings for batteries and fuel cells due to their high conductive surface area [Ramya, 2008; Lee et al., 2004]. As illustrated in Table 8.1, the as-synthesized conductive PPY nanostructures can be selectively dispersed in solutions and solvents. They have potential application as nanosensors for aqueous solutions and solvents, such as aqueous solutions, acetone, butanone,  $\text{CCl}_4$ ,  $\text{CHCl}_3$  (chloroform), etc. The current response curves shown in Figure 8.6 illustrate the different responses of PPY nanosensor to distilled water, acetone, toluene, and others. Since the sensor conductivity is proportional to the current passing through the sensor while applying a fixed D. C. voltage of 500 mV, the curves of current vs. measuring time in Figure 8.6 show that the sensor conductivity changes in an opposite manner when the sensor is wetted by water and acetone. Water increases the nanosensor conductivity sharply while acetone decreases the conductivity drastically. It is because when using the distilled water to wet the sensor bridge, which is made of thin porous PPY nanofilm (thickness: about 500 nm), some PPY colloidal particles dissolve in water, fill the pores of the film and increase the conductive cross-section area of the sensor bridge greatly. As a result, the sensor current increases largely. However, acetone and butanone will shrink thin PPY films due to their adsorption on the PPY, which results in a reduced conductive cross-section area. As such, the current decreases. Noting that if removing the PPY film away from the sensor bridge, the circuit current was kept zero under the low voltage of 500 mV even after adding the distilled water on the bridge. Figure 8.6 also shows that the PPY sensor response to liquid  $\text{N}_2$  is similar to that with acetone. It is because liquid  $\text{N}_2$  also shrinks the thin PPY film. Further investigation with  $\text{CCl}_4$ , chloroform, toluene, and their mixtures on the PPY sensors show that the

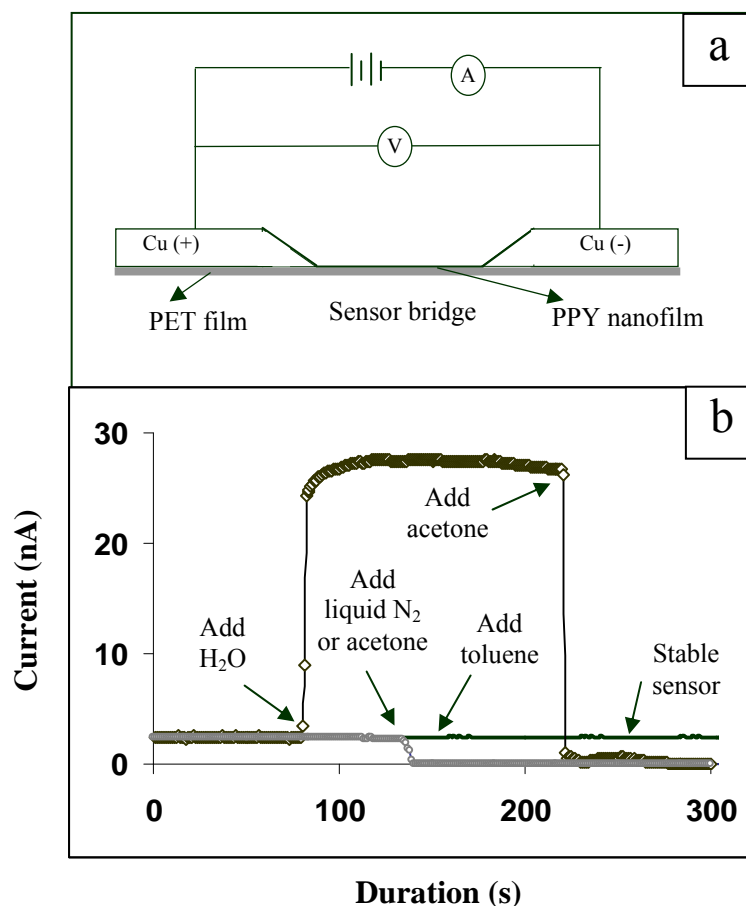


**Figure 8.6** PPY nanosensor measurement circuit (a) and measurement results (b). In (b), the line (—) stands for sensor results without any addition (before 150 s) and addition of liquid toluene (at 150 s), while (—○—) and (—◇—) stand for addition of liquid N<sub>2</sub> or acetone, and addition of distilled water then acetone, respectively.

conductivity of the sensor is almost constant because the as-synthesized colloidal PPY dispersion is immiscible with these solvents. Figure 8.6 displays the situation when toluene is added to the sensor.



### **8.4 Conclusions**

Very stable liquid PPY dispersions with conductive, magnetic, and phase-convertible properties were synthesized by using  $\text{FeCl}_3$  as oxidizer and two specific surfactants as steric stabilizers. Based on the unique properties of the as-synthesized PPY, different shape and size of functional nano-/micro-structures or sensors can be prepared by assigning different fabrication procedures. Thus, the prepared polymers have potential to be widely used in advanced microelectronics and nanotechnology areas.

**CHAPTER 9**

**CONCLUSIONS AND RECOMMENDATIONS FOR FUTURE  
WORK**

The present research work has attempted to develop simple methods for the preparation of fine nanostructures and nanopatterns via gas plasma processes and polymer modification. For plasma polymerization and deposition in dry ambience at room temperature, the works described in Chapter 3 to 7 demonstrated that plasma processing is a powerful tool for preparing nanostructured fluoropolymer materials from monomers of different properties, or single monomer. These works also show that although the parameters of plasma polymerization can significantly affect the deposition rates, properties, and the reproducibility of the resulting polymers [Shi, 1996; Fu et al., 2003; Barton et al., 2003; Bhat and Upadhyay, 2003], the parameters can be used as variables for achieving various morphologically different nanostructured polymers, even if using single monomer. It was also verified that plasma polymerization, a relatively simple and fast polymerization tool, can overcome the process difficulty in the preparation of types of fluoropolymers.

By utilizing different parameters in plasma polymerization and deposition (such as the input RF power, system pressure, and glow discharge duration), bulk fluoropolymer films and films of nanospheres can be synthesized from the fluoromonomers with different boiling points and molecular weight, such as perfluoroheptane, Zonyl<sup>TM</sup>, hexafluorobenzene, and pentafluorostyrene. Nanoporous nanospheres and films can be fabricated from one fluoromonomer (such as heptadecafluorodecyl acrylate, pentafluorostyrene) by further choosing the polymerization parameters carefully. By using the two inverse functions of plasma process (viz. polymerization and etching), mesoporous nanostructures, such as different pore size of mesoporous

poly(heptadecafluorodecyl acrylate) films and nanospheres can also be fabricated from the bulk nanospheres. Finally, by controlling the monomer concentration (at low level) and plasma RF power (at high level) as well as choosing different glow discharge time, 2 – 3 dimensional linearly aligned fluoropolymer nanoparticles were successfully prepared on the hydrogen-terminated silicon wafers under the induction of Si crystalline surface and electric field in the plasma chamber. Therefore, by means of plasma processing, not only normal solid polymer nanofilms and nanospheres can be prepared, but nanoporous polymer nanofilms and nanospheres can also be readily fabricated, and the size of the pores and spheres are controllable by using different methods and parameters (shown in Chapter 4, 5, and 6). This is one distinguishing advantage of plasma processes in comparison to other chemical polymerization methods. In addition, in compare to commonly reported bulk or macroporous polymer films from low energy of plasma polymerization and deposition at a high monomer concentration and low input RF power (usually  $\leq 200$  W) [Shi, 1996; Fu et al., 2003; Barton et al., 2003; Bhat and Upadhyay, 2003], this work demonstrated high energy of plasma polymerization and deposition, which could easily achieve finer uniform polymer nanospheres, mesoporous films, and other nanostructures. For example, under high energy of plasma process, the plasma system was also shown to be a useful tool on the self-assembly of 2 and 3 dimensional nanostructures in a dry ambience at room temperature. The high plasma energy was readily achieved by using the mentioned high input power of  $\geq 400$  W, lower monomer concentration (by choosing higher b. p. monomer and reducing monomer feeding time), and other stated means.

Furthermore, the as-prepared fluoropolymer nanostructures from high energy of plasma process not only have different nanostructure morphologies, but also possess specific characteristics comparing to conventional or low energy plasma polymerization and deposition, such as high hydrophobicity, good chemical stability, low dissipation factor, and very high porosity ratio, resulting in ultra-low dielectric constant. Thus, they may have various potential specific applications, such as low  $\kappa$  fillers, pigments, hosts for optically active compounds, and coating layer in chip packaging [Liu et al., 2004; Huo et al., 1997; Ozin, 1992]. The as-synthesized porous fluoropolymer nanostructures were also demonstrated to have new functions in comparison to bulk films from low energy plasma process, such acting as substrates for selective adsorption of CO<sub>2</sub> and O<sub>2</sub> gases. In addition, in order to widen the applications of the as-prepared porous nanospheres, magnetic nanoparticles were readily adsorbed on these porous organic nanospheres via different methods to impart magnetic property, as shown in Chapter 5 and 6. It is known that porous magnetic nanospheres are important and can be utilized for the delivery and controlled release of drugs [El-Kareh, et al., 1997], as well as supporters for catalysts [Suresh, et al., 1998].

Based on the fabrication processes and nanostructural results of the fluoropolymers, it suggests that if the developed methods on plasma polymerization and deposition are extended to other monomers, such as pyrrole, a series of different organic nanostructured materials can possibly be synthesized. Pyrrole, an important electro-active monomer, is known to be similar as fluoromonomers in difficulty to fabricate nano-/micro-devices by using normal conventional polymerizations, as it also always encounters the processibility issues. Thus, the use of plasma processes to prepare different types of

nanostructured polypyrroles will be one of my future investigation objectives. In this investigation, kinds of polypyrrole nanostructures possessing conductive, semi-conductive, and non-conductive properties will be fabricated via assigning different plasma parameters, such as plasma RF power and monomer concentration, in the polymerizations. Currently, in terms of plasma polymerization, pyrrole is only used for the preparation of thin conductive polymer films [Roth and Graupner, 1993; Kumar and Sharma, 1998; Lee et al., 2005]. In addition, since the as-synthesized fluoropolymer nanostructures have distinguished properties, investigating more applications for the as-prepared nanostructured fluoropolymers and polypyrroles would be another motivation in the future works.

The work described in Chapter 8 on polymer modification reveals that the chemical modification is a versatile tool in the preparation of nanostructured polymers, which possess unique properties beyond the limitations of current polymers. By using specific surfactants to modify polypyrrole, the modified polymer was shown to be readily fabricated into functional 0 – 3 dimensional conductive nanostructures via different simple processes. These nanostructures are impossible to be achieved by the polypyrroles without chemical-modification. Nowadays in the fabrications and applications of nanostructured polymers, there are still a lot of limitations for these polymers that need to be overcome, such as the upper-limited conductivity and magnetism of polymers, energy conversion for organic solar cells, and so on. Therefore, further developments on the fabrications of nanostructured polymers with breakthrough-distinguished characteristics via chemical and physical modifications should be the basis of my future research plan in the area of polymer modification.

---

**REFERENCES****A:**

Alivisatos, A. Semiconductor clusters, nanocrystals and quantum dots, *Science* 271, pp.933-937, 1996.

Analysis of diffusional effects in porous supports. Webpage: [www.lsbu.ac.uk /biology](http://www.lsbu.ac.uk/biology)

Austin, M. D., H. X. Ge, W. Wu, M. T. Li, Z. N. Yu, D. Wasserman, S. A. Lyon, S. Y. Chou. Fabrication of 5 nm linewidth and 14 nm pitch features by nanoimprint lithography, *Appl. Phys. Lett.* 84(26), pp.5299-5301, 2004.

**B:**

Baksh, M. M., M. Jaros, J. T. Groves. Detection of molecular interactions at membrane surfaces through colloid phase transitions, *Nature* 427, pp.139-141, 2004.

Ballauff, M. Nanoscopic polymer particles with a well-defined surface - Synthesis, characterization and properties, *Macromol. Chem. Phys.* 204(2), pp.121-127, 2003.

Barsan, N., U. Weimar. Conduction model of metal oxide gas sensors, *J. Electroceramics* 7, pp.143-167, 2001.

Barton, D., R. D. Short, S. Fraser, J. W. Bradley. The effect of ion energy upon plasma polymerization deposition rate for acrylic acid, *Chem. Commun.* pp.348-349, 2003.

Beamson, G., D. Briggs. High-resolution XPS of organic polymers, *The Scienta ESCA 300 Database*, John Willey & Sons, New York, 1993.

Benseddik, E., A. Bonnet, S. Lefrant. Transport properties in polypyrrole powders in PPY-PVA composites - Evidence for bipolaronic clusters, *J. Appl. Polym. Sci.* 68, pp.709-711, 1998.

Berndt, J., S. Hong, E. Kovacevic, I. Stefanovic, J. Winter. Dust particle formation in low pressure Ar/CH<sub>4</sub> and Ar/C<sub>2</sub>H<sub>2</sub> discharges used for thin film deposition, *Vacuum* 71, pp.377-390, 2003.

Bhat, N. V., D. J. Upadhyay. Adhesion aspects of plasma polymerized acetonitrile and acrylonitrile on polypropylene surface, *Plasma Polym.* 8(2), pp.99-118, 2003.

Bhushan, B. *Handbook of Nanotechnology*, 2<sup>nd</sup> ed., Springer Press, 2006.

Biederman, H., Osada, Y. *Plasma Technology: 3. Plasma Polymerization Processes*, Elsevier Science Publishers, New York, 1992.

Billmeyer, F. W. Textbook of Polymer Science, 3<sup>rd</sup> ed., John Wiley & Sons, New York, 1984.

Black, C. T., C. B. Murray, R. L. Sandstrom, S. H. Sun. Spin-dependent tunneling in self-assembled cobalt-nanocrystal superlattices, *Science* 290, pp.1131-1134, 2000.

Boal, A. K., F. Ilhan, J. E. Derouchey, T. Thurn-Albrecht, T. P. Russell, V. M. Rotello. Self-assembly of nanoparticles into structured spherical and network aggregates, *Nature* 404 (6779), pp.746-748, 2000.

Boltau, M., S. Walheim, J. Mlynek, G. Krausch, U. Steiner. Surface-induced structure formation of polymer blends on patterned substrates, *Nature* 39, pp.877-878, 1998.

Borini, S., A. M. Rossi, L. Boarini, G. Amato. Patterning of porous silicon by electron beam lithography, *J. Electrochem. Soc.* 150(5), pp.1-3, 2003.

Boufendi, L., A. Plain, J. Ph. Blondeau, A. Bouchoule, C. Laure, M. Toogood. Measurements of particle size kinetics from nanometer to micrometer scale in a low-pressure argon-silane radio-frequency discharge, *Appl. Phys. Lett.* 60(2), pp.169-171, 1992.

Boufendi, L., J. Gaudin, S. Huet, G. Viera, M. Dudemaine. Detection of particles of less than 5 nm in diameter formed in an argon-silane capacitively coupled radio-frequency discharge, *Appl. Phys. Lett.* 79(26), pp.4301-4303, 2001.

Boufendi, L., J. Hermann, A. Bouchoule, B. Dubreuil. Study of initial dust in an Ar-SiH<sub>4</sub> discharge by laser induced particle explosive evaporation, *J. Appl. Phys.* 76(1), pp.148-153, 1994.

Breyta, G., C. J. Knors, H. Ito, R. Sooriyakumaran. Photoresist composition, US Patent 5492793, 1996.

Bronstein, L. M., S. Polarz, B. Smarsly, M. Antonietti. Sub-nanometer noble-metal particle host synthesis in porous silica monoliths, *Adv. Mater.* 13, pp.1333-1336, 2001.

### C:

Calderon, J. G., R. B. Timmons. Pulsed plasma polymerization of acryloyl chloride: functionalization of surfaces with acid chloride groups, *Polymer Preprints*, 38, pp.1073-1076, 1997.

Callister, W. D. Materials Science and Engineering - An Introduction, 6<sup>th</sup> ed., John Wiley & Sons, NJ, 2003.



- Callister, W. D. Materials science and engineering, an introduction, Wiley International Edition, 6<sup>th</sup> ed., John Wiley and Sons, Inc. 2003.
- Cawdery, N., T. M. Obey, B. Vincent. Colloidal dispersions of electrically conducting polypyrrole particles in various media, *J. Chem. Soc., Chem. Commun.* *10*, pp.1189 – 1190, 1988.
- Che, S., Z. Liu, T. Ohsuna, K. Sakamoto, O. Terasaki, T. Tatsumi. Synthesis and characterization of chiral mesoporous silica, *Nature* *429*, pp.281-284, 2004.
- Chen, W., A. Y. Fadeev, M. C. Hsieh, D. Oner, J. Youngblood, T. J. McCarthy. Ultrahydrophobic and ultralyophobic surfaces - Some comments and examples, *Langmuir* *15(10)*, pp.3395-3399, 1999.
- Chen, Y. W., C. W. Chen, S. C. Tseng, J. Huang, Y. Z. Wu. Surface modification of bi-axially expanded poly(tetrafluoroethylene) by plasma polymerization of ethylene, *Surf. Coat. Technol.* *176*, pp.148-156, 2004.
- Chen, Y. W., W. C. Wang., W. H. Yu., E. T. Kang., K. G. Neoh., R. H. Vora., C. K. Ong., L. F. Chen. Ultra-low-k materials based on nanoporous fluorinated polyimide with well-defined pores via the RAFT-moderated graft polymerization process. *J. Mater. Chem.* *14*, pp.1406-1412, 2004.
- Cheng, Z. P., X. L. Zhu, Z. L. Shi, K. G. Neoh, E. T. Kang. Polymer microspheres with permanent antibacterial surface from surface-initiated atom transfer radical polymerization, *Ind. Eng. Chem. Res.* *44(18)*, pp.7098-7104, 2005.
- Childress, J. R., R. E. Fontana Jr. Magnetic Recording read head sensor technology, *C. R. Physique* *6*, pp.997-1012, 2005.
- Chin, B. D., O. O. Chin. Dispersion stability and electrorheological properties of polyaniline particle suspensions stabilized by poly (vinyl methyl ether), *J. Colloid Interface Sci.* *234*, pp.344-350, 2001.
- Choi, W. J., Tuteja A., Mabry J. M., Cohen R. E., McKinley G. H. A modified Cassie–Baxter relationship to explain contact angle hysteresis and anisotropy on non-wetting textured surfaces, *J. Colloid Interface Sci.*, *339*, pp.208–216, 2009.
- Chow, G. M., R. L. Holtz, A. Pattnaik, A. S. Edelstein. Alternative approach to nanocomposite synthesis by sputtering, *Appl. Phys. Lett.* *56*, pp.1853-1855, 1990.
- Chronakis, I. S., S. Grapenson, A. Jakob. Conductive polypyrrole nanofibers via electrospinning - Electrical and morphological properties, *Polymer.* *47*, pp.1597-1603, 2006.

Clark, N., A. Vanderslice, R. Grove III, R. R. Krchnavek. Time-dependent exposure dose of hydrogen silsesquioxane when used as a negative electron-beam resist, *J. Vac. Soc. Technol. B* 24(6), pp.3073-3076, 2006.

Coppée, V. M. Geskin, R. Lazzaroni, P. Damman. Formation of nanostructured polymer surfaces from combined relaxation and crystallization, *Macromol.* 37, pp.244-247, 2004.

Corma, A., F. Rey, J. Rius, M. J. Sabater, S. Valencia. Supramolecular self-assembled molecules as organic directing agent for synthesis of zeolites, *Nature* 431, pp.287-290, 2004.

Coulson, S. R., I. S. Woodward, J. P. S. Badyal, S. A. Brewer, C. Willis. Plasma chemical functionalization of solid surfaces with low surface energy perfluorocarbon chains, *Langmuir* 16, pp.6287-8293, 2000.

Cruz-Silva, R., E. Amaro, A. Escamilla, M.E. Nicho, S. Sepulveda-Guzman, L. Arizmendi, J. Romero-Garcia, F. F. Castillon-Barraza, M. H. Farias. Biocatalytic synthesis of polypyrrole powder, colloids, and films using horseradish peroxidase, *J. Colloid Interface Sci.* 328, pp.263-269, 2008.

Cui, Y., C. M. Lieber. Functional nanoscale electronic devices assembled using silicon nanowire building blocks, *Science* 291, pp.851-853, 2001.

Cui, Z. *Micro-Nanofabrication*, Higher Education Press, Springer, 2005.

### D:

Dai, L. M., H. J. Griesser, A. W. H. Mau. Surface modification by plasma etching and plasma patterning, *J. Phys. Chem. B.* 101(46), pp.9548-9554, 1997.

Ding, Y., Y. Hu, L. Y. Zhang, Y. Chen, X.Q. Jiang. Synthesis and magnetic properties of biocompatible hybrid hollow spheres. *Biomacromol.* 7(6), pp.1766-1772, 2006.

Ding, Z., J. N. Chen, S. Y. Gao, J. B. Chang, J. F. Zhang, E. T. Kang. Immobilization of chitosan onto poly-L-lactic acid film surface by plasma graft polymerization to control the morphology of fibroblast and liver cells, *Biomaterials* 25, pp.1059-1067, 2004.

Drug formulation technology for compounds administered by inhalation, [http://www.allp.com/PulmoSpheres/PS\\_WHITE.HTM](http://www.allp.com/PulmoSpheres/PS_WHITE.HTM).

Dry polymer electrolytes with high conductivity and modulus for secondary lithium metal batteries. <http://www.lbl.gov/Tech-Transfer/techs/lbml2200.html>.

**E:**

Eleftheriou, E., T. Antonakopoulos, G. K. Binnig, G. Cherubini, M. Despont, U. Durig, M. A. Lantz, H. Pozidis, H. E. Rothuizen, P. Vettiger. Millipede-A MEMS-based scanning-probe data-storage system, *IEEE. Trans. Magn.* 39(2), pp.938-945, 2003.

El-Kareh, B., G. B. Bronner, S. E. Schuster. The evolution of DRAM cell technology, *Solid State Technol.* 5, pp.89-93, 1997.

El-Kareh, B., G. B. Bronner, S. E. Schuster. The National Technology Roadmap for Semiconductors (Sematech, 1994), *Solid State Technol.* 5, pp.89-101, 1997.

El-Zahab, B., H. F. Jia, P. Wang. Enabling multienzyme biocatalysis using nanoporous materials, *Biotechnol. Bioeng.* 87(2), pp.179-183, 2004.

**F:**

Falconnett, D., D. Pasqui, S. Park, R. Eckert, H. Schiff, J. Gobrecht, R. Barbucci, M. Textor. A novel approach to produce protein nanopatterns by combining nanoimprint lithography and molecular self-assembly, *Nano Lett.* 0(0), pp.A-F, 2004.

Feldkamp, U., C. M. Niemeyer, Rotational Design of DNA Nanoarchitecture. *Angew. Chem. Int. Ed.* 45, pp.1856-1876, 2006.

Fennimore, A. M., T. D. Yuzvinsky, W. Q. Han, M. S. Fuhrer, J. Cumingsand, A. Zetti. Rotational actuators based on carbon nanotubes, *Nature* 424, pp.408-410, 2003.

Fu, M. X., Y. F. Zhu, R. Q. Tan, G. Q. Shi. Aligned polythiophene micro- and nanotubes, *Adv. Mater.* 13(24), pp.1874-1877, 2001.

Fischer, P. B., K. Dai, E. Chen, S. Y. Chou. 10 nm Si pillars fabricated using electron-beam lithography and reactive ion etching and HF etching, *J. Vac. Sci. Technol. B.* 11(6), pp.2524-2527, 1993.

Fonash, S. J. Plasma processing damage in etching and deposition, *IBM J. Res. Develop.* 43, pp.103-107, 1999.

Fontana, R. E., J. Katine, M. Rooks, R. Viswanathan, J. Lille, S. MacDonald, E. Kratschmer, C. Tsang, S. Nguyen, N. Robertson, P. Kasiraj. E-beam writing - A next generation lithography approach for thin-film head critical features, *IEEE Trans. Magn.* 38, pp.95-100, 2002.

Früchtel, J. S., K. Pflugseder, H. Gstach. Symmetric building blocks and combinatorial functional group transformation as versatile strategies in combinatorial chemistry, *Biotechnol. and Bioengin.* 71(2), pp.94-103, 2001.

Fu, G. D., E. T. Kang, K. G. Neoh. Deposition of nanostructured fluoropolymer films on silicon substrates via plasma polymerization of allylpentafluorobenzene, *J. Phys. Chem. B* *107*, pp.13902-13910, 2003.

Fu, G. D., Y. Zhang, E. T. Kang, K. G. Neoh. Nanoporous ultra-low- $\kappa$  fluoropolymer composite films via plasma polymerization of allylpentafluorobenzene and magnetron sputtering of poly(tetrafluoroethylene), *Adv. Mater.* *16(9-10)*, pp.107-120, 2004.

Fu, G. D., Z. H. Shang, L. Hong, E. T. Kang, K. G. Neoh. Preparation of cross-linked polystyrene hollow nanospheres via surface-initiated atom transfer radical polymerizations, *Am. Chem. Soc. O*, pp.A-E, 2005.

Fu, G. D., Z. H. Shang, L. Hong, E. T. Kang, K. G. Neoh. Preparation of cross-linked polystyrene hollow nanospheres via surface-initiated atom transfer radical polymerizations, *Macromol.* *4(3)*, pp.A-E, 2005.

### G:

Gad-el-Hak, M. MEMS - Applications, 2<sup>nd</sup> ed., Taylor & Francis Group. CRC Press. 2002.

Gao, H., X. B. Wu, J. T. Li, G. T. Wu, J. Y. Lin, K. Wu, D. S. Xu. Hydrogen adsorption of open-tipped insufficiently graphitized multi-walled carbon nanotubes, *Appl. Phys. Lett.* *83(16)*, pp.3389-3391, 2003.

Gaponik, N. P., D. V. Talapin, A. L. Rogach, A. Eychmuller. Electrochemical synthesis of CdTe nanocrystal/polypyrrole composites for optoelectronic applications, *J. Mater. Chem.* *10*, pp.2163-2166, 2000.

Gayr, S., G. Vergason, V. Etten. Plasma polymerization - Theory and Practice, 43<sup>rd</sup> Annual Technical Conference Proceedings-Denver, pp.267-271, 2000.

Ghosh, P., S. B. Kar. Modification of non-newtonian flow behavior of aqueous solution of poly(vinyl alcohol), Conducting polypyrrole prepared by in situ polymerization of pyrrole, *J. Appl. Polym. Sci.* *91*, pp.3731-3734, 2004.

Gole, J. L., A. Fedorov, P. Hesketh, C. Burda. From nanostructures to porous silicon sensors and photocatalytic reactors, *Phys. Stat. Sol. I*, pp.S188-S197, 2004.

Gourgon, C., C. Perret, G. Micouin, F. Lazzarino, J. H. Tortai, O. Joubert, J. P. E. Grolier. Influence of pattern density in nanoimprint lithography, *J. Vac. Sci. Technol. B* *21(1)*, pp.98-105, 2003.

Grenier, C. R. G., W. Pisula, T. J. Joncheray, K. Müllen, J. R. Reynolds. Regiosymmetric poly(dialkylphenylenedioxythiophene)s - Electron-rich and stackable  $\pi$ -conjugated nanoribbons, *Angew. Chem. Int. Ed.* *46*, pp.714-717, 2007.

Gubbins, D., E. Herrero-Bervera, Encyclopedia of geomagnetism and paleomagnetism, Springer, 2006.

Guerin, D. C., D. D. Hinshelwood, S. Monolache, F. S. Denes, V. A. Shamanian. Plasma polymerization of thin films - Correlations between plasma chemistry and thin films character, *Langmuir* 18, pp.4118-4123, 2002.

### H:

Haba, Y., E. Segal, M. Narkis, G. I. Titelman, A. Siegmann. Polyaniline-DBSA/polymer blends prepared via aqueous dispersions, *Synth. Met.* 110, pp.189-193, 2000.

Hadjadi, M. A., A. Beorchia, P. R. I. Cabarrocas, L. Boufendi, S. Huet, J. L. Bubendorff. Effects of the substrate temperature on the growth, properties of hydrogenated nanostructured silicon thin films, *J. Phys. D: Appl. Phys.* 34, pp.690-697, 2001.

Hahn, J., P. State, R. Frankel. Magnetic microbes show a knack for nano-engineering, <http://sciencenow.sciencemag.org/cgi/content/full/2005/422/2>.

Halik, M., H. Klauk, U. Zschieschang, G. Schmid, C. Dehm, M. Schütz, S. Maisch, F. Effenberger, M. Brunnbauer, F. Stellacci. Low-voltage organic transistors with an amorphous molecular gate dielectric, *Nature* 431, pp.963-966, 2004.

Hamada, J. I., Y. Ushio, K. Kazekawa, T. Tsukahara, N. Hashimoto, H. Iwata. Embolization with cellulose porous beads, I: An experimental study, *AJNR* 17, pp.1895-1899, 1996.

Han, J., S. X. Zheng. Highly porous polysilsesquioxane networks via hydrosilylative polymerization of macrocyclic oligomeric silsesquioxane, *Macromol.* 41(13), pp.4561-4564, 2008.

Han, L. C. M., R. B. Timmons, W. W. Lee. Pulsed plasma polymerization of an aromatic perfluorocarbon monomer - Formation of low dielectric constant and high thermal stability films, *J. Vac. Sci. Technol. B* 18(2), pp.799-804, 2000.

Han, L. C. M., R. B. Timmons, W. W. Lee, Y. Y. Chen, Z. B. Hu. Pulsed plasma polymerization of pentafluorostyrene - Synthesis of low dielectric constant films, *J. Appl. Phys.* 84(1), pp.439-444, 1998.

Han, L. M., R. B. Timmons, W. W. Lee. Pulsed plasma polymerization of an aromatic perfluorocarbon monomer - Formation of low dielectric constant, high thermal stability films. *J. Vac. Sci. & Tech. B.* 18, pp.799-801, 2000.

- Han, L. M., R. B. Timmons, W. W. Lee, Y. Chen, Z. Hu. Pulsed plasma polymerization of pentafluorostyrene - Synthesis of low dielectric constant films, *J. Appl. Phys.* *84*, pp.439-444, 1998.
- Hao, L. Y., C. L. Zhu, W. Q. Jiang, C. N. Chen, Y. Hu, Z. Y. Chen. Sandwich Fe<sub>2</sub>O<sub>3</sub>-SiO<sub>2</sub>-PPy ellipsoidal spheres and four types of hollow capsules by hematite olivary particles, *J. Mater. Chem.* *14*, pp.2929-2934, 2004.
- Harriott, L. R. Limits of lithography, *Proceed. IEEE.* *89(3)*, pp.366-374, 2001.
- Hayakawa, T., M. Yoshinari, K. Nemoto. Characterization and protein-adsorption behaviour of deposited organic thin film onto titanium by plasma polymerization with hexamethyldisiloxane, *Biomaterials* *25*, pp.119-127, 2004.
- Heeger, A. J. Semiconducting and metallic polymers - The fourth generation of polymeric materials (Nobel Lecture), *Angew. Chem. Int. Ed.* *40*, pp.2561-2611, 2001.
- Hirst, P. H., G. R. Pitcairn, J. G. Weers, T. E. Tarara, A. R. Clark, L. A. Dellamary, G. Hall, J. Shorr, S. P. Newman. In vivo lung deposition of hollow porous particles from a pressurized metered dose inhaler, *Pharm. Res.* *19(3)*, pp.258-286, 2002.
- Hofmeister, H., P. T. Miclea, W. Mörke. Metal nanoparticle coating of oxide nanospheres for core-shell structures, *Part. Part. Syst. Charact.* *19*, pp.359-365, 2002.
- Hsiao, R. Fabrication of magnetic recording heads and dry etching of head materials, *IBM J. Res. Develop.* *43*, pp.89-102, 1999.
- Hu, F. X., K. G. Neoh, E. T. Kang, Synthesis and in vitro anti-cancer evaluation of tamoxifen-loaded magnetite/PLLA composite nanoparticles, *Biomater* *27*, pp.5725-5733, 2006.
- Hu, W. C., G. H. Bernstein, K. Sarveswaran, M. Lieberman. Low temperature development of PMMA for sub-10 nm electron beam lithography, *IEEE.* *52*, pp.825-827, 2003.
- Hu, W. C., K. Sarveswaran, M. Lieberman, G. H. Bernstein. Sub-10 nm electron beam lithography using cold development of poly(methylmethacrylate), *J. Vac. Sci. Technol. B.* *22(4)*, pp.328-335, 2004.
- Hu, W. Ultra-high resolution (UHR) electron beam lithography (EBL), <http://www.utdallas.edu/~walter.hu/research/ebl.htm>.
- Huang, H. H., C. S. Sreekanth, C. S. Seet, G. Q. Xu, L. Chan, Thermal and photoinduced desorption and decomposition of Fe(Co)(5) on clean and oxygen-modified Ru(001), *J. Phys. Chem.* *100(46)*, pp.18138-18144, 1996.

Hulvat, J. F., S. I. Stupp. Liquid-crystal templating of conducting polymers, *Angew. Chem. Int. Ed.* **42**, pp.128-131, 2003.

Huo, Q., J. Feng, F. Schüth, G. D. Stucky. Preparation of mesoporous silica spheres, *Chem. Mat.* **9**, pp.14-17, 1997.

### I:

Ibn-Elhaj, M., M. Schadt. Optical polymer thin films with isotropic and anisotropic nano-corrugated surface topologies, *Nature* **410**, pp.796-799, 2001.

Inagaki, N. *Plasma Surface Modification and Plasma Polymerization*, Technical Publication, Pennsylvania, USA, pp.101-312, 1996.

### J:

Jang, J. S., J. W. Bae. Formation of polyaniline nanorod/liquid crystalline epoxy composite nanowires using a temperature-gradient method, *Adv. Funct. Mater.* **15**, pp.1877-1882, 2005.

Jeong, J. Y., S. E. Babayan, A. Schütze, V. J. Tu, J. Park, I. Henins, G. S. Selwyn, R. F. Hicks. Etching polyimide with a non-equilibrium atmospheric-pressure plasma jet, *J. Vac. Sci. Technol. A* **17**, pp.2581-2585, 1999.

Jia, H. F., G. Y. Zhu, P. Wang. Catalytic behaviors of enzymes attached to nanoparticles: the effect of particle mobility, *Biotech and Bioengin.* **84**, pp.406-411, 2003.

### K:

Kalinin, S. V., D. A. Bonnell, T. Alvarez, X. J. Lei, Z. H. Hu, R. Shao, J. H. Ferris. Ferroelectric lithography of multicomponent nanostructures, *Adv. Mater.* **16**, pp.9-10, 2004.

Kalkan, A. K., S. H. Bae, H. D. Li, D. J. Hayes, S. J. Fonash. Nanocrystalline Si thin films with arrayed void-column network deposited by high density plasma, *J. Appl. Phys.* **88(1)**, pp.555-561, 2000.

Kang, E. T., G. H. Neoh, T. C. Tan, Y. K. Ong. Polymerization and oxidation of pyrrole by organic electron acceptors, *J. Polym. Sci.* **25**, pp.2143-2153, 1987.

Keating, C. D., M. J. Natan. Striped metal nanowires as building blocks and optical tags, *Adv. Mater.* **15**, pp.451-454, 2003.

Kim, H. II., S. S. Kim. Fabrication of reverse osmosis membrane via low temperature plasma polymerization, *J. Membr. Sci.* **190**, pp.21-33, 2001.

Kim, Y. B., J. K. Choi, J. A. Yu, J. W. Hong. Synthesis and characterization of a non-aqueous conductive microgel coated with poly(aniline)-DBSA in a colloidal dispersion, *Synth. Met.* *131*, pp.79-85, 2002.

Komaba, S., A. Amano, T. Osaksa. Electroluminescence properties of electropolymerized poly(para-phenylene) films by means of electrochemical oxidation and reduction, *J. Electroanal. Chem.* *430*, pp.97-102, 1997.

Komaba, S., M. Seyama, T. Momma, T. Osaka. Potentiometric biosensor for urea based on electropolymerized electroinactive polypyrrole, *Electrochimica Acta* *42(3)*, pp.383-388, 1997.

Kosek, J., Z. Grof, M. Marek, G. Salejova. Morphogenesis of growing polymer particles, [http://cnd.vscht.cz/~jkk/research/p\\_mesoscale.html](http://cnd.vscht.cz/~jkk/research/p_mesoscale.html).

Kumar, D., R. C. Sharma. Advances in conductive polymers, *Eur. Polym. J.* *34*, pp.1053-1060, 1998.

## L:

Legendijk, A., Treichel, H., Uram, K. J., Jones, A. C. Low-Dielectric Constant Materials, II, *Mater. Res. Soc.*, Pittsburgh, PAA, *443*, pp.91-450, 1998.

Lammertink, R. G. H., M. A. Hempenius, J. E. van den Enk, V. Z. H. Chan, E. L. Thomas, G. J. Vansco. Nanostructured thin films of organic-organometallic copolymers - One-step lithography with poly(ferrocenylsilanes) by reactive ion etching, *Adv. Mater.* *12*, pp.98-102, 2000.

Lau, C. B., T. Tang, B. T. Huang. Preparation of macroporous functionalized polymer beads by a multistep polymerization and their application in zirconocene catalysts for ethylene polymerization, *J. Polym. Sci.* *41*, pp.873-880, 2003.

Lazzari, M., M. A. López-Quintela. Block copolymers as a tool for nanomaterial fabrication, *Adv. Mater.* *15(19)*, pp.1583-1593, 2003.

Lee, B., V. Seshadri, G. A. Sotzing. Water dispersible low band gap conductive polymer based on thieno (3,4-b) thiophene, *Synth. Met.* *152*, pp.177-180, 2005.

Lee, H., J. Y. Kim, J. H. Park, Y. G. Joe, T. H. Lee, Performance of polypyrrole-impregnated composite electrode for unitized regenerative fuel cell, *J. Power Sourc.* *131(1-2)*, pp.188-193, 2004.

Lee, H. S., S. A. Kim, S. J. Ahn, H., W. Lee. Positive and negative patterning on a palmitic acid langmuir-blodgett monolayer on Si surface using bias-dependent atomic force microscopy lithography, *Appl. Phys. Lett.* *81(1)*, pp.138-140, 2002.



- Lee, W. L. Photoresist stripping composition and method, US Patent 4395348, 1983.
- Lee, W., M. K. Jin, W. C. Yoo, E. S. Jang, J. H. Choy, J. H. Kim, K. Char, J. K. Lee. Nanostructured metal surfaces fabricated by a nonlithographic template method, *Langmuir* 20, pp.287-290, 2004.
- Lehn, J. M. Supramolecular Chemistry Concepts and Perspectives (Textbook), Wiley VCH, Weinheim, 1995.
- Lei, S. B., L. J. Wan, C. Wang, C. L. Bai. Direct observation of the ordering and molecular folding of poly[(*m*-phenylenevinylene)-*co*-(2,5-dioctoxy-*p*-phenylenevinylene)], *Adv. Mater.* 16(9-10), pp.828-831, 2004.
- Leich, M. A., N. M. Mackie, K. L. Williams, and E. R. Fisher, Pulsed plasma polymerization of benzaldehyde for retention of the aldehyde functional group, *Macromolecules* 31, pp.7618-7626, 1998.
- Lemieux, M. C., S. Minko, D. Usov, M. Stamm, V. Tsukruk. Tunable microstructure and nanomechanical properties in a binary polymer brush, *Polym. Mater. Sci. Eng.* 89, pp.274-275, 2003.
- Li, C., D. H. Zhang, S. Han, X. L. Liu, T. Tang, C. W. Zhou. Diameter-controlled growth of single-crystalline In<sub>2</sub>O<sub>3</sub> nanowires and their electronic properties, *Adv. Mater.* 15(2), pp.143-146, 2003.
- Li, G. L., D. L. Zeng, L. Wang, B. Y. Zong, K. G. Neoh, E. T. Kang, Hairy hybrid nanoparticles of magnetic core, fluorescent silica shell, and functional polymer brushes, *Macromolecules*, 3b2 (ver. 9), pp.4-7, 2009.
- Li, X. H., X. G. Zhang, H. L. Li. Preparation and characterization of pyrrole/aniline copolymer nanofibrils using the template-synthesis method, *J. Appl. Polym. Sci.* 81, pp.3002-3007, 2001.
- Lide, D. R., H. P. R. Frederikse, CRC Handbook of Chemistry and Physics - A ready-reference book of chemical and physical data, 76<sup>th</sup> ed., CRC Press, Boca Raton, FL, pp.115-117, 1995.
- Lin, T. J., B. H. Chun, H. K. Yasuda, D. J. Yang, J. A. Antonelli. Plasma polymerized organosilanes as interfacial modifiers in polymer-metal systems, *J. Adhesion Sci. Tech.* 5(10), pp.893-904, 1991.
- Lin, T. J., J. A. Antonelli, D. J. Yang, H. K. Yasuda, F. T. Wang. Plasma treatment of automotive steel for corrosion protection - a dry energetic process for coatings, *Progr. in Org. Coat.* 31, pp.351-361, 1997.

- Ling, Q. D., S. L. Lim, Y. Song, C. X. Zhu, S-H. D. Chan, E. T. Kang, K. G. Neoh. Nonvolatile polymer memory device based on bitable electrical ditching in a thin film of poly (n-vinylcarbazole) with covalently bonded C-60, *Langmuir* *23*, pp.312-319, 2007.
- Liu, J., Y. H. Lin, L. Liang, J. A. Voigt, D. L. Huber, Z. R. R. Tian, E. Coker, B. Mckenzie, M. J. Mcdermott. Templateless assembly of molecularly aligned conductive polymer nano-wires - A new approach for oriented nanostructures, *Chem. Eur. J.* *9(3)*, pp.605-611, 2003.
- Liu, L., P. Li, S. A. Asher. Entropic trapping of macromolecules by mesoscopic periodic voids in a polymer hydrogel, *Nature* *397(6715)*, pp.141-144, 1999.
- Liu, S. C., D. F. O'Brien. Stable polymeric nanoballoons - Lyophilization and rehydration of cross-linked liposomes, *J. Am. Chem. Soc.* *124*, pp.6037-6042, 2002.
- Liu, X. Q., Y. P. Guan, Z. Y. Ma, H. Z. Liu, Surface modification and characterization of magnetic polymer nanospheres prepared by miniemulsion polymerization. *Langmuir* *20* (23), pp.10278-10282, 2004.
- Liu, X. Y., X. B. Ding, Z. H. Zheng, Y. X. Peng, A. S. C. Chan, C. W. Yip, X. P. Long. Synthesis of amphiphilic magnetic microspheres by dispersion copolymerization of styrene and poly(ethylene oxide) macromonomer, *Polym. Int.* *52*, pp.235-240, 2003.
- Lopes, W. A., H. M. Jaeger. Hierarchical self-assembly of metal nanostructures on diblock copolymer scaffolds, *Nature* *414*, pp.735-738, 2001.
- Lu, Y., A. Pich, H. J. P. Adler. Synthesis and characterization of polypyrrole dispersions prepared with different dopants, *Macromol. Symp.* *210*, pp.411-417, 2004.
- Lu, Y. F., H. Y. Fan, A. Stump, T. L. Ward, T. Rieker, C. J. Brinker. Aerosol-assisted self-assembly of mesostructured spherical nanoparticles, *Nature* *398*, pp.223-226, 1999.
- Lubguban, J., T. Rajagopalan, N. Mehta, B. Lahlouh, S. L. Simon, S. Gangopadhyay. Low-k organosilicate films prepared by tetravinyltetramethyl-cyclotetrasiloxane, *J. Appl. Phys.* *92(2)*, pp.1033-1038, 2002.
- Lupitsky, R., Y. Roiter, C. Tsitsilianis, S. Minko. From smart polymer molecules to responsive nanostructured surfaces, *Langmuir* *21*, pp.8591-8593, 2005.

## M:

- Madou, M. J. *Fundamentals of Microfabrication - The Science of Miniaturization*. 2<sup>nd</sup> ed., CRC Press. <http://www.biomems.net>. 2002.

- Maggioni, G., S. Carturan, V. Rigato, G. D. Mea. Glow discharge vapour deposition polymerization of polyimide thin coatings, *Surf. Coat. Technol.* *142-144*, pp.156-162, 2001.
- Maier, G. Low dielectric constant polymers for microelectronics, *Prog. Polym. Sci.* *26*, pp.3-65, 2001.
- Makhlouki, M., M. Mustapha, A. Bonnet, A. Conan, A. Pron, S. Lefrant. Transport properties in polypyrrole-PVA composites - Evidence for hopping conduction, *J. Appl. Sci.* *44*, pp.443-446, 1992.
- Maluf, N., K. Williams. *An Introduction to Microelectromechanical Systems Engineering*. 2<sup>nd</sup> ed., Artech House. 2004.
- Mandal, T. K., B. M. Mandal. Ethylhydroxyethylcellulose stabilized polypyrrole dispersions, *Polym. Commun.* *36*, pp.1911-1913, 1995.
- Marcilla, R., C. Pozo-Gonzalo, J. Rodriguez, J. A. Alduncin, J. A. Pomposo, D. Mecerreyes. Use of polymeric ionic liquids as stabilizers in the synthesis of polypyrrole organic dispersions, *Synth. Met.* *156*, pp.1133-1138, 2006.
- Martin, S. J., J. P. Godschalx, M. E. Mills, E. O. Shafer II, P. H. Townsend. Development of a low-dielectric-constant polymer for the fabrication of integrated circuit interconnect, *Adv. Mater.* *12(23)*, pp.1769-1777, 2000.
- Martinu, L., H. Biederman, J. Nedbal. Dielectric properties of fluorocarbon and chlorofluorocarbon films plasma polymerized in an r.f. glow discharge, *Thin Solid Films* *136*, pp.11-19, 1986.
- Matsui, S. Nanostructure fabrication using electron beam - Its application to nanometer devices, *Proceed. IEEE.* *85(4)*, pp.528-534, 1997.
- Meng, H., D. F. Perepichka, F. Wudl. Facile solid-state synthesis highly conducting poly(ethylenedioxythiophene), *Angew. Chem. Int. Ed.* *42*, pp.121-123, 2003.
- Menon, A. K., B. K. Gupta. Nanotechnology - A data storage perspective, *Nanostruct. Mater.* *11(8)*, pp.965-986, 1999.
- Merhari, L., K. E. Gonsalves, Y. Hu, W. He, W. S. Huang, M. Angelopoulos, W. H. Bruenger, C. Dzionk, M. Torkler. Nanocomposite resist systems for next generation lithography, *Microelectron. Eng.* *63*, pp.391-403, 2002.
- Merkle, R. C. Self replicating systems and low cost manufacturing, <http://www.zyvex.com/nanotech/selfRepNATO.html>.
- Mijs, W. J. *New methods for polymer synthesis*, Plenum Press, New York, 1992.

Minne, S. C., Ph. Flueckiger, H. T. Soh, C. F. Quate. Atomic force microscope lithography using amorphous silicon as a resist and advances in parallel operation, *J. Vac. Sci. Technol. B* *13*(3), pp.1380-1385, 1995.

Minoux, E., O. Groening, K. B. K. Teo, S. H. Dalai, L. Gangloff, J. P. Schnell, L. Hudanski, I. Y. Y. Bu, P. Vincent, P. Legagneux, G. A. J. Amaratunga, W. I. Milne. Achieving high-current carbon nanotube emitters, *Nano Lett.* *0*(0), pp.A-E, 2005.

Moseler, M., U. Landman. Formation and stability and breakup of nanojets, *Science* *289*, pp.1165-1169, 2000.

### N:

Nalwa, H. S. Handbook of Low and High Dielectric Constant Materials and Their Application - Materials and Processing, Academic Press, San Diego, CA, pp.4, 1999.

Nam, J. M., C. S. Thaxton, C. A. Mirkin. Nanoparticle-based bio-bar codes for the ultrasensitive detection of proteins, *Science* *301*, pp.1884-1886, 2003.

Nguyen, C. V., K. R. Carter, C. J. Hawker, J. L. Hedrick, R. L. Jaffe, R. D. Miller, J. F. Remenar, H. W. Rhee, P. M. Rice, M. F. Toney, M. Trollas, D. Y. Yoon. Low-dielectric nanoporous organosilicate films prepared via inorganic/organic polymer hybrid templates, *Chem. Mater.* *11*(11), pp.3080-3085, 1999.

Nguyen, S. V. High-density plasma chemical vapour deposition of silicon-based dielectric films for integrated circuits, *IBM J. Res. Develop.* *43*, pp.109-126, 1999.

Nitta, K., K. Sato, T. Shimamaki, K. Hayakawa, S. Y. Kuramoto. Chemical-sensitization photoresist composition, US Patent 5945517, 1999.

### O:

Ohno, K., Y. Tsujii, T. Fukuda. Synthesis of a well-defined glycopolymers by atom transfer radical polymerization, *J. Polym. Chem.* *36*, pp.2473-2481, 1998.

Ohuchi, F. S., T. J. Lin, J. A. Antonelli, D. J. Yang. Preparation and in-situ characterization of polycarbosilane thin films by d.c. plasma-enhanced deposition, *Thin Solid Films*, *245*, pp.10-16, 1994.

Olmedo, L., P. Hourquebie, F. Jousse. Microwave properties of conductive polymers, *Synth. Met.* *69*, pp.205-208, 1995.

Osaks, T. Electrochemical aspects of advanced electronic materials, *Electrochem. Acta* *37*(6), pp.989-995, 1992.

Osaka, T., T. Fuduka, H. Kanagawa, T. Momma. Application of electroinactive polypyrrole film to the pH sensor electrode, *Sens. and Actuators B*, 13-14, pp.205-208, 1993.

Osaks, T., T. Momma, S.I. Komaba, H. Kanagawa. Electrochemical process of formation of an insulating polypyrrole film, *Sens. and Actuators B* 372, pp.201-207, 1994.

Ozin, G.A. Nanochemistry - Synthesis in diminishing dimensions, *Adv. Mater.* 4, pp.612-649, 1992.

Øye, G., V. Roucoules, L. J. Oates, A. M. Cameron, N. R. Cameron, P. G. Steel, J. P. S. Badyal. Plasma chemical amine functionalization of porous polystyrene spheres - The importance of particle size, *J. Phys. Chem. B* 107, pp.3496-3499, 2003.

### P:

Park, M., C. Harrison, P. M. Chaikin, R. A. Register. Block copolymer lithography - Periodic arrays of similar to 10(11) holes in 1 square centimeter, *Science* 276 (5317), pp.1401-1404, 1997.

Percec, V., C. H. Ahn, G. Ungar, D. J. P. Yearley, M. Moller, S. S. Sheiko. Controlling polymer shape through the self-assembly of dendritic side-groups, *Nature* 391, pp.161-164, 1998.

Phoenix, C. Developing Molecular manufacturing, <http://www.crnano.org/developing.htm>.

Pich, A., Y. Lu, H. J. P. Adler, T. Schmidt, K. F. Arndt. Dispersion polymerization of pyrrole in the presence of poly(vinyl methyl ether) microgels, *Polym.* 43, pp.5723-5729, 2002.

Pozidis, H., W. Haberle, D. Wiesmann, U. Drechsler, M. Despont, T. R. Albrecht, E. Eleftheriou. Demonstration of thermomechanical recording at 641 Gbit/in<sup>2</sup>, *IEEE. Trans. Magn.* 40(4), pp.2531-2536, 2004.

Puntes, V. F., K. M. Krishnan, A. P. Alivisatos. Colloidal nanocrystal shape and size control - The case of cobalt, *Science* 291, pp.2115-2117, 2001.

### Q:

Qin, G. H., Q. Wang, M. Nie. Polypyrrole-Fe<sub>3</sub>O<sub>4</sub> magnetic nanocomposite prepared by ultrasonic irradiation, *Macromol. Mater. Eng.* 291, pp.68-74, 2006.

Øye, G., V. Roucoules, L. J. Oates, A. M. Cameron, N. R. Cameron, P. G. Steel, J. P. S. Badyal. Plasmachemical amine functionalization of porous polystyrene spheres - The importance of particle size, *J. Phys. Chem. B* *107*, pp.3496-3499, 2003.

## R:

Rai-Choudhury, P. Handbook of Microlithography - Micromachining and Micro-Fabrication. Vol. 1: Microlithography. SPIE Press, Vol. PM 39. 2007.

Ramos, T. Nanoporous silica for low- $\kappa$  dielectrics. In: A. Lagendijk, H. Treichel, K. J. Uram, A.C. Jones. (Eds.) Low-dielectric Constant Materials, II, Vol. 443. Mater. Res. Soc., Pittsburgh, PAA, p 91, 1997.

Ramya, R., M. V. Sangaranarayanan, Analysis of polypyrrole-coated stainless steel electrodes — Estimation of specific capacitances and construction of equivalent circuits, *J. Chem. Sci.* *120*, pp.25-31, 2008.

Rana, S., J. Dubuc, M. Bradley, P. White. The synthesis of the cyclic antibacterial peptide Kawaguchipectin B on 11 different DVB cross-linked PS resins, *Tetrahedron Lett.* *41*, pp.5135-5139, 2000.

Reisberg, S., L.A. Dang, Q.A. Nguyen, B. Piro, V. Noel, P.E. Nielsen, L.A. Le, M.C. Pham. Label-free DNA electrochemical sensor based on a PNA-functionalized conductive polymer, *Talanta* *76(1)*, pp. 206-210, 2008.

Robinson, A. P. G., R. E. Palmer, T. Tada, T. Kanayama, M. T. Allen, J. A. Preece, K. D. M. Harris. Rapid Communication: 10 nm scale electron beam lithography using a triphenylene derivative as a negative/ positive tone resist, *Phys. D: Appl. Phys.* *32*, pp.75-78, 1999.

Roger, W. W., J. Miles, T. Olson. Recording technologies for terabit per square inch systems, *IEEE Trans. Magn.* *38*, pp.1711-1718, 2002.

Rosei, F., M. Schunack, P. Jiang, A. Gourdon, E. Lægsgaard, I. Stensgaard, C. Joachim, F. Besenbacher. Organic molecules acting as templates on metal surfaces, *Science* *296(55-66)*, pp.328-331, 2002.

Ross, C. A. Patterned magnetic recording media, *Anno. Rev. Mater. Res.* *31(35)*, pp.203-235, 2001.

Roth, S., W. Graupner. Conductive polymers - Evaluation of industrial applications, *Synth. Met.* *55*, pp.3623-3631, 1993.

Rupprecht, L., A. J. Epstein. Conductive polymers and plastics in industrial applications, Columbus, Ohio, pp. 43210, 1999.

Ryan, J. V., A. D. Berry, M. L. Anderson, J. W. Long, R. M. Stroud, V. M. Cepark, V. M. Browning, D. R. Rolison, C. I. Merzbacher. Electronic connection to the interior of a mesoporous insulator with nanowires of crystalline RuO<sub>2</sub>, *Nature* *406*, pp.169-172, 2000.

## S:

Saifullah, M. S. M., K. R. V. Subramanian, D. J. Kang, D. Anderson, W. T. S. Huck, G. A. C. Jones, M. E. Welland. Sub-10 nm high-aspect ratio patterning of ZnO using an electron-beam, *Adv. Mater.* *17*, pp.1757-1761, 2005.

Salem, A. K., F. R. A. J. Rose, R. O. C. Oreffo, X. B. Yang, M. C. Davies, J. R. Mitchell, C. J. Roberts, S. J. B. Tendler, P. M. Williams, K. M. Shakesheff. Porous polymer and cell composites that self-assemble in situ, *Adv. Mater.* *15*(3), pp.210-213, 2003.

Sandrin, L., M. S. Silverstein, E. Sacher. Fluorine incorporation in plasma-polymerised octofluorocyclobutane, hexafluoropropylene and trifluoroethylene, *Polymer* *42*(8), pp.3761-3769, 2001.

Saravanan, C., R. C. Shekar, S. Palaniappan. Synthesis of polypyrrole using benzoyl peroxide as a novel oxidizing agent, *Macromol. Chem. Phys.* *207*, pp.342-348, 2006.

Saunders, B. R., J. M. Saunders, J. Mrkic, E. H. Dunlop. A study of polypyrrole/poly (n-isopropylacrylamide-co-acrylamide) dispersions - Electrically conducting polymer dispersions stabilized by copolymers with lower critical solution temperatures, *Phys. Chem. Chem. Phys.* *1*, pp.1563-1568, 1999.

Saxena, V., B. D. Malhotra. Prospects of conducting polymers in molecular electronics, *Curr. Appl. Phys.* *3*, pp.293-305, 2003.

Savage, P. E. Organic chemical reactions in supercritical water, *Chem. Rev.* *93*, pp.791-800, 1991.

Schmedake, T. A., F. Cunin, J. R. Link, M. J. Sailor. Standoff detection of chemicals using porous silicon "smart dust" particles, *Adv. Mater.* *14*, pp.1270-1272, 2002.

Scholz, S. M., R. Vacassy, L. Lemaire, J. Dutta, H. Hofmann. Nanoporous aggregates of ZnS nanocrystallites, *Appl. Organomet. Chem.* *12*, pp.327-335, 1998.

Seidel, R., M. Liebau, G. S. Duesberg, F. Kreupl, E. Unger, A. P. Graham, W. Hoenlein. In-situ contacted single-walled carbon nanotubes, contact improvement by electroless deposition, *Nano Lett.* *3*(7), pp.965-968, 2003.

Serizawa, T., K. Hamada, M. Akashi. Polymerization within a molecular-scale stereoregular template, *Nature* *429*, pp.52-55, 2004.

- Service, R. F. Assembling the supersmall and ultrasensitive, *Science* 294, pp.2462-2463, 2001.
- Service, R. F. Small clusters hit the big time, *Science* 271, pp.920-922, 1996.
- Sermon, P., B. Knut, S. McClatchie. *Semiconductor Fabtech - Low-k Dielectric IC Fabrication*, 11<sup>th</sup> ed., 82, pp.1-30, 2001.
- Shi, F. F. Recent advances in polymer thin films prepared by plasma polymerization synthesis and structural characterization, *Surf. Coat. Technol.* 82, pp.1-15, 1996.
- Shi, F. F. Surface and coating, *Tech.* 82, pp.1-12, 1996.
- Singer, N. Self-assembled nanospheres may help against disease or terrorism, or as fillers and coatings, *Sandia National Laboratories* 51(6), pp.1-3, 1999.
- Singer, P. Low dielectrics - The search continues, *Semicond. Int.* 19(3), pp.88-96, 1996.
- Skotheim, T. A., R. L. Elsenbaumer, J. R. Reynolds. *Handbook of conducting polymers*, Marcel Dekker, Inc. 1997, [www.amazon.com /dp/0824700503](http://www.amazon.com/dp/0824700503).
- Snyder, G. J., J. R. Lim, C. K. Huang, J. P. Fleurial. Thermoelectric microdevice fabricated by a MEMS-like electrochemical process, *Nature Mater.* 2, pp.528-530, 2003.
- Spychaj, T., A. Bartkowiak. Polyvalent metal cation modified dextran hydrogels - Nonsize exclusion applications, *Polym. for Adv. Technol.* 9, pp.138-144, 1997.
- Srinivasarao, M., D. Collings, A. Philips, S. Patel. Three-dimensionally ordered array of air bubbles in a polymer film, *Science* 292, pp.79-82, 2001.
- Srivastav, V., R. Pal, H. P. Vyas. Overview of etching technologies used for HgCdTe, *Opto-Electron. Rev.* 13, pp.197-211, 2005.
- Steen, M. L., W. C. Flory, N. E. Capps, E. R. Fisher. Plasma modification of porous structures for formation of composite materials, *Chem. Mater.* 13, pp.2749-2752, 2001.
- Stevens, M. P. *Polymer Chemistry - An introduction*, Oxford University Press, New York, 1999.
- Stradner, A., H. Sedgwick, F. Cardinaux, W. C. K. Poon, S. U. Egelhaaf, P. Schurtenberger. Equilibrium cluster formation in concentrated protein solutions and colloids, *Nature* 432, pp.492-495, 2004.
- Stupp, S. I., V. Lebonheur, K. Walker, L. S. Li, K. E. Huggins, M. Keser, A. Amstutz. Supramolecular materials - Self-organized nanostructures, *Science* 276, pp.384-389, 1997.



Sun, S. H., C. B. Murray, D. Weller, L. Folks, A. Moser. Monodisperse FePt nanoparticles and ferromagnetic FePt nanocrystal superlattices, *Science* 287, pp.1989-1992, 2002.

Sun, S. H., H. Zeng, D. B. Robinson, S. Raoux, P. M. Rice, S. X. Wang, G. X. Li. Monodisperse MFe<sub>2</sub>O<sub>4</sub> (M= Fe, Co, Mn) Nanoparticles, *J. Am. Chem. Soc.* 126, pp.273-279, 2004.

Sun, W., N. P. Kherani. A three-dimensionally porous silicon p-n diode for betavoltaics and photovoltaics, *Adv. Mater.* 17, pp.1230-1233, 2005.

### T:

Takahashi, K., K. Tachibana. Solid particle production in fluorocarbon plasmas. I. Correlation with polymer film deposition, *J. Vac. Sci. Technol. A* 19(5), pp.2055-2060, 2001.

Takahashi, K., T. Mitamura, K. Ono, Y. Setsuhara. Characterization of porosity and dielectric constant of fluorocarbon porous films synthesized by using plasma-enhanced chemical vapor deposition and solvent process, *Appl. Phys. Lett.* 82(15), pp.2476-2478, 2003.

Takizawa, P. A., J. L. Derisi, J. E. Wilhelm, R. D. Vale, Plasma membrane compartmentalization in yeast by messenger RNA transport and a septic diffusion barrier, *Science* 290, pp.341-344, 2000.

Teare, D. O. H., C. G. Spanos, P. Ridley, E. J. Kinmond, V. Roucoules, J. P. S. Badyal. Pulsed plasma deposition of super-hydrophobic nanospheres, *Chem. Mater.* 14(11), pp.4566-4571, 2002.

Teare, D. O. H., D. C. Barwick, W. C. E. Schofield, R. P. Garrod, L. J. Ward, J. P. S. Badyal. Substrate-independent approach for polymer brush growth by surface atom transfer radical polymerization, *Langmuir* 21, pp.11425-11430, 2005.

Technical Report - Electrically conductive polymers, *Mater. Design* 12(3), pp.163-165, 1991.

Tsapis, N., D. Bennett, B. Jackson, D. A. Weitz, D. A. Edwards. Trojan particles - Large porous carrier nanoparticles for drug delivery, *PNAS* 99(19), pp.12001-12005, 2002.

Tseng, A. A., K. Chen, C. D. Chen, K. J. Ma. Electron beam lithography in nanoscale fabrication recent development, *IEEE Trans. Electron. Packag. Manufact.* 26(2), pp.248-252, 2003.

Tsujii, Y., M. Ejaz, S. Yamamoto, T. Fukuday. Fabrication of patterned high-density polymer graft surfaces. II. Amplification of EB-patterned initiator monolayer by surface-initiated atom transfer radical polymerization, *Polymer* 43, pp.3837-3841, 2002.

### U:

Ugelstad, J., A. Berge, T. Ellingsen, R. Schmid, T. N. Nilsen, P. C. Mork, P. Stenstad, E. Horness and O. Olsvik. Preparation and application of new monosized polymer particles, *Prog. Polym. Sci.*, 17, pp. 87-161, 1992.

### V:

Valsesia, A., P. Colpo, M. M. Silvan, T. Meziani, G. Ceccone, F. Rossi. Fabrication of nanostructured polymeric surfaces for biosensing devices, *Nano Lett.* 4(6), pp.1047-1050, 2004.

Van Roon, J. L., E. Groenendijk, H. Kieft, C. G. P. H. Schroën, J. Tramper, H. H. Beeftink. Novel approach to quantify immobilized-enzyme distributions, *Biotechnol. Bioeng.* 89(6), pp.661-669, 2005.

Vekilov, P.G., F. Rosenberger. New factors for protein crystal perfection on the Earth and under reduced gravity. Protein Crystal Growth Conference, Panama City, Florida, USA, April 28-30, 1996.

Verveer, P. J., F. S. Wouters, A. R. Reynolds, P. I. Bastiaens. Quantitative imaging of lateral ErbB1 receptor signal propagation in the plasma membrane, *Science* 290, pp.1567-70, 2000.

Voigt, A., H. Elsner, H. G. Meyer, G. Gruetzner, micro resist technology, [http://www.nanolithography.gatech.edu/resists/ma-N\\_2403\\_Poster\\_Ebeam.pdf](http://www.nanolithography.gatech.edu/resists/ma-N_2403_Poster_Ebeam.pdf).

Vos, R., M. Lux, K. Xu, W. Fyen, C. Kenens, T. Conrad, P. Mertens, M. Heyns, Z. Hatcher, M. Hoffman. Removal of submicrometer particles from silicon wafer surfaces using HF-based cleaning mixtures, *J. Electrochem. Soc.* 148, pp.683-691, 2001.

### W:

Wada, T., S. Haraichi, K. Ishii, H. Hiroshima, M. Komuro. SiO<sub>2</sub>/poly-Si electron beam resist process for nanofabrication, *J. Vac. Sci. Technol.* 14, pp.1850-1854, 1996.

Wallace, G. G. Conductive electroactive polymers, CRC press, 2008.

- Wanekaya, A. K., W. Chen, N. V. Myung, A. Mulchandani. Nanowire-based electrochemical biosensors, *Electroanalysis* *18*(6), pp.533-550, 2006.
- Wang, C. F, S. Y. Xie, S. C. Lin, X. Cheng, X. H. Zhang, R. B. Huang, L. S. Zheng. Glow discharge growth of SnO<sub>2</sub> nano-needles from SnH<sub>4</sub>, *Chem. Commun.* *12*, pp.1766-1767, 2004.
- Wang, H. Y., S. M. Park. Polypyrrole-based optical probe for a hydrogen peroxide assay, *Analyt. Chem.* *79*, pp.240-245, 2007.
- Wang, W. Z., O. K. Varghese, C. M. Ruan, M. Paulose, C. A. Grimes. Synthesis of CuO and Cu<sub>2</sub>O crystalline nanowires using Cu(OH)<sub>2</sub> nanowire templates, *J. Mater. Res.* *18*(12), pp.2756-2759, 2003.
- Wang, Y., X. J. Wang, X. H. Chuai, N. Fu, Z. Z. Cui, M. B. Yi, D. M. Zhang, B. Yang. Synthesis and properties of novel crosslinkable second-order nonlinear optical polymers based on 2,3,4,5,6-pentafluorostyrene, *Polym. Int.* *53*, pp.1103-1112, 2004.
- Wang, T. F., T. J. Lin, D. J. Yang, J. A. Antonelli, H. K. Yasuda. Corrosion protection of cold-rolled steel by low temperature plasma interface engineering I, Enhancement of E-coat adhesion, *Progr. in Org. Coat.* *28*, pp.291-297, 1996.
- Ward, L. J., W. C. E. Schofield, J. P. S. Badyal. Atmospheric pressure glow discharge deposition of polysiloxane and SiO<sub>x</sub> films, *Langmuir* *19*, pp.2110-2114, 2003.
- Ward, L. J., W. C. E. Schofield, J. P. S. Badyal. Atmospheric pressure plasma deposition of structurally well-defined polyacrylic acid films, *Chem. Mater.* *15*, pp.1466-1469, 2003.
- Watanabe, E., Y. Tanaka, G. Goto, T. Ohminato, T. Okabe. 1234 Mechanical properties of cast Fe-Pt magnetic alloys, [http://iadr.confexd.com/iadr/2002SanDiego/techprogram/abstract\\_17853.htm](http://iadr.confexd.com/iadr/2002SanDiego/techprogram/abstract_17853.htm).
- Wessling, B. Dispersion as the link between basic research and commercial applications of conductive polymers (polyaniline), *Synth. Met.* *93*, pp.328-332, 1998.
- Wessling, B. Dispersion-The key tool for understanding, improving and using conductive polymers and organic metals, *Synth. Met.* *152*(1-3), pp.5-8, 2005.
- White, N. M., J. D. Turner. Thick-film sensors - Past, present and future. *Meas. Sci. Technol.* *8*, pp.1-20, 1997.
- Winther-Jensen, B., N. Clark, P. Subramanian, R. Helmer, S. Ashraf, G. Wallace, L. Spiccia, D. MacFarlane. Application of polypyrrole to flexible substrates, *J. Appl. Polym. Sci.* *104*, pp.3938-3947, 2007.

Woodward, I., W. C. E. Schofield, V. Roucoules, J. P. S. Badyal. Super-hydrophobic surfaces produced by plasma fluorination of polybutadiene films, *Langmuir* *19*, pp.3432-3438, 2003.

Wuang, S. C., K. G. Neoh, E. T. Kang, D. W. Pack, D. E. Leckband. Heparinized magnetic nanoparticles - In-vitro assessment for biomedical applications, *Adv. Funct. Mater.* *16*, pp.1723-1730, 2006.

Wuang, S. C., K. G. Neoh, E. T. Kang, D. W. Pack, D. E. Leckband, Polypyrrole nanospheres with magnetic and cell-targeting capabilities, *Macromol. Rapid Commun.* *28*, pp.816-821, 2007.

Wuang, S. C., K. G. Neoh, E. T. Kang, D. W. Pack, D. E. Leckband, Synthesis and functionalization of polypyrrole-Fe<sub>3</sub>O<sub>4</sub> nanoparticles for applications in biomedicine, *J. Mater. Chem.*, *17*, pp.3354-3362, 2007.

### X:

Xiao, X. C., J. W. Elam, S. Trasobares, O. Auciello, J. A. Carlisle. Synthesis of a self-assembled hybrid of ultrananocrystalline diamond and carbon nanotubes, *Adv. Mat.* *17*, pp.1496-1500, 2005.

Xing, S. X., G. K. Zhao. Morphology and thermostability of polypyrrole prepared from SDBS aqueous solution, *Polymer Bulletin* *57*, pp.933-943, 2006.

Xu., D., E. T. Kang, K. G. Neoh, Y. Zhang, A. A. O. Tay, S. S. Ang, M. C. Y. Lo, K. Vaidyanathan. Selective electroless plating of copper on (100)-oriented single crystal silicon surface modified by UV-induced coupling of 4-vinylpyridine with the H-terminated silicon, *J. Phys. Chem. B* *106*, pp.12508-12516, 2002.

Xu, D. S., G. L. Guo, Y. G. Guo, Y. L. Zhang, L. L. Gui. Nanocrystal size control by bath temperature in electrodeposited CdSe thin films, *J. Mat. Chem.* *13*(2), pp.360-364, 2003.

### Y:

Yang, B. J., Y. H. Wu, B. Y. Zong, Z. X. Shen. Electrochemical synthesis and characterization of magnetic nanoparticles on carbon nanowall templates, *Nano Lett.* *2*(7), pp.751-754, 2002.

Yang, D. J., W. L. Jolly. Decarbonylation of 2-germaacetic acid in aqueous solutions, *Inorg. Chem.* *17*(3), pp.621-624, 1978.

- Yang, G. H., S. W. Oh, E. T. Kang, K. G. Neoh. Plasma polymerization and deposition of linear, cyclic and aromatic fluorocarbons on (100)-oriented single crystal silicon substrates, *J. Vac. Sci. Technol. A*. *20(6)*, pp.1955-1963, 2002.
- Yang, G. H., Y. Zhang, E. T. Kang, K. G. Neoh, A. C. H. Huan, D. M. Y. Lai. Plasma polymerization of allylpentafluorobenzene on copper surfaces, *J. Mater. Chem.* *12*, pp.426-431, 2002.
- Yang, G. H., Y. Zhang, E. T. Kang, K. G. Neoh. Deposition of ultrathin fluoropolymer films on Si(100), GaAs (100) surfaces by RF magnetron sputtering of poly(tetrafluoroethylene-co-hexafluoropropylene), *J. Phys. Chem. B*. *107(12)*, pp.2780-2787, 2003.
- Yang, S., P. Mirau., J. N. Sun., D. W. Gidley. Characterization of nanoporous ultra low-k thin films templated by copolymers with different architectures, *J. Radiation Phys. Chem.* *68*, pp.351-356, 2003.
- Yang, X. T., L. G. Xu, S. C. Ng, S. O. H Chan. Magnetic and electrical properties of polypyrrole-coated  $\gamma$ -Fe<sub>2</sub>O<sub>3</sub> nanocomposite particles, *Nanotech.* *14*, pp.624-629, 2003.
- Yao, S., U. Beginn, T. Gress, M. Lysetska, F. Würthner. Supramolecular polymerization and Gel formation of bis(merocyanine) dyes driven by dipolar aggregation. *J. Am. Chem. Soc.* *126 (26)*, pp.8336-8348, 2004.
- Yasuda, H. New insights into aging phenomena from plasma chemistry, *Nuclear Instruments, Methods Phys. Res.* *515*, pp.15-30, 2003.
- Yasuda, H. Plasma polymerization, *Thin Solid Films* *144*, L107-L109, 1986.
- Yasuda, H. Plasma Polymerization. Academic, Orlando, 1985.
- Yasuda, H. K. Plasma polymerization and plasma interactions with polymeric materials, *Applied Polymer Symposium Series 46*, John Wiley & Sons, New York, 1990.
- Yasuda, H. K. Plasma Polymerization and Plasma Treatment - *Applied Polymer Symposium 38*, John & Wiley Sons, New York, 1984.
- Yi, D. K., D. Y. Kim. Polymer nanosphere lithography - Fabrication of an ordered trigonal polymeric nanostructure, *Chem. Commun.* pp.982-983, 2003.
- Yin, Y. D., Y. Lu, B. Gates, Y. N. Xia. Template-assisted self-assembly - A Practical route to complex aggregates of monodispersed colloids with well-defined sizes, shapes and structures, *J. Am. Chem.* *123*, pp.8718-8729, 2001.
- Ying, J. Y. Nanostructural tailoring - Opportunities for molecular engineering in catalysis, *AIChE Journal* *46(10)*, pp.1902-1906, 2000.

Yu, S., T. K. S. Wong., X. Hu., K. Pita., V. Ligatchev. Synthesis and characterization of templating low dielectric constant organosilicate films, *J. Electrochem. Soc.* *151*, pp. F123-F127, 2004.

Yuan, Y. J., H. P. Hentze, W. M. Arnold, B. K. Marlow, M. Antonietti. Fabrication of nanostructured silica using a triblock copolymer template, *Nano Lett.* *2(12)*, pp.1359-1361, 2002.

## Z:

Zhang, K. Q., X. Y. Liu. In situ observation of colloidal monolayer nucleation driven by an alternating electric field, *Nature* *429(6993)*, pp.739-43, 2004.

Zhang, L. J., M. X. Wan. Self-assembly of polyaniline from nanotubes to hollow microspheres, *Adv. Func. Mater.* *13*, pp.815-820, 2003.

Zhang, L. Y., G. X. Cheng, C. Fu. Molecular selectivity of tyrosine-imprinted polymers prepared by seed swelling and suspension polymerization, *Polym. Int.* *51*, pp.687-692, 2002.

Zhang, L. Z., J. C. Yu, Z. Zheng, C. W. Leung. Fabrication of hierarchical porous iron oxide films utilizing the Kirkendall effect, *Chem. Commun.* pp.112-113, 2005.

Zhang, Q. M., H. F. Li, M. Poh, F. Xia, Z. Y. Cheng, H. S. Xu, C. Huang. An all-organic composite actuator material with a high dielectric constant, *Nature* *419*, pp.284-287, 2002.

Zhang, Y., E. T. Kang, K. G. Neoh, S. S. Ang, A. C. H. Huan. Surface passivation of (100)-Oriented GaAs with ultrathin fluoropolymer films deposited by radio frequency magnetron sputtering of poly(tetrafluoroethylene), *J. Electrochem. Soc.* *150(3)*, pp.F53-59, 2003.

Zhang, Y., G. H. Yang, E. T. Kng, W. Huang, A. C. Huan, S. Y. Wu, K. G. Neoh. Deposition of fluoropolymer films on Si(100) surfaces by Rf magnetron sputtering of poly(tetrafluoroethylene), *Langmuir* *18(16)*, pp.6373-6380, 2002.

Zhang, Y., K. L. Tan, G. H. Yang, X. P. Zhou, E. T. Kang, K. G. Neoh. Thermal imidization of poly(amic acid) on Si(100) surface modified by plasma polymerization of glycidyl methacrylate, *J. Adhesion. Sci. Technol.* *14(13)*, pp.1723-1744, 2000.

Zheng, W. M., F. Gao, H. C. Gu. Magnetic polymer nanospheres with high and uniform magnetite content, *J. Mag. Mater.* *288*, pp.403-410, 2005.

Zong, B. Y., Z. H. Shang, E. T. Kang, K. G. Neoh, Magnetic mesoporous fluoropolymer nanospheres from plasma process and adsorption of surface-functionalized magnetic nanoparticles, *Plasma Process. Polym.* *4*, pp.390-397, 2007.

- Zong, B. Y., G. C. Han, Y. K. Zheng, Z. B. Guo, K. B. Li, L. Wang, J. J. Qiu, Z. Y. Liu, L. H. An, P. Luo, H. L. Li, B. Liu. Ultrasoft and high magnetic moment NiFe film electrodeposited from a  $\text{Cu}^{2+}$  contained solution, *IEEE Trans. Magn.* *42(10)*, pp.2775-2777, 2006.
- Zong, B. Y., G. C. Han, Y. K. Zheng, L. H. An, T. Liu, K. B. Li, J. J. Qiu, Z. B. Guo, P. Luo, H. M. Wang, B. Liu, A general approach to semi-metallic, ultra-high-resolution, electron-beam resists, *Adv. Funct. Mater.* *19*, pp.1-7, 2009.
- Zong, B. Y., Y. H. Wu, B. J. Yang, P. Luo, L. Wang, J. J. Qiu, K. B. Lin. Synthesis of iron oxide nanostructures by annealing electrodeposited Fe-based films, *Chem. Mater.* *17*, pp.1515-1520, 2005.
- Zou, X. P., E. T. Kang, K. G. Neoh, C. Q. Cui, T. B. Lim. Surface modification of poly(tetrafluoroethylene) films by plasma polymerization of glycidyl methacrylate for adhesion enhancement with evaporated copper, *Polym.* *42*, pp.6409-6418, 2001.
- Zou, X. P., E. T. Kang, K. G. Neoh, W. Huang. Modification of Si(100) surface by plasma-enhanced graft polymerization of allylpentafluorobenzene, *J. Adhesion, Sci. Technol.* *15(13)*, pp.1655-1672, 2001.
- Zou, X. P., E. T. Kang, K. G. Neoh, Y. Zhang, K. L. Tan, C. Q. Cui, T. B. Lim. Plasma polymerization and deposition of glycidyl methacrylate on Si (100) surface for adhesion improvement with polyamide, *Polym. Adv. Technol.* *12*, pp.583-595, 2001.

### List of Publications

Fu, G. D., B.Y. Zong, E. T. Kang, K. G. Neoh, C. C. Lin, D. J. Liaw, Nanoporous low-dielectric constant polyimide films via poly(amic acid)s with RAFT-graft copolymerized methyl methacrylate side chains, *Industrial & Engineering Chemistry Research*, 43(21), pp.6723-6730, 2004.

Xu, F. J., S. C. Mang, B. Y. Zong, E. T. Kang, K. G. Neoh, Immobilization of functional oxide nanoparticles on silicon surface via Si-C bonded polymer brushes, *Journal of Nanoscience and Nanotechnology*, 6(5), pp.1458-1463, 2006.

Zong, B.Y., Z. H. Shang, E. T. Kang, K. G. Neoh, Magnetic mesoporous fluoropolymer nanospheres from plasma processes and adsorption of surface-functionalized magnetic nanoparticles, *Plasma Processes and Polymers*, 4(4), pp.390-397, 2007.

Li, G. L., D. L. Zeng, L. Wang, B. Y. Zong, K. G. Neoh, E. T. Kang, Hairy hybrid nanoparticles of magnetic core, fluorescent silica shell, and functional polymer brushes, *Macromolecules*, 3b2 (ver. 9), pp.4-7, 2009.